Immobilizing arsenic in anoxic groundwater by iron and nitrate treatment: divergence driven by reactive organic carbon

Zengyi Li

A thesis submitted for the degree of Doctor of Philosophy

UNIVERSITY OF EAST ANGLIA

School of Biological Sciences

May 2024

“Our increase of knowledge, assuming that we are successful, is like that of a traveller approaching a mountain through a haze: at first only certain large features are discernible, and even they have indistinct boundaries, but gradually more detail becomes visible and edges become sharper.”

Bertrand Russell,
Human Knowledge: Its Scope and Limits

Abstract

Groundwater arsenic (As) of natural origin is a global issue affecting the health of an estimated 100-200 million people in >70 countries. In situ remediation has proven to be challenging due to the unstable nature of iron (Fe) oxide in anoxic groundwater. Efforts made to stimulate minerals (trans)formations in reducing groundwater for arsenic immobilization via iron and nitrate augmentation in laboratory and field experiments have shown promise. However, the mechanisms governing the formation of stable minerals to sequester arsenic are still poorly understood. While laboratory studies overwhelmingly favor the formation of mixed Fe(II)-Fe(III) oxides such as nano-magnetite for arsenic immobilization, field observations suggest the likely significant role of sulfur (S) minerals. This study suggests a divergence driven by reactive organic carbon (ROC), if indeed the processes regulating Fe/S mineral (trans)formation in oligotrophic groundwater are microbially mediated, aiming to further understand the controlling mechanisms and improve the treatment approach.

To ascertain the likely complex combinations of Fe and/or S minerals responsible for arsenic sequestration in anoxic groundwater systems, experiments were conducted in the field kept under anoxic conditions, using 8 columns packed with freshly collected aquifer sediment from a depth of 10 m and consisted of fine sand with 10.6 mg/kg arsenic and 0.36% total organic carbon. The column experiments lasted over 2 months. Pre-treatment equilibrium took 11 days. All columns were fed with fresh natural groundwater containing 89±6 μg/L As(III) (109±9 μg/L total-As). The treatment took 10 days. In addition to 2 control columns characterized by 0.79±0.07 mmol/L of influent sulfate, the experiments included 2 columns each for (a) reactive organic carbon (ROC) amendments (1 mmol/L acetate/lactate), and with/without (b) 5 mmol/L Fe(II)-nitrate supplementation. Post treatment, all columns returned to groundwater-fed only and lasted 50 days.

Fe(II)-nitrate treatments nearly doubled absorbed arsenic in sediments, with

phosphate extractable arsenic increasing from 0.75 mg/kg to 1.13±0.27 mg/kg, equivalent to accumulation of 0.11 μmol of this "strongly-absorbed" arsenic, while sequestering 1.68±0.02 μmol arsenic based on influent-effluent mass balance. The wide difference, together with 0.56 μmol arsenic associated with acidic-volatile-sulfide, suggest that sulfate reduction resulted in precipitation of sulfide minerals as a major arsenic sink. ROC-amendment alone enhanced arsenic mobilization, with 0.12 and 0.22 μmol arsenic released from solid to aqueous phase during acetate- and lactate-amendment, respectively. In contrast, lactate-amendment combined with Fe(II)-nitrate treatment increased HCl-extractable Fe(III) in sediments from 88 to 125 mg/kg, while inhibited sulfide precipitation, especially increased 25% phosphate-extractable "strongly-absorbed" As. Laboratory column experiments using artificial groundwater with lactate also found lower sulfide precipitation after Fe(II)-nitrate treatment. Lactate coupled to Fe(II)-nitrate treatment, or acetate alone, increased reactive Fe(III) in sediments, and inhibited sulfate reduction.

Microbial community obtained by 16s rRNA sequencing exhibited dramatic changes in all sediment samples collected at the end of the experiments compared to the initial sediment. Significant enrichment in nitrate-dependent iron-oxidizers were evident in end-point column sediments for Fe(II)-nitrate augmentation, and especially so with additional lactate-amendment. Interestingly, lactate-amendment alone significantly enriched sulfate reducers, but acetate-amendment did not. Consistent with the aforementioned chemistry changes, ROC amendment combined with Fe(II)-nitrate treatment resulted in lower abundance of sulfate reducers, and may contributed to the lack of sulfide precipitation observed in these columns.

In conclusion, by shedding light on coupled biogeochemical cycles of arsenic, iron and sulfur, the findings are vital for the development of effective *in situ* mitigation technology which calls for augmentation of ROC together with iron and nitrate.

Acknowledgement

The study is supported by a split-site PhD programme offered in collaboration between the University of East Anglia (UEA) and Southern University of Science and Technology (SUSTech).

I am especially grateful to Tom Clarke, my primary supervisor, for his patient guidance and generous support over the years. I also have benefited a lot from Andy Gates's invaluable insights and help. Yan Zheng has been my supervisor at SUSTech, I can not thank her enough for her dedication to the study.

I would like to thank Eileen Yu and Matthew Sullivan, who meticulously read my earlier drafts and guided me through the final stages. I also thank Jonathan Todd for his invaluable advice.

I thank Benjamin Bostick, Athena Nghiem, and Jing Sun for bringing me into this field of study, and for all the guidance and instructions. My work also benefited a lot from discussions with Yu-Min Chou, Xiaodong Jiang, Weijie Zhang, Xingxing Wang, Alex Furman, Shehong Li, Bhasker Rathi, Douglas Kent, and Henning Prommer.

Fieldwork was a pivotal component of this study, involving accumulatively 10 months spent solely in the Yinchuan Plain. Thanks must be given to Yuqin Sun, who established the research site and taught me how to plan, prepare and do field work successfully. Special thanks to Baoling Yang for being a great helper and companion, particularly during my insanely long field-based experiments, and many a day and night of analysis and discussion afterwards. Alex Palomo and Yanhua Duan helped me a lot with methods and analysis. I must thank all other members of the meritorious Yinchuan Field Crew during the past few years, including Long Han, Shuangbao Han, Songlin Liu, Yuehong Gu, Huiying Dai, Lulu Ma, Meng Ma, Zhanwen Cheng and Yunjie Ma, without you the study would have been impossible. I also thank all other past and present members of the Water Quality & Health Lab for various supports, Xiaofei Yuan, Xiaolong Yu, Weishi Wang, Anne Imig, Zhen Tan, Ruipeng Kang, Rui

Jiang, Pingqing Yi, Xiaobao Tuo, Tianci Jiang, Xi Zeng, Saloni Choudhary, Chao Wang, Zhen Yang, Xiaoxin Feng, Zhixiong Huang, Hongxue Ma and Wanning Zhang. I am grateful to Guangyao Chen, Chunmei Ji, Renze Wang and many more at Qianjin Farm, for their help, assistance and care. My preliminary study was conducted inside the Lasdun Wall, where I received a lot of help from Marcus Edwards, Andrew Loveday, Beth Williams, Graham Chilvers, and Stuart Rix, while spent some really nice time with mates of Lab 2.30, Joseph Shepherd, Kabiru Usman, Lauren Mills, Yinghong Gu, Yi Zeng, Gareth Ashworth... I also cherish many a field trip unrelated to this study, such as our Cambodia project & field investigation, with Yan, Jingyu Liu, Xin Wu, Kongkea Phan and students at IU.

Life during my PhD could have been more struggling and frustrating, particularly with the pandemic outbreak and countless quarantines afterwards that repeatedly upset my plans. Special thanks to Wensi Guo, Jingyu, Xin, Bin Xu, and Yuxia Yang, my PhD comrades. I also deeply appreciate the company of many other friends. Shiyu Tang, Zicheng Feng, Mengmeng Gao, Xinqi Luo of the SUSTech Philharmonic worked closely with me to initiate the New Year Concert amid the challenging pandemic situations. Zishen Zhang, Yejun Ding, Qiuchi Zhang, Tianyu Wang, Xuehui Pi, Lingyu Zhao, Jiayuan Dong, Zhong Lyu, Yangshen Li, Binyang Lyu, Weijie Yan, James Fung, and many a Dakang Ouyang kept me company through the ebbs and flows, so did Bach and Radio 3.

Lastly, I thank my parents for their unconditional support throughout the years, and our long-time friend, Dr Xinrong Liu (1923-2016), who had equipped me with the critical capabilities necessary to explore this intricate world.

List of contents

List of tables

List of figures

Nomenclature

AGW	Artificial groundwater
ARM	Anhysteretic remanent magnetization
As(III)	Arsenite
As(V)	Arsenate
AVS	Acidic-volatile sulfide
AVS-SEM	Simultaneously extracted metal with AVS
Cl-ext Fe	HCl extractable iron from sediments
DIW	De-ionized water
DO	Dissolved oxygen
Fe(II)	Ferrous iron
Fe(III)	Ferric iron
FORC	First order reverse curve
FRB	Fe(III)-reducing bacteria
GW	Groundwater
HIRM	Hard isothermal remanent magnetization
IRM	Isothermal remanent magnetization
IRM_{-100mT}	IRM imparted at -100 mT
IRM_{-300mT}	IRM imparted at -300 mT
Lac	Lactate
MCL	Maximum contaminant level
MLW	Multi-level well
NDFO	Nitrate-dependent Fe(II) oxidation
ORP	Oxidation reduction potential
P-ext As	Phosphate extractable arsenic from sediments
SD	Single domain
SIRM	Saturated isothermal remanent magnetization
SP	Super-paramagnetic
SIRM	Saturated isothermal remanent magnetization
SRB	Sulfate-reducing bacteria (and archaea)
χ_{lf}	Low-frequency magnetic susceptibility
χ_{hf}	High-frequency magnetic susceptibility

Chapter 1 Introduction

1.1 Arsenic in anoxic groundwater

1.1.1 Groundwater arsenic: a global health problem

One major challenge facing humanities today is the widespread occurrence of elevated arsenic (As) concentrations in groundwater, which threatens the health of an estimated 220 million people in more than 70 countries (Podgorski and Berg, 2020; Ravenscroft et al., 2009). Groundwater, though hidden and invisible, accounts for 99% of all liquid freshwater on earth (Shiklomanov, 1993). It provides drinking water for almost half of the world's population, irrigation water for nearly half of the global food production, and industrial water for about one third of the industrial consumption (UNESCO-IGRAC, 2018).

The World Health Organization (WHO) has listed arsenic as one of the 10 chemicals of major public health concern and recommended a guideline concentration of < 10 μg/L for drinking water, yet the health risks from exposure to low arsenic concentrations are still very much uncertain (Ahmad and Bhattacharya, 2019). Whether the WHO guideline is sufficiently low enough to protect human health from arsenic exposure has been frequently questioned based on risk assessment and statistical analysis (Ahmad et al., 2020; Saint-Jacques et al., 2018; Schmidt, 2014). With increasing concern over the health impact of arsenic exposure, and developing capability to detect arsenic at low levels, tougher standards for allowable arsenic concentrations were adopted in some regions and countries in recent years. For example, the New Jersey Department of Environmental Protection lowered the maximum contaminant level (MCL) to 5 μg/L for arsenic in drinking water in 2006 (Rockafellow-Baldoni et al., 2018). In the Netherlands, a guideline of < 1 μg/L for drinking water was agreed upon voluntarily in 2015 (Ahmad et al., 2020).

Irrigation with arsenic-rich groundwater poses other risks, since 20% of the global

crop production are from arsenic hazard areas (Alam et al., 2021). It can reduce crop productivity and impact global food production (Huhmann et al., 2017). Arsenic-containing groundwater also accumulates arsenic in rice grains, contaminating food crops and resulting in arsenic concentration in rice exceeding tolerable level (Dittmar et al., 2010). Exposure to arsenic via arsenic-accumulated crops brings further health concerns. WHO has set up the allowable standard of < 0.3 mg/kg arsenic in rice, while the European Union set a maximum concentration of 0.1 mg/kg inorganic arsenic for rice used for infant and children's food (Gu et al., 2020).

1.1.2 A brief history of groundwater arsenic discoveries

Detection of arsenic in natural waters has been known for over 100 years, since the earliest measurement in 1885 by Fresenius, and the earliest report of poisoning from well water in 1898 (Ravenscroft et al., 2009). Since well-water poisoning was found in West Bengal (India) in the 1980s, the extent of arsenic contamination started to be recognized with growing attentions. It was brought to the attention of scientists worldwide when a landmark conference was organized in 1995 (Chowdhury et al., 1997), and has been widely referred to as the largest mass poisoning in the world and perhaps in human history (Nordstrom, 2000). Combining prediction model and statistics, it was recently estimated that the potentially exposed population to be 94 to 220 million (Podgorski and Berg, 2020).

The causes of elevated arsenic concentration in these groundwater systems are complicated because of the numerous pathways. Initially, oxidation of arsenic-laden pyrite by atmospheric oxygen invasion was considered as the mechanism of arsenic releasing (Nordstrom, 2000), however further observations on oxic and anoxic wells in Bangladesh found that reductive dissolution of arsenic-laden iron oxyhydroxides was the geogenic cause of the problem (Nickson et al., 1998; Nickson et al., 2000). Later research found authigenic sulfide precipitation does not constitute a significant arsenic sink due to low initial sulfate in groundwater, hence arsenic mobilized under iron-reducing conditions remained mobile under sulfate-reducing conditions (Zheng

et al., 2004).

Since 2000, more discoveries were reported in many parts of the world, and most of the arsenic in groundwater were found to be geogenic in origin (Fendorf et al., 2010). Recent analysis of sediment data from the Yellow River Basin and the Ganges-Brahmaputra-Meghna Delta down-gradient of the Tibetan Plateau evidenced the excess sediment arsenic enrichment by redox trapping of groundwater arsenic during discharge, redefining the geological origin of high arsenic concentrations in groundwater and sediment (Han et al., 2023).

The key to mitigating elevated arsenic in groundwater throughout the world is the mechanisms controlling arsenic mobilization and immobilization, behind which redox reactions and the coupled biogeochemical cycling of iron, nitrate and sulfur play significant roles (O'Day et al., 2004; Zheng et al., 2004).

1.1.3 Sources and mobilization of arsenic in groundwater

Arsenic is a minor element with an abundance of 4.8 mg/kg in the earth's upper crust. The heterogeneous distribution of arsenic in the crust is linked to its presence in groundwater (Mukherjee et al., 2019; Zheng, 2007). Elevated groundwater arsenic concentrations have been widely reported in Asia, South America and North America, occurring usually in sedimentary basins with flat topography, late Pleistocene to Holocene shallow aquifers of fluvial or lacustrine plains, with sequences of sediment of several to over 10 kilometers deposited during rapid subsidence.

High arsenic concentrations in groundwater are usually associated with young mountain belts, such as the Himalayan orogenic system in Asia, the Cordillera Mountains in North America, and the Andean orogenic system in South Ameria, where sediment arsenic originated. In West Bengal (India) and Bangladesh, it was suggested that mobilizable arsenic in arsenic-laden iron oxyhydroxides were derived from weathering and oxidation of sulfide deposits in the Ganges basin (Nickson et al., 1998), the Gondwana coal seams in the Rajmahal basin, and the isolated outcrops in

the Darjeeling Himalayas (Chowdhury et al., 1999). Provenance studies of typical areas in China, where elevated concentrations of arsenic were detected in Quaternary aquifers, found sedimentary arsenic sources in the Carboniferous-Permian coal-bearing rocks of the Hengshan and Hongshou Mountains around Datong Basin (Xie et al., 2011), and Langshan mountain near Hetao Basin (Guo et al., 2016).

Sedimentary arsenic are not necessarily mobilizable, hence not the direct source of groundwater arsenic. The enrichment of highly mobilizable arsenic in anoxic aquifer sediments has been revealed likely due to post-depositional redox trapping of arsenic and iron during groundwater recharge or discharge, according to recent sediment provenance study (Han et al., 2023). While post-depositional redox condition changes resulted in the enrichment of arsenic in sediment, it was evidenced that coupled reductive dissolution of As(V) and Fe(III) minerals was behind the elevated concentrations of arsenic in groundwater (Sun, 2021; Sun et al., 2021). Recently reported negative correlation between groundwater arsenic concentration and sulfate/chloride ratio in the Yinchuan Plain (China) indicates that arsenic enrichment in groundwater is accompanied by sulfate consumption, and likely due to the reduction of arsenic-laden Fe(III) oxyhydroxides by sulfide (Feng et al., 2022).

The occurrence of elevated concentrations of arsenic around the globe are essentially the results of reductive dissolution of iron (oxyhydr)oxides in aquifer sediments that contains arsenic, as widely accepted (McArthur et al., 2001; Nickson et al., 1998; Nickson et al., 2000; Smedley and Kinniburgh, 2002). Microbially driven reductive dissolution or transformation of arsenic-laden iron minerals in anoxic aquifer sediments leads to the significant release of arsenic to groundwater (Fendorf et al., 2010; Horneman et al., 2004; Smedley and Kinniburgh, 2002; Tufano and Fendorf, 2008).

Fe(III) minerals, if reactive, can be reduced by free sulfide and dissolute, producing dissolved Fe(II) and releasing arsenic to groundwater (Sun et al., 2016c). When there is no reactive Fe(III) mineral available to reduce, and low concentration of dissolved

Fe(II) to precipitate with, the excess dissolved sulfide could be found in a sulfate-reducing groundwater. With sulfide activity (concentration) increases, arsenic could be mobilized as its solubility enhanced by the formation of thiolated compounds (Burton et al., 2011; Keimowitz et al., 2007; Sun et al., 2016c).

While sulfate reduction is capable of producing biological sulfides and enhancing arsenic mobilization through reduction of arsenate and ferric iron, or thiolation of arsenic, it can also stimulate arsenic immobilization by forming sulfide minerals with arsenic and iron, substitution within sulfide minerals, or forming sorption complex (Bostick and Fendorf, 2003; Burton et al., 2011; Burton et al., 2014; Liu et al., 2022). Nonetheless, arsenic-bearing sulfide minerals are susceptible to oxidative dissolution resulted from redox condition changes, such as pH rising, dissolved Fe(III) and/or DO increasing, and release arsenic to groundwater (Lengke et al., 2009; Stolze et al., 2022). Relatively stable solid sulfide precipitates, such as FeAsS and As_2S_3, can also be rapidly oxidized during environmental perturbations (Bostick, 2001).

Arsenic mobilization and immobilization in groundwater systems are in permanent dynamic equilibrium. When suitable geochemical sinks are present, they are capable of re-immobilizing the once mobilized arsenic in groundwater.

1.1.4 Sinks and immobilization of arsenic in groundwater

Arsenic mostly accumulates in sulfides and (oxyhydr)oxides. The two major mineralogical sinks mobilize and sequester arsenic in groundwater systems under different redox conditions, hence the single most important fact that controls arsenic concentrations in groundwater systems are redox transformations.

Major mineralogical arsenic sinks were found to be sulfide minerals, such as pyrite in the Bengal Basin (McArthur et al., 2001; Ravenscroft et al., 2005). Arsenic can be trapped by forming minerals of orpiment, realgar, arsenopyrite, or sulfide minerals of iron, copper, lead and zinc, which are normally unstable in the presence of oxygen. Arsenic-laden pyrite found in West Bengal appeared to be secondary or authigenic,

rather than primary sulfide from the source (Chowdhury, 1998; Chowdhury et al., 1999; Nordstrom, 2000), while under sulfate-reducing conditions, authigenic sulfide precipitation does not seem to constitute a significant arsenic sink (Zheng et al., 2004). Such sulfide-rich iron minerals, reported to contain most of the arsenic in deep aquifer sediments of the Bengal Basin (Lowers *et al*., 2007), are also capable of sequestering arsenic from groundwater by chemical adsorption and co-precipitation (Bostick and Fendorf, 2003; Pi et al., 2017). Niazi and Burton reported that in reducing aquatic environment under neutral pH condition, both arsenite and arsenate (at 0.01-1.00 mM) sorption to particulate FeS were not significantly affected by the presence of phosphate (at 0.01-1.00 mM) (Niazi and Burton, 2016). FeS is also an important source of Fe(II) and S(-II) species that enhance the reduction of heavy metals like Cr(VI) (Gong *et al*., 2017).

Oxide and hydroxide minerals of iron can adsorb arsenic, yet are normally unstable in anaerobic environments. While iron (oxyhydr)oxides are major sources of highly mobilizable arsenic under reducing conditions, when their presence is allowed under suitable redox conditions, they could still serve as primary sinks and sequester much of the arsenic from groundwater (Lu et al., 2010). Some reactive Fe(III) oxides, such as ferrihydrite and goethite, can go through partial reduction under reducing conditions and transformed to Fe(II) minerals or mixed valence Fe(II/III) minerals, apart from reductive dissolution (Hansel et al., 2005; Tufano et al., 2009). The transformation processes could release and redistribute arsenic to mobilizable phases on the sediment's surface, while retain iron on the solid phase (Horneman et al., 2004). Certain mixed valence Fe(II/III) minerals, such as magnetite, are thermodynamically stable even under reducing conditions, hence an ideal sink for arsenic immobilization in typical anoxic groundwater systems (Sun et al., 2016a).

Dissolved arsenic concentration in groundwater is highly related to surface complexation reactions, namely the adsorption and desorption processes of the arsenic oxyanions on mineral surfaces (Dixit and Hering, 2003; Rawson *et al*., 2016). These processes are primarily associated with mixed valence Fe(II/III) minerals and Fe(III)

(hydr)oxides (Sun *et al*., 2016a). To quantify the arsenic sorption processes, Sun et al. (2018) further proposed a conceptual model considering multiple types of iron minerals, characterized by different surface site densities, including newly formed ferrihydrite, magnetite, and natural amorphous to crystalline Fe(III) oxides.

Apart from adsorption, co-precipitation with iron minerals, such as magnetite, is also considered to be an important immobilization process of both arsenite and arsenate (Rawson *et al*., 2016; Rawson *et al*., 2017):

$$Fe^{2+} + 2Fe^{3+} + 2H_3AsO_3 + H_2O \rightarrow FeO_4As_2O_3(s) + 8H^+$$

$$Fe^{2+} + 2Fe^{3+} + 2H_3AsO_5 + H_2O \rightarrow FeO_4As_2O_5(s) + 8H^+$$

The fate and transport of arsenic in sedimentary aquifers are primarily controlled by the redox conditions in subsurface environment, and the spatial distribution (often heterogeneous) of reactive minerals that adsorb, incorporate, or co-precipitate with arsenic. While iron minerals can effectively immobilize arsenic in several ways, their presence and transformation are controlled by the coupled iron, nitrogen and sulfur cycling in groundwater systems.

1.2 Iron mineral (trans)formation in anoxic aquifer

1.2.1 Iron (hydr)oxides (trans)formation in anoxic aquifer

Sedimentary minerals in subsurface environments are primarily influenced by pH, Eh, dissolved Fe(II) concentrations and anion activities (Curtis and Spears 1968). As the most abundant transitional element on Earth surface, iron plays a pivotal role in various biogeochemical processes within groundwater systems (Borch et al., 2009).

Ferric oxyhydroxides (oxide-hydroxides) are various forms of FeOOH, such as the thermodynamically unstable lepidocrocite γ-FeOOH, and the relatively stable form of goethite α-FeOOH. The hydrate forms of them are formulated as $FeOOH \cdot nH_2O$, represented by ferric hydroxide $FeOOH \cdot H_2O$, or $Fe(OH)_3$, formed from precipitation

of dissolved Fe(III) at pH between 6.5 and 8.0:

$$Fe^{3+} + 3OH^- \rightarrow Fe(OH)_3(s)$$.

Aquifers with high arsenic concentration in groundwater are mostly anoxic and Fe(III)-reducing (Nickson et al., 2000; Polizzotto et al., 2005). In such systems, the reductive dissolution of iron (hydr)oxides is a crucial process of mineral transformation that releases dissolved ferrous iron (Hansel et al., 2005; Rawson et al., 2017):

$$Fe(OH)_3(s) + 3H^+ + e^- \rightarrow Fe^{2+} + 3H_2O$$.

This reduction can be achieved with various electron donors, including hydrogen sulfide (Dos Santos Afonso and Stumm, 1992). When dissolved iron exists as ferrous iron in anoxic solutions, they can precipitate similarly and form ferrous hydroxide:

$$Fe^{2+} + 2OH^- \rightarrow Fe(OH)_2(s)$$.

Ferrous hydroxide is a precursor of magnetite. It can transform into magnetite under anaerobic conditions and at temperature > 70 °C, known as the Schikorr reaction, but the transformation can also proceed slowly in anoxic groundwater systems under much lower temperature (Paar et al., 2015):

$$3Fe(OH)_2(s) \rightarrow Fe_3O_4(s) + H_2 + 2H_2O$$.

Besides being reduced to dissolved Fe(II), Fe(III) hydroxides can also be partially reduced in the presence of dissolved ferrous iron, and transform into mixed-valence Fe(II/III) minerals, such as magnetite (Hansel et al., 2005; Tufano et al., 2009):

$$Fe^{2+} + 2Fe(OH)_3(s) \rightarrow Fe_3O_4(s) + 2H^+ + 2H_2O$$.

Magnetite, the output of this reductive transformation of ferrihydrite, has been found stable under typical Fe(III)-reducing conditions of high arsenic groundwater (Sun et al., 2016a). Incubation of sediments from Bangladesh aquifers have found that arsenic could only be mobilized when Fe(III) oxyhydroxides had been sufficiently reduced and transformed into reactive iron minerals (van Geen et al., 2004). While indigenous

microbes in Bangladesh aquifers are capable of mobilizing most of the labile arsenic fraction with the supply of organic substrate, the process didn't release much of the iron to the solution. While these geochemical reactions Within the solid-solution interaction system, arsenic mobilization and immobilization are controlled by various physical, chemical and biological processes.

1.2.2 Coupled (bio)geochemical cycling of iron and nitrogen in anoxic aquifer

Within the solid-solution interaction system of groundwater aquifer, iron mineral (trans)formation and arsenic (im)mobilization are controlled by various physical, chemical and biological processes. Nitrogen cycle plays critical roles in the redox transformations of arsenic species (Jönsson and Sherman 2008) and iron species in groundwater and sedimentary minerals (Korom, 1992). Since Senn and Hemond (2002) demonstrated that nitrate oxidizes Fe(II), forming Fe(III) oxides that in turn sequester arsenic in Mystic Lake, MA, similar processes have been found in Cape Code aquifer (Smith et al., 2017). Zhao et al. (2013) further illustrated that this oxidation is biological. It is worth further considering the role of nitrate in Fe(III) oxide (trans)formation that impact arsenic cycling in groundwater systems.

In anoxic groundwater system, Fe(II) and Fe(III) hydroxides can transform into magnetite in the presence of nitrate, although with chloride or sulfate present, they can also transform into poorly crystalline goethite or lepidocrocite (Jang et al., 2003). Laboratory efforts made by co-injection of Fe(II) and nitrate in anoxic aquifer sediments achieved success in producing nano-particulate magnetite, in which case nitrate-dependent Fe(II) oxidation (NDFO) played an important role (Sun et al., 2016a; Sun et al., 2016b).

NDFO is a critical process in subsurface environments, oxidizing Fe(II) to Fe(III) while reducing nitrate to nitrogen gas, driven by the activity of NDFO bacteria (Jamieson et al., 2018; Straub et al., 1996). The complete reaction can be simplified as:

$$10Fe^{2+} + 2NO_3^- + 12H^+ \rightarrow 10Fe^{3+} + N_2(g) + 6H_2O$$.

The mechanism has been reported in various anaerobic environments (Hafenbradl et al., 1996; Ratering and Schnell, 2001; Zhang et al., 2018).

Jamieson et al. (2018) further identified and quantified the intermediate processes during NDFO, and developed process-based numerical models considering the contributions of both biotic and abiotic reactions. In this framework, processes were restricted by heterotrophic nitrate reduction to nitrite:

$$CH_3COO^- + 4NO_3^- \rightarrow 4NO_2^- + H_2O + HCO_3^- + CO_2(g)$$,

and nitrite reduction to nitrogen gas:

$$3CH_3COO^- + 8NO_2^- + 8H^+ \rightarrow 4N_2(g) + 7H_2O + 3HCO_3^- + 3CO_2(g)$$.

During the process, dissolved Fe(II) can be oxidized by nitrate, producing nitrite:

$$2Fe^{2+} + NO_3^- + 2H^+ \rightarrow 2Fe^{3+} + NO_2^- + H_2O$$,

or by biogenic nitrite generated from both heterotrophic nitrate reduction and NDFO processes:

$$4Fe^{2+} + 2NO_2^- + 5H_2O \rightarrow 4FeOOH(s) + N_2O(g) + 6H^+$$.

Poorly crystalline Fe(III) hydroxides, form during the process, had been proved to be well-suited electron acceptor in microbial Fe(III) reduction (Straub et al., 2004).

$$3Fe(OH)_3(s) + 3e- \rightarrow 3Fe_3O_4(s) + 2H^+ + 2H_2O$$.

The reductive re-crystallization of amorphous ferric hydroxides, similar to partial oxidation of Fe(II), results in the formation of mixed-valence Fe(II/III) oxides (Sun et al., 2016a; Sun et al., 2016b).

Microbes are the key to the biogeochemical cycling of iron in aquifer systems (Lovley et al., 2022). Evidences are emerging that microbes play an important role in the formation of mixed valence iron minerals such as magnetite (Byrne et al., 2015; Chaudhuri et al., 2001), which, given its stability under typical Fe(III)-reducing conditions, can achieve long term immobilization of arsenic in groundwater systems

(Sun et al., 2016a; Sun et al., 2016b). In a previous column study, sterilized sand columns inoculated with only Fe(II)-oxidizing *Acidovorax* sp. Strain. BoFeN1 and Fe(III)-reducing *Geobacter sulfurreducens*, feeding with Fe(II) and nitrate, similarly achieved magnetite formation and arsenic sequestration with natural sediments columns (Li, 2018), presumably indicating that the Fe(II)-oxidizers and Fe(III)-reducers play major roles in the processes of mixed valence Fe(II/III) mineral (trans)formation by iron and nitrate treatment. Straub et al. (2004) also demonstrated the possibility and likely significant role of anaerobic microbial iron cycling in the electron flow network in anoxic environments, by showing that non-toxic benzonate completely oxidized with nitrate only in co-culture experiments of lithoautotrophic nitrate-reducing Fe(II)-oxidizers and Fe(III)-reducer *Geobacter bremensis*, while neither nitrate or benzonate was utilized during either of the separate incubation experiment. While Fe(III)-reducing bacteria (FRB) in the subsurface environment is important for the transformation of iron hydroxides to mixed-valence Fe(II/III) minerals, NDFO microorganisms can oxidize including solid-phase Fe(II), likely plays an important role in mixed valence Fe(II/III) mineral formation, such as magnetite (Weber et al., 2006; Weber et al., 2001). Key microbes participating in the process include also denitrifying microbes that generate nitrite from nitrate as an intermediate that oxidize Fe(II) efficiently (Melton *et al*., 2014). The reaction is fast and in fact no nitrite was detected in effluent sample during laboratory column experiments of Fe(II)-nitrate treatment (Sun *et al*., 2016a). Field experiments (Sun, 2021) showed evidences that nitrate was consumed so rapidly that a large portion of Fe(II) remained not oxidized or precipitated in groundwater, the denitrification of nitrate may also significantly contributed to reactions other than Fe(II) and As(III) oxidation, which also is interesting for investigators to look into in the future. Presumably, the more Fe(II) oxidation coupled with nitrate reduction there is, the more arsenic will be sequestered in sediment by the newly formed Fe(III) or mixed valence Fe(II/III) oxides. If this reaction is microbially driven, there needs to be labile organic carbon around for the microbes, unless it's not a heterotroph. While Wang et

al. (2017) called for chemoautotrophic denitrification by Fe(II) oxidation, commonly studied species such as *Acidovorax* sp. Strain BoFeN1, requires 1 mmol/L acetate as electron donor for complete oxidization of 4 mmol/L Fe(II) to Fe(III) (Kappler et al., 2005).

The *in situ* formation of Fe(II/III) (hydr)oxides for arsenic immobilization consist of the following processes: nitrate-dependent oxidation of Fe(II) to less soluble Fe(III), while nitrite also plays a role in the oxidation process (Wang et al., 2018; Xiu et al., 2016); simultaneous precipitation of arsenic, Fe(III) and Fe(II) and formation of hydroxides like green rust, or oxides like magnetite (Sun, Chillrud et al. 2016); further nitrate/nitrite reduction and slow oxidation, transforming Fe(II,III) hydroxides to magnetite (Hansen, Koch et al. 1996, Hansen and Koch 1998); partially reduction of the unstable ferrihydrites to Fe(II,III) hydroxides in reducing aquifer (Sun, Chillrud et al. 2016). Nitrate-dependent microbial oxidation is also a key process to transform As(III) into less soluble As(V) (Melton *et al*., 2014), thus arsenic can be sequestered in the newly formed iron minerals (Wang *et al*., 2018; Xiu *et al*., 2016). The process of arsenic immobilization is likely to includes: nitrate-dependent As(III) oxidation to As(V), which is more favourable than Fe(II) oxidation (Xiu, Guo et al. 2016, Wang, Liu et al. 2018); arsenic incorporating into iron oxides structure (Sun *et al*., 2016a), during which iron can be partially replaced by arsenic in the newly formed oxides or hydroxides; arsenic precipitating at iron oxides surface (Amstaetter *et al*., 2009); and arsenic adsorbed at iron oxides surface (Raven *et al*., 1998).

1.2.3 Coupled (bio)geochemical cycling of iron and sulfur in anoxic aquifer

Sulfate reduction and sulfide minerals has been proposed by many for simple and inexpensive *in situ* remediation of groundwater arsenic (Keimowitz et al., 2007; Kirk et al., 2004; Mozumder et al., 2020; Pi et al., 2017). While arsenic is critically associated with at least hundreds of minerals for its capability of substituting for P(V), Si(IV), Al(III), Fe(III) in many mineral structures, it is primarily concentrated in sulfide minerals (mostly pyrite) in crustal rocks (Bowell et al., 2014; Kirk Nordstrom,

2012).

Microbial sulfate reduction produces dissolved sulfide, a strong reductant capable of reducing arsenate rapidly (Rochette et al., 2000). Dissolved sulfide were detected in typical anoxic groundwater systems with elevated arsenic concentrations, yet the concentrations were usually lower than 1 mg/L, with arsenic sulfide (As_2S_3) account for up to 43% of the sediment arsenic (Sun, 2021). It was not detected in effluents during an existed column experiment fed with artificial groundwater containing sulfate and treated with iron and nitrate (Sun *et al*., 2016a). Reaction with reactive Fe(III) oxides, such as ferrihydrite, may served as a major cause for the absence or low concentration of dissolved sulfides in these cases, for sulfide is capable of reducing and dissolving Fe(III) (hydr)oxides, releasing Fe(II) or producing iron sulfide precipitation (Dos Santos Afonso and Stumm, 1992; Sun *et al*., 2016c). Dissolved sulfide removal (oxidation) by ferrihydrite under flow-through conditions were also detected and examined (Poulton et al., 2002; Poulton et al., 2003). The reactions are surface-controlled rapid processes coupled to microbial sulfate reduction (Kocar et al., 2010; Poulton et al., 2004):

$$2Fe(OH)_3(s) + HS^- + 5H^+ \rightarrow 2Fe^{2+} + S(s) + 6H_2O,$$

$$2Fe(OH)_3(s) + 3HS^- + 3H^+ \rightarrow 2FeS(s) + S(s) + 6H_2O.$$

Sulfate reduction, in the presence of abundant iron hydroxides while low dissolved sulfide, can promote the transformation of Fe(III) minerals to amorphous FeS (Kocar et al., 2010). Ferrous mono-sulfide (FeS), commonly known as mackinawite, is a major constituent of acid-volatile-sulfides (AVS), ubiquitous in anoxic environments from sulfate reduction, and a precursor to the (trans)formation of more stable sulfide minerals such as pyrite and greigite. Iron sulfide (FeS) is known for being capable of removing heavy metals and arsenic, and is relatively stable under reducing conditions.

Sulfur cycling in groundwater systems is also highly related to microbial activities. Sulfate reducing bacteria, such as *Desulfobulbus*, *Desulfosporosinus* and *Desulfovibrio*, can utilize sulfate as electron acceptor and oxidize organic carbon

sources (Xia et al., 2019). Column experiments, fed with artificial groundwater containing sulfate and lactate, was inoculated with sulfate reducing bacteria *Desulfovibrio vulgaris* and found it capable of mediating the transformation of ferrihydrite to amorphous FeS (Kocar et al., 2010). Nitrogen species also participate in sulfur cycling. Anaerobic ammonium oxidation (anammox) bacteria has been found playing important roles in the biogeochemical cycling of nitrogen (Arrigo, 2005; Van de Graaf et al., 1995). Recent studies also reported that sulfate can serve as electron acceptor for anaerobic ammonia oxidation coupled with sulfate reduction, or so-called Sulfammox (Grubba et al., 2021; Liu et al., 2021; Makinia et al., 2021; Rios-Del Toro and Cervantes, 2019). In coastal wastewater systems, organic matter was found to favor heterotrophic denitrifiers over sulfammox bacteria. Meanwhile, chemolithotrophic denitriers were found capable of oxidizing sulfide while reducing nitrate (Cardoso et al., 2006).

In microbially mediated reactions, it is organic carbon that often serves as the prefered electron donor, oxidized from organic carbon to inorganic form. Electron acceptors such as oxygen, nitrate, sulfate and iron oxides, however, usually co-exist in nature. If the processes of certain iron mineral (trans)formation are indeed microbial, then presumably reactive organic carbon (ROC) amendment in the system could enhance microorganism growth and stimulate (trans)formation of wanted iron mineral.

ROC is commonly added in laboratory experiment to stimulate microbial activity, especially in the (artificial) groundwater to mimic reducing conditions (Sun et al., 2016a; Sun et al., 2016b; Sun et al., 2016c). The choice of ROC source to stimulate microbial activities can have significant impacts on the efficiency and sustainability of bio-remediation strategies for iron mineral transformation and arsenic immobilization. Acetate and lactate are both organic carbon sources that can stimulate microbial metabolism in reducing environments, leading to the transformation of iron minerals and immobilization of arsenic. However, they have different chemical properties that can influence microbial activity and the resulting biogeochemical reactions. Acetate is a simpler organic molecule that can be more easily metabolized

by a wider range of microorganisms, leading to more rapid microbial growth and iron mineral transformation. The accumulation of acetate can also inhibit microbial activity and biogeochemical reactions, as it can promote the growth of sulfate-reducing bacteria (SRB) that compete with FRB for electron donors. Lactate, on the other hand, is a more complex organic molecule that is metabolized more slowly by microorganisms. It can promote the growth of a more specific group of microorganisms that are specialized in iron mineral transformation and arsenic immobilization. The amendment of lactate is commonly applied to stimulate sulfate reduction (Burton et al., 2011; Burton et al., 2014), reductive Fe(III) minerals dissolution and transformation to magnetite (Tufano and Fendorf, 2008). ‘

Desulfuromonas can carry on sulfur reduction, while *Desulfovibrio* spp. Can disproportionate sulfur, SRB also play major roles in anaerobic carbon cycling, capable of utilizing various substrates from methane, carbon monoxide and methanol, to sugars, amino acids, and substrates degraded from polymeric organic compounds by other microbes (Muyzer and Stams, 2008). Incomplete degradation of organic compounds to acetate is the main metabolic pathways for SRB. Some SRB can completely oxidize organic carbon to CO2, while few can go through both pathways depend on available substrates.

Lactate, for its superiority as an organic substrate, can be completely oxidized by some SRB:

$$2CH_3CHOHCOO^- + 2SO_4^{2-} \rightarrow 2HS^- + 4HCO_3^- + H^+,$$

although most SRB can only incompletely degrade lactate to acetate:

$$2CH_3CHOHCOO^- + SO_4^{2-} \rightarrow 2CH_3COO^- + HS^- + 2HCO_3^- + H^+$$

Few SRB can consume acetate alone (Neculita et al). *Desulfobacterium*, *Desulfotomaculum*, *Desulfococcus* spp., *Desulfobacca acetoxidans* are capable of acetate oxidation coupling autotrophic CO_2 fixation (acetyl-CoA pathway) (Oude Elferink et al., 1999), while *Desulfobacter postgatei* can convert acetate to CO_2 and

NADH (a modifide citric acid cycle) (Brandis-Heep et al., 1983). When acetate degrading bacteria are not present, acetate accumulation may lower the pH and inhibit the growth of SRB, for the optimal pH for neutrophil SRB is between 7.0 and 7.8 (Kikot 2010, Sharma 2014). Apart from organic substrates, carbon monoxide, carbon dioxide or hydrogen can also be the sole electron donors for some autotrophic SRB in anaerobic sludge bioreactors (van Houten et al., 2006; van Houten et al., 1997).

The microbially mediated processes, if can be selectively stimulated, may be the key to controlling iron mineral (trans)formation in anoxic groundwater and subsequent removal of arsenic. Kirk et al. (2004) proposed groundwater arsenic remediation by simply injecting sulfate and stimulating bacterial sulfate reduction, in order to produce sulfide and subsequently precipitate with arsenic and iron, and emphasized the competition between FRB and SRB controlled by dissolved ferric iron concentration, as did Xia et al. (2019). While amendment of ROC for stimulation of sulfate reduction is common, natural sulfate-reducing groundwater usually contains very low total organic carbon (TOC), e.g. all samples TOC < 2 mg/L from the Mahomet aquifer's sulfate-reducing zones (Kirk et al., 2004). Groundwater from sulfate-reducing zones in the shallow aquifer of the Yinchuan Plain exhibits not only a low concentration of organic carbon, but also a significantly low bioavailability of the already limited organic carbon (Dai, 2022). How ROC augmentation may affect the carbon-poor groundwater systems and regulate different microbial activities for the transformation of minerals in sediments, deserves further investigation.

1.3 Mitigation strategies and challenges

1.3.1 Mitigation strategies for groundwater arsenic

To mitigate groundwater arsenic problem and reduce exposure, policy makers usually look for alternative water sources, centralize water treatment and supply, or at least promote household implementation of accessible arsenic treatment technologies.

While technologies are various, they either remove arsenic from water, or transform the dissolved arsenic into insoluble forms. Various *ex situ* technologies, including adsorption, ion exchange, membrane filtration, oxidation, and coagulation, have demonstrated efficacy in household or centralized water treatment (Patel et al., 2023). For rural household lacking access to centralized water supply, the point of use (POU) treatment using iron-based material could cost US$2,740 per installation and US$1.00 per day of maintenance, on average, to treat a small volume (< 6 L/day per person) of water (Yang et al., 2020). The application of such technologies to treat larger volumes of water, often necessary for irrigation, is economically impractical. Furthermore, the dispersed nature of irrigation wells in rural areas poses additional challenges.

In fact, irrigation accounts for 85-90% of groundwater pumped in Bangladesh and West Bengal, and mostly for growing arsenic-accumulating rice crop (Ravenscroft et al., 2009). Mitigation could be achieved by switching to deeper wells and using low-arsenic groundwater, although it may unintentionally draw down arsenic from upper aquifers, while the cost of implementation is usually high. Local farmers could also choose to grow crops that require less irrigation or uptake less arsenic, but their preference for rice is the result of long time selection, hence very difficult to change.

To In recent decades, *in situ* remediation approaches shed light on the issue. A typical remediation strategy usually aims to form a permeable reactive barrier (PRB) or wall (Benner et al., 1997) *in situ* with materials capable of sequestering the contaminants. The barrier intercepts the path of contamination plume advection, subsequently reduces the concentration and prevents the migration of contaminants.

1.3.2 *In situ* remediation: one well at a time

A significant portion of population depends on private wells for drinking and irrigation purposes. Private wells are the smallest water supply, popular in the rural area for being low-cost and minimal maintenance requirement, yet benefit the least from treatment technologies in terms of suitability and economy of scale (Zheng, 2017). Development of simple and stable remediation strategies for private wells are

vital to reduce arsenic exposure among dispersed rural population.

Natural iron oxide minerals, such as hematite, magnetite, and goethite, have been found effective at immobilizing arsenic by adsorption (Aredes et al., 2012). Nano-material research have found iron oxides based materials capable of efficient arsenic removal in water (Jang, Min et al. 2006, Pena, Meng et al. 2006). However, for *in situ* remediation, stable adsorption of arsenic with iron oxides are still facing many difficulties, especially under reducing conditions, which is typical in most elevated arsenic concentration aquifers of the world (Smedley and Kinniburgh 2002, Zheng, Stute et al. 2004). An iron-oxide based nano-material with not only high efficiency but also better stability is the key to removing arsenic efficiently and keeping immobilized arsenic from releasing again in reducing aquifer.

Recently process studies showed possibilities in stable arsenic immobilization by mixed-valence iron oxides such as nano-particulate magnetite (Tufano and Fendorf 2008, Sun, Chillrud et al. 2016). A treatment by iron and nitrate achieved long term arsenic removal in anoxic groundwater by *in situ* formation of mixed valence Fe(II/III) oxides, such as magnetite, through (a) chemical or biological oxidation of Fe(II) to form magnetite, (b) denitrifiers producing nitrite by utilizing organic carbon, and (c) dissolved Fe(II) reacting with ferrihydrite and forming magnetite (Sun et al., 2016a; Sun et al., 2016b). While arsenite is considered to be oxidized during the treatment of Fe(II) and nitrate, it is still possible for kinetically reduction of arsenate to arsenite to occur. Sun (2015) explored the potential of enhanced remediation for groundwater arsenic contamination by *in situ* formation of iron minerals as a dispersed reactive filter or PRB. The approach applies Fe(II) and nitrate injection(s) in anoxic groundwater aquifer, producing within sediments iron minerals thermodynamically stable under reducing conditions, such as magnetite, and achieved long-term arsenic immobilization during laboratory column experiments, showed excellent ability in *in situ* arsenic sequestration, managed to keep effluents arsenic concentrations lower than 10 μg/L (Sun et al., 2016a), the WHO guideline of drinking water standard, for more than 100 pore volumes, while magnetite persisted as conditions turned reducing

again. It was estimated that a single well treatment can produce approximately 1300 m^3 of arsenic-safe (≤ 50 μg/L) irrigation water, sufficient for irrigating 1000 m^2 of land for an entire rice cultivation season in the arid Yinchuan Basin, at a low cost of US$0.08 per m^3, as simulated based on pilot push-pull tests (**Figure 1.1**) (Sun, 2021). These recent progresses are crucial advances towards the goal to successfully remove arsenic from groundwater in reducing aquifer, however the possibility that the results may lead to other unexpected problems, and the effectiveness of the treatment when facing environmental variability, remains significant to be further studied.

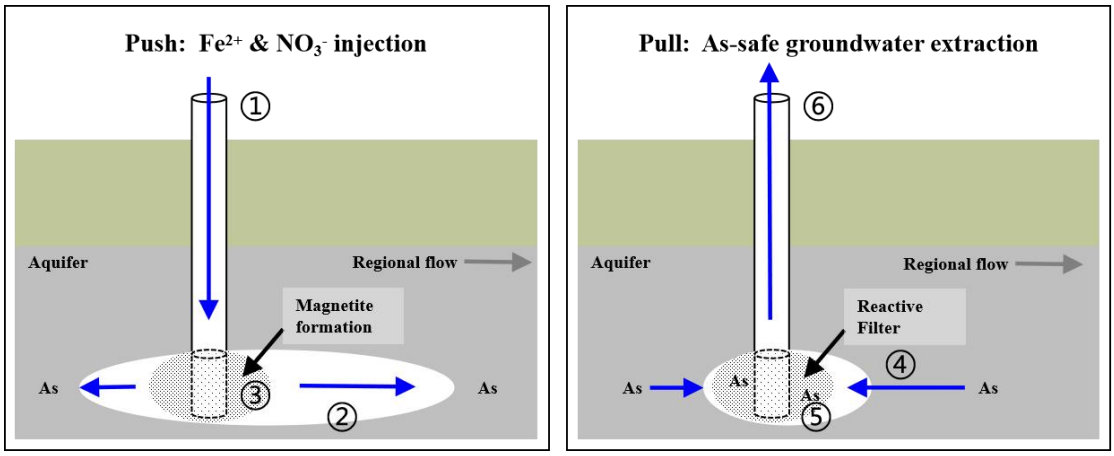

Figure 1.1 Single well push-pull approach: The single well push-pull is an effective and low-cost approach to remediate a single well for low-arsenic irrigation water supply. As the figure shown, the groundwater aquifer is illustrated as the gray area underground, with the gray arrow showing regional groundwater flow direction to the right, while the blue arrows showing the push-pull of groundwater. The "push" is conducted through injection of Fe(II) and nitrate reagents into a single well (①), their diffusion in the aquifer (②) can produce magnetite particles in aquifer sediments (③), forming *in situ* a permeable reactive barrier (round area with black dots) serving as a filter surrounding the well screen (the bottom of the well in dash line). The "pull" is during groundwater extraction from the well, with groundwater flowing (④) through the reactive filter and arsenic adsorbed by magnetite (⑤) , providing arsenic-safe groundwater for irrigation (⑥). Figure adapted from Sun (2021).

Process-based, numerical modelling approaches have been developed and tested, to help understand iron mineral formation and arsenic mobility (Jamieson et al., 2018; Rawson et al., 2016; Rawson et al., 2017), yet the network and the inter-plays between different processes are still not well understood. Single well push-pull tests in the field further examined the effectiveness at site scale, but preferential flow path

and heterogeneity in aquifer significantly affected the *in situ* experiment, while uncontrollable environmental variability also disturbed the tracer recovery, leaving processes such as denitrification after nitrate injection remain unexplained (Sun, 2021). To successfully immobilize arsenic in anoxic groundwater by *in situ* remediation, environmental variability must be taken into careful consideration for the development, improvement and implement of mitigation strategies.

1.3.3 Challenges from environmental variability

While *in situ* remediation approaches are promising, challenges from environmental variability are still many, such as the presence of other chemical species (e.g. sulfate and phosphate) that strongly impact mineral transformation and arsenic immobilization.

Sulfate is ubiquitous in groundwater systems, stable in aerobic environment but can be reduced in anoxic, sulfate-reducing conditions, producing sulfides that precipitate with iron (Miao et al., 2012). While the iron and nitrate treatment aims to form mixed valence Fe(II/III) oxides, it may come up with different results if abundant sulfate is present in groundwater, as evidenced in the field push-pull experiment (Sun, 2021), since iron mineral formation and transformation is highly dependent on and sensitive to the environmental characteristics. Previous laboratory column experiment with sulfate in influent also found iron minerals formed mostly as sulfate green rust according to XAS (X-ray absorption spectrocscopy) analysis (Li, 2018). Sun et al. (2016a) performed laboratory column experiments on iron (as ferrous sulfate) and nitrate treatment, and found iron sulfides the second most abundant iron minerals in end-point sediments.

Phosphate interference from natural groundwater presents another problem, since phosphate strongly competes with arsenic species for adsorption sites in iron sulfides (Han et al., 2020; Niazi and Burton, 2016) and (hydr)oxides (Goldberg, 2002; Hongshao and Stanforth, 2001; Manning and Goldberg, 1996), due to its similar ionic radius and acid dissociation constant with arsenate (O'reilly et al., 2001), hence

affecting the mobilization and immobilization of arsenic in water systems (Dixit and Hering, 2003; Smedley and Kinniburgh, 2002). In practice, phosphate (usually in the form of KH_2PO_4) solutions of various concentrations have been widely applied for the extraction of adsorbed phase of arsenic from iron oxides (Jackson and Miller, 2000; Keon et al., 2001; Sun et al., 2021), proving its effectiveness for desorption of arsenic from iron oxides, one of the major sink for arsenic in natural groundwater system, and the mineral we intended to form by iron and nitrate treatment.

1.4 Thesis aim and objectives

Efforts made to stimulate minerals (trans)formation in anoxic groundwater for arsenic immobilization via iron and nitrate augmentation in laboratory and field experiments have shown promise. However, the mechanisms governing formation of stable minerals to sequester arsenic are still poorly understood. While laboratory studies overwhelmingly favor the formation of mixed Fe(II/III) oxides such as nano-particulate magnetite for arsenic immobilization, field observations suggest the likely significant role of sulfur minerals. If indeed the processes regulating iron and sulfur mineral (trans)formation are microbially mediated, as many existing researches suggested, ROC augmentation may be necessary since the groundwater is oligotrophic.

This study aims to further understand the controlling mechanisms of iron mineral transformation and arsenic immobilization in anoxic groundwater systems, and improve the iron and nitrate treatment approach, by investigating the divergence driven by ROC augmentation during the treatment, and examining the impact of sulfate reduction and phosphate interference from the environment, using experimental approaches balanced between artificial (laboratory) and natural (field) conditions.

The more specific objectives are as follows:

(a) To investigate how ROC augmentation impact iron and sulfur cycling in carbon-poor anoxic groundwater systems, and its potential in improving the application of iron and nitrate treatment.

(b) To examine the impact of sulfate reduction and sulfide precipitation on iron mineral transformation and arsenic immobilization in anoxic groundwater aquifers.

(c) To test and evaluate the iron and nitrate treatment approach for arsenic immobilization with phosphate interference from groundwater, and to guide the development and improvement of future mitigation strategies for groundwater arsenic contamination.

Chapter 2 Materials and Methods

This chapter first provides information of the research sites in Yinchuan Plain, China, briefly reports data from the field investigations prior to the experiments to profile the arsenic and iron speciation in critical extractable phases of sediments, and identified the sediment sample we chose to perform experiment. Then it describes the materials and experimental designs for 2 field-based column experiment studies later presented in *Chapter 3* and *Chapter 4,* and a laboratory based column experiment study later presented in *Chapter 5*. Lastly, it provides in detail various analytical methods applied in this study for aqueous (groundwater and effluent) and solid (sediment) sample analyses, in laboratory and in the field.

2.1 Site description and field investigation

2.1.1 Geographical and geological background

The Yinchuan Basin is a semi-arid area (annual rainfall < 200 mm/year) lying in northwestern China, with the Helan Mountain to its west, desert in the north, and loess in the south, as shown in **Figure 2.1**. The Yellow River, originating in the Tibetan Plateau, runs through the Yinchuan Basin from south to north with large amount of debris. The plain has substantially accumulated up to 2000 metre thick of Quaternary sediments resulted from a high subsidence rate, with multiple layers of alluvial and lacustrine deposits. Its groundwater system consists of 2 deep confined aquifers and an unconfined shallow aquifer between the depths of 10 and 40 m. The shallow unconfined aquifer in the region has been reported to contain 3 to 177 μg/L (n=142) of dissolved arsenic in its groundwater, while its groundwater table fluctuates between 0.1 to 5 meters below ground level (Han et al., 2013). We have been working on groundwater arsenic in the Yinchuan Basin for years, with several well-maintained research sites established and multi-level observation wells installed. Sediment cores and groundwater samples of high spatial resolution from the sites have been studied

(Sun et al., 2021), while pilot field push-pull tests of arsenic immobilization by iron and nitrate treatment were performed in 2 of the research sites in 2017 and 2018 (Sun, 2021). The resources, infrastructure and preliminary field data already available made the sites best suited for field-based experimental researches.

The study area is located in the northern plain of Yinchuan Basin. We focused on an approximately 2.5 kilometre profile between two study sites: YCA (38°49'48.20"N, 106°21'14.04"E) adjacent to the Sand Lake and next to paddy rice fields irrigated with Yellow River water through a network of irrigation canals; YCB (38°50'41.53"N, 116°22'24.57"E) located in a corn field irrigated by groundwater (depth 60 m) containing dissolved arsenic > 100 μg/L (Sun et al., 2021). Given the relatively saline soil in the local area, irrigation activities during the past few decades could have significant impact on the groundwater composition, as natural and anthropogenic changes in hydrological cycle most likely affect these shallow aquifer first (Stute et al., 2007).

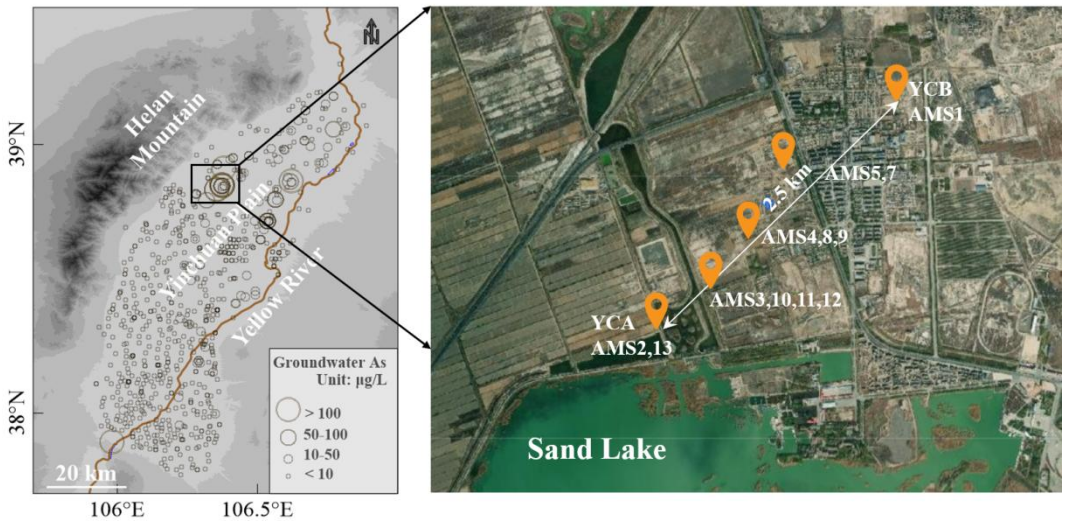

Figure 2.1 Research site and sampling locations in northern Yinchuan Plain: Elevated concentration of arsenic in shallow (depth < 50m) groundwater is commonly found in the Yinchuan Plain. The concentrations of arsenic in shallow groundwater were obtained from 579 wells in the region (Han et al., 2013). High-resolution sampling of sediment cores and groundwater were performed along a 2.5 km profile in the research site to analyze the spacial-heterogeneous distribution of arsenic and iron species, so as to select the ideal sediment sample for experiment.

2.1.2 Field investigation and sampling

Our research sites located in the Qianjing Farm, Pingluo County. Multi level wells (MLW) were at first established by China Geological Survey in 2012 for groundwater sampling and observation, at sites YCA (38°49′48.20″N, 106°21′14.04″E) and YCB (38°50′41.53″N, 106°22′24.57″E). From year 2017 to 2018, we performed continuous sediment cores sampling using split spoon sampler, at site YCA (to a depth of 30 m) and YCB (to a depth of 40 m), at high-spatial resolution. In May 2021, a series of continuous sediment cores named after sites AMS1 to AMS13 (**Table 2.1**), with depths ranging between 9 and 20.5 m (n=13), were obtained with AMS Power Probe 9520-VTR (Art's Manufacturing & Supply, Inc.) along a line drawn between the two research sites, making up a profile of the shallow subsurface, as illustrated below in **Figure 2.1**.

Table 2.1 Sediment core sampling information

Site	Depth (m)	Coordinate			
AMS1	12.5	106°22′24.5″	E	38°50′41.9″	N
AMS2	19.5	106°21′31.9″	E	38°49′51.4″	N
AMS3	19.5	106°21′46″	E	38°50′3″	N
AMS4	20.5	106°21′46″	E	38°50′3″	N
AMS5	19.5	106°22′7.3″	E	38°50′29.4″	N
AMS6	9	106°26′50.2″	E	38°53′58.2″	N
AMS7	19.5	106°22′7.1″	E	38°50′28.6″	N
AMS8	16.5	106°21′52.6″	E	38°50′20.8″	N
AMS9	16.5	106°21′54.5″	E	38°50′20.6″	N
AMS10	15	106°21′54.5″	E	38°50′20.6″	N
AMS11	13.5	106°21′29.7″	E	38°29′59.6″	N
AMS12	13.5	106°21′29.7″	E	38°29′59.6″	N
AMS13	15	106°21′32.4″	E	38°49′51.4″	N

The ID, depth, and coordinate of the sites for sediment core sampling.

Fresh groundwater were sampled from 2 major types of wells, steel tube wells (with an inner diameter of 15 cm) and multi-level observation wells (MLW, with an inner diameter of approximately 2 cm), or collected during core drilling using AMS PowerProbe direct push drilling technology (Art's Manufacturing & Supply, Inc.). Groundwater pumping were conducted with either peristaltic pumps (Geotech

Environmental Equipment Geopump™ Peristaltic Pump Series II Kit, or Solinst® Peristaltic Pump Model 410) for multi-level observation wells, or a submerged pump (Proactive Environmental Products® Mega-monsoon) for steel tube wells. All groundwater samples were taken after pumping out at least 2 pore volumes of the well's pore water. Sediments were sampled as continuous cores using direct push drill rigs (AMS PowerProbe). The sediment cores were acquired in 1.5 meter long PVC tubes, immediately cut into sections, sealed with preservative film, vacuum packaged in Mylar bags, and stored under -20°C.

2.1.3 High-resolution profile of the shallow aquifer: characterizing mobilizable arsenic and reactive iron species in sediments

During the field investigation, high resolution chemical extraction of sediments was performed on site immediately after sampling, followed by profiling the concentrations and speciation of extractable iron and arsenic (**Figure 2.2**). As will be detailed in *2.5.5 Chemical extraction for reactive iron and exchangeable arsenic*, phosphate extraction was applied to extract strongly adsorbed As(III)/As(V) through anion exchange. HCl extraction aims at reactive Fe(II)/Fe(III) from amorphous and low crystalline iron minerals, for reactive Fe(II) in minerals has been found more reactive for NDFO than dissolved Fe(II) (Grabb et al., 2017; Liu et al., 2019; Rakshit et al., 2008; Sørensen and Thorling, 1991), characterization of the reactive phase of iron species in sediments are important in this study.

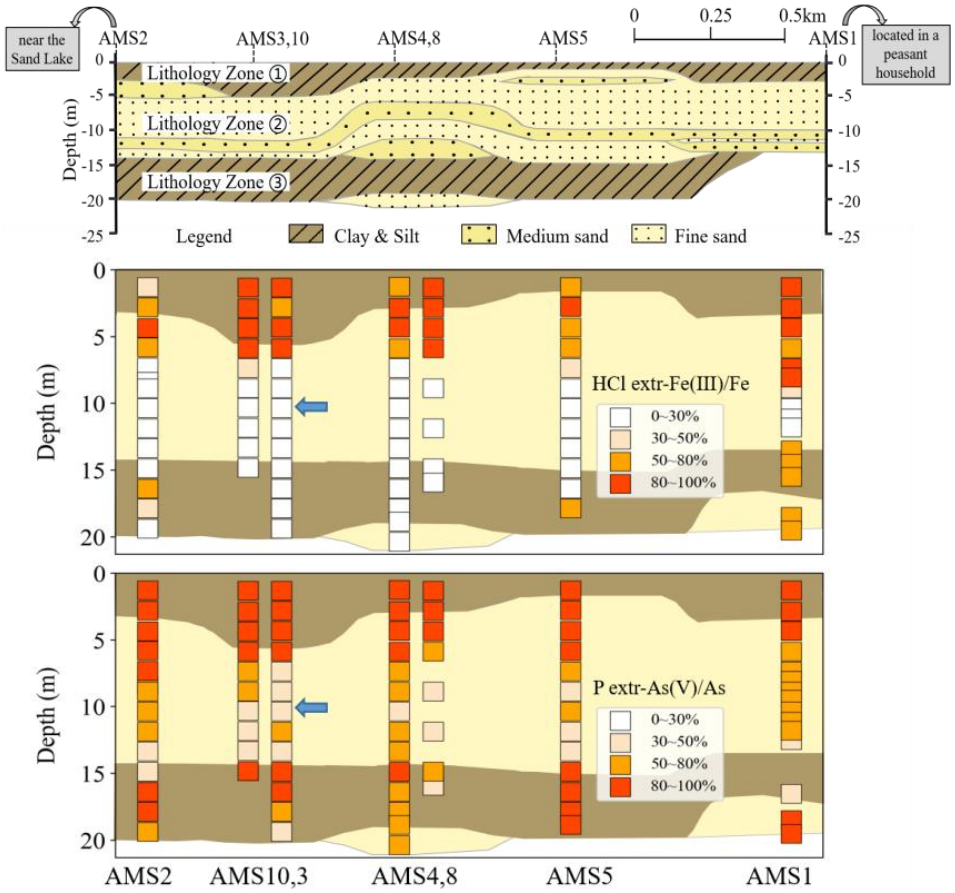

Figure 2.2 Profile lithology, extractable Fe(III)/Fe and As(V)/As of sediment: We illustrate here the spatial distribution of arsenic and iron species of phosphate extractable (P extr-) and HCl extractable (HCl extr-) factions in sediment of the sampling profile. As shown in the top figure, the shallow aquifer is characterized by a layer of clay and silt (lithology zone ①), a layer of medium to fine sand (lithology zone ②), and another layer of clay and silt (lithology zone ③). As shown in the middle and bottom figures, each of the square boxes represents the results of a sediment sample from the depth, and each line of boxes represent a sediment core. Due to higher resolution of sampling, some of the square boxes are partly covered by others, but the depth it represents and the result displayed in color shade are not mistaken. In the first layer above the depth approximately 7 metre, HCl extr-Fe in sediments were mostly ferric iron, while P extr-As were mostly arsenate. The second layer consists of mostly medium to fine sand contain much higher reducing portion of HCl ext-Fe(II) and P ext-As(III) in the sediments, indicating the aquifer is an iron reducing environment. The blue arrow shows where the sediment AMS3-7, selected for the field-based experiment, was sampled.

2.2 Field based column experiments

While *in situ* field experiments, such as single well push-pull, can provide the most realistic perspectives, they are usually exhausting and subject to variable conditions in

the field. In this study, we will try to avoid heterogeneity and preferential flow by performing 1-dimensional column simulation. Column experiments provide a one-dimensional simulation of the natural groundwater flowing system, hence simplifying the observation and examination of certain geochemical processes. In previous column studies, artificial groundwater was frequently used as a substitute feed solution (Benner et al., 2002; Saalfield and Bostick, 2009; Sun et al., 2016a), but its resemblance with natural groundwater is highly doubtful. Very few studies of groundwater arsenic applied field-based column experiments to approach nearly *in situ* conditions, by continuously pumping groundwater to supply the experimental system (Mihajlov, 2014; Mozumder et al., 2020), as further improvement to the experimental design, making the simulation more close to the natural conditions while retaining the advantage of the simplified 1-dimensional experimental design.

The field-based column experiments were performed on site under simulated groundwater flow condition, using freshly pumped natural groundwater containing elevated concentration of arsenic (**Figure 2.3**). An overflow of fresh groundwater was maintained by continuously pumping from an observation well, in order to make anoxic groundwater available as influent to the columns. The design also made it possible to keep the system anoxic by submerging the column settings in a box of overflowing groundwater. The experimental design is for the studies presented in *Chapter 3* and *Chapter 4*.

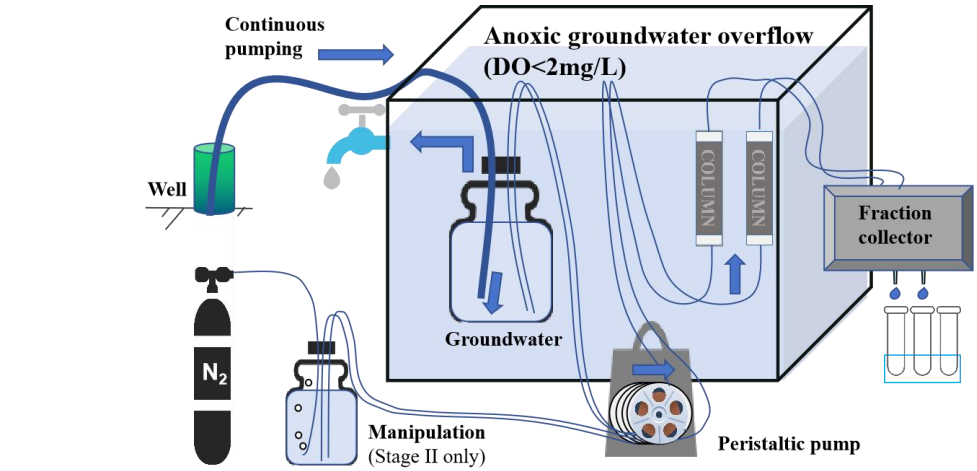

Figure 2.3 Field-based column experiment set-up: Fresh groundwater was continuously extracted from an observation well YCB-MLW5 with peristaltic pump, at a rate 10 L/hour, then diverted into an overflowing Pyrex bottle (1 L) inside an overflowing water tank (16 L), continuously refreshed to maintain near-anoxic (DO < 2 mg/L). Columns and tubing connectors were submerged into the water, and covered with aluminum foil to avoid light intrusion. A multi-channel peristaltic pump extracted groundwater from the bottle and injected into the columns from the bottom, while the effluents out of the top outlet of the columns were collected with an automatic fraction collector at set intervals. During the treatment, reagents were continuously purged with nitrogen gas during the injection.

2.2.1 Materials

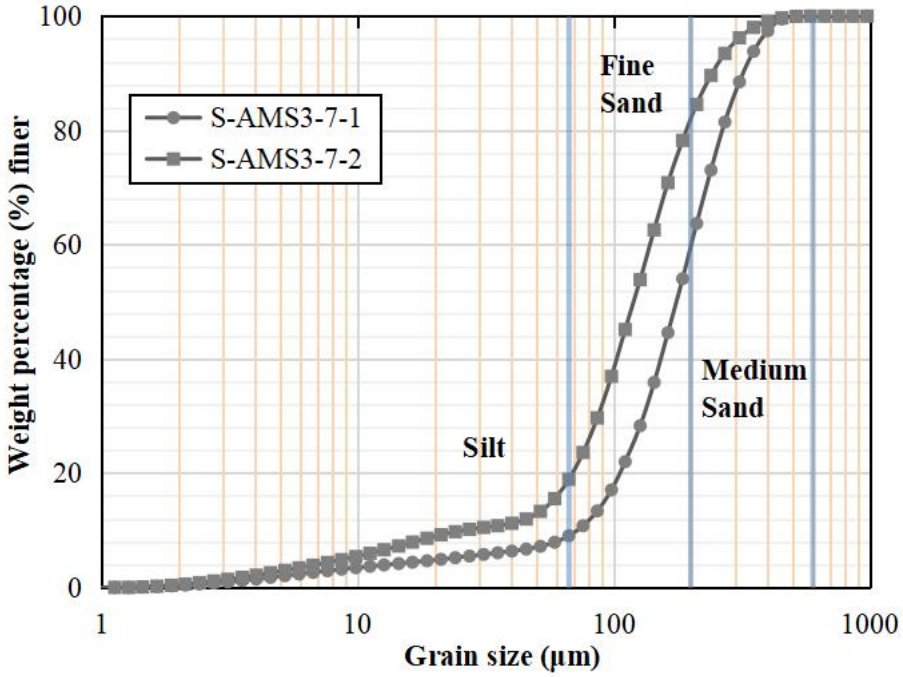

Figure 2.4 Grain size distribution of sediment sample S-AMS3-7 (n=2): The weight percentage (%) of the grains with sizes finer than the grain size are plotted against the grain size (x axis). The grain sizes are plotted on the logarithmic scale. The grain sizes are classified into silt (< 62 µm), fine sand (62 to 200 µm) and medium sand (200 to 600 µm), using the size ranges as shown in *2.5.1 Grain sizes*.

The sediment sample chosen for the experiment was S-AMS3-7, consists of 86±7% fine to medium grained brown sands (**Figure 2.4**), collected from a saturated shallow aquifer at the depth between 9 and 10 m, at the site AMS3. Its phosphate extractable As(V)/As and HCl extractable Fe(III)/Fe were relatively low (**Figure 2.2**). During the field sampling, the sediments were continuously sampled in 1.5 m long PVC tubes, then immediately cut into sub-samples (approximately 20 cm) for preservation, sealed and vacuum-packed in Mylar bags with packs of de-oxidizer to avoid oxygen, and stored frozen under -20℃ before use.

The columns are made from polycarbonate tubes (15 mm ID, 20 mm OD, 10 cm long net adapters, 13 cm long). Column length packed with sediments was 10 cm, and volume was 17.7 ml. The pore volume (PV) was estimated to be 6.2 mL with the porosity of 0.35. Sealed PVC tubes containing sediments were firstly unpacked inside

a glove bag filled with N_2 gas. Sediments were then homogenized in a sterilized beaker, and wet-packed into the columns. Both ends of the column were packed with sterilized glass wool for stable solution distribution during the experiment. After connectors were installed, the junctures were sealed with silicone and let dry for 2 hours in the glove bag.

The source groundwater chosen as influent for the experiments was from a 39.5 m depth observation well YCB-MLW5 of a multi-level well Q47 at YCB site, near AMS1. The arsenic concentration and speciation of the groundwater were similar with the groundwater sampled from AMS3 site (GW-AMS3-2, depth 9 m), as will be detailed in **Chapter 3**. A peristaltic pump (Geopump™) was settled for continuously pumping from the well and directing the source groundwater to the experimental system as influent. The influent GW for all columns was spiked with a conservative tracer bromide (1 mmol/L or 80 mg/L Br as 103 mg/L NaBr), for a short period within 24 hours, at the beginning (pre-treatment) and before the end of the experiment (post-treatment), respectively. The injections were performed by diluting 10 mL 100 mmol/L NaBr stock solution with fresh groundwater to 1 L in a 1 L Pyrex bottle. The bottle was continuously purged with nitrogen gas to avoid oxygen.

Besides freshly pumped groundwater, there were also solutions made and preserved in Pyrex bottles for manipulations. These solutions were continuously purged with nitrogen gas before (> 12 hours) and during feeding, and refreshed every 24 hours during the treatment or amendment period. These solutions were:

Br-GW (groundwater with 3 mmol/L NaBr) was made by diluting 3 mL 100 mmol/L NaBr stock solution in 100 mL groundwater, for the 4 GW experiments.

NO_3-Br-GW (groundwater with 15 mmol/L $NaNO_3$ and 3 mmol/L NaBr) was made by dissolving 128 mg $NaNO_3$ in 100 mL Br-GW, for the 4 GW+Fe+NO_3 experiments.

Fe-DIW (15 mmol/L $FeCl_2$ solution) was made by dissolving 298 mg $FeCl_2 \cdot 4H_2O$ (Macklin, 99.95%) in 100 mL de-ionized water (DIW, purged with nitrogen gas for 24 hours before use) instead of groundwater to avoid precipitation.

ROC stock solution (1 mol/L sodium lactate or acetate) was made by dissolving 9.334 g of 60% sodium lactate $C_3H_5NaO_3$, or 4.102g sodium acetate CH_3COONa with DI water, in a 50 mL volumetric flask, and stored in fridge at 4°C.

ROC-GW (3 mmol/L sodium acetate or lactate) was made by diluting 0.9 mL ROC stock solution with fresh groundwater to 300 mL in a 300 mL Pyrex bottle.

During the iron and nitrate treatment, GW (ROC-GW for the ROC augmentation experiments), Fe-DIW (DIW for the blank treatment experiments) and NO_3-Br-GW (Br-GW for the blank-treated experiments) were mixed at a ratio of 1:1:1 through tubing. The final influent should contain for iron and nitrate treatment experiments 1 mmol/L NaBr, 5 mmol/L $FeCl_2$ and 5 mmol/L $NaNO_3$, while for blank treatment experiments 1 mmol/L NaBr only. For the ROC augmentation experiments, the final influent should also contain 1 mmol/L acetate or lactate.

2.2.2 Experimental design

The experimental designs for each experiments, adapted from successful column experiments (Sun et al., 2016a; Sun et al., 2018). The experiments all went through the 3 periods, including a treatment as described below and in **Table 2.2**.

Pre-treatment: For the experimental system to equilibrate and stabilize under simulated groundwater flowing conditions. All 8 columns were fed with fresh groundwater solely as influent for approximately 40 PV (pore volumes).

Treatment: For manipulations with/without Fe(II)-nitrate and with/without ROC amendment. Columns GW+Fe+NO_3 a, GW+Fe+NO_3 b, GW+Fe+NO_3+ace, GW+Fe+NO_3+lac were treated with 5 mmol/L $FeCl_2$ and 5mmol/L $NaNO_3$ simultaneously in influent during a reaction period of 10 days and for approximately 27 PV. Additionally, influent for GW+Fe+NO_3+ace were amended with 1 mmol/L sodium acetate, while for GW+Fe+NO_3+lac, with 1 mmol/L sodium lactate, during the treatment. Meanwhile, columns GW a, GW b, GW+ace, GW+lac were blank treated without the chemicals in influent, for the same period of 10 days. During the

treatment, influent for GW+ace and GW+lac were amended with 1 mmol/L sodium acetate and 1 mmol/L sodium lactate, respectively.

Table 2.2 Field-based column experiments

Experiment	Treatment
GW+Fe+NO_3 a	5 mmol/L $FeCl_2$+$NaNO_3$
GW+Fe+NO_3 b	
GW+Fe+NO_3+ace	5 mmol/L $FeCl_2$+$NaNO_3$ 1 mmol/L acetate
GW+Fe+NO_3+lac	5 mmol/L $FeCl_2$+$NaNO_3$ 1 mmol/L lactate
GW a	blank
GW b	
GW+ace	blank 1 mmol/L acetate
GW+lac	blank 1 mmol/L lactate

The experiments all went through the following periods: **Pre-treatment**: 2.6 PV/day for 40 PV, equilibrium of experiments system with fresh groundwater. **Treatment**: 27 PV at 2.6 PV/day for 27 PV, iron and nitrate treatment by simultaneous injection of $FeCl_2$ and $NaNO_3$, or blank treatment without the chemicals, with and without ROC augmentation. **Post-treatment**: 2.6 PV/day for 25 PV, flushing; 5.4 PV/day for 230 PV, long-term observation.

Post-treatment: For observation of results from different manipulations. After the treatment finished, influent for all columns were set back to fresh groundwater, then after a period of approximately 25 PV, the flow rate were increased from approximately 2.6 PV/day to 5.4 PV/day, and continued until the end of the experiment.

2.2.3 Sample collection and analysis

During the experiment, samples of influent groundwater and effluents from the column outlets were collected regularly. Monitoring of pH, ORP, EC, TDS, salinity, as well as titration for alkalinity, and spectrophotometric analyses of Fe(II), NO_3^-, NO_2^-, ammonia, and sulfide, were performed regularly on site. Groundwater samples were filtered (0.45 μm, PES membrane, ANPEL) and stored at 4 ℃ for major ion analysis, filtered (0.45 μm, PES membrane, ANPEL) and acidified with 1% HNO_3 (GR, CNW

technologies) for trace element analysis, filtered (0.45 μm, PES membrane, ANPEL) and preserved with 20 mmol/L EDTA for arsenic species analysis. Trace elements, major ions, DOC, and arsenic species were then analyzed in laboratory. Sediment samples before and after the experiment were extracted with 1 mol/L HCl and 1 mol/L sodium phosphate immediately after collection. Sediments and groundwater filters were frozen under -80℃ before DNA extraction. Analytical methods are detailed in *2.4 Aqueous sample analysis* and *2.5 Solid sample analysis*.

2.3 Laboratory based column experiments

This experimental design is for the study presented in *Chapter 5*. Sediment used in this experiment is from the YCA core at the depth of 23.5 metre.

2.3.1 Materials

Artificial groundwater (AGW) used in the experiment was prepared as shown in **Table 2.3**.

Table 2.3 Artificial groundwater composition

Components	Molar concentration	Mass concentration
NH_4Cl	0.02 mmol/L	1.1 mg/L
KCl	1.00 mmol/L	74.6 mg/L
$CaCl_2$	0.40 mmol/L	44.4 mg/L
$MgSO_4$	0.40 mmol/L	48.1 mg/L
P (as Na_2HPO_4)	0.01 mmol/L	310 μg/L
As (as $NaAsO_2$)	3.00 μmol/L	225 μg/L
$C_3H_5O_3Na$	1.00 mmol/L	112 mg/L
Fe (as $FeSO_4$ in Fe-AGW)	10.0 mmol/L	560 mg/L
$NaNO_3$ (in Nitrate-AGW)	10.0 mmol/L	0.85 g/L

Fresh Fe(II)-containing AGW (Fe-AGW) solution was prepared by dissolving 1.39 g $FeSO_4 \cdot 7H_2O$ in 0.5 L AGW that was previously bubbled with nitrogen gas for 24 hours. Fe(II) concentration was 10 mmol/L (560 mg/L) in the influent solution. Nitrate-containing AGW (Nitrate-AGW) was prepared by dissolving 0.43 g $NaNO_3$ in 0.5 L AGW that was previously bubbled with nitrogen gas for 24 hours. Nitrate concentration was 10 mmol/L in the influent solution. AGW was bubbled with nitrogen gas for 24 hours before use.

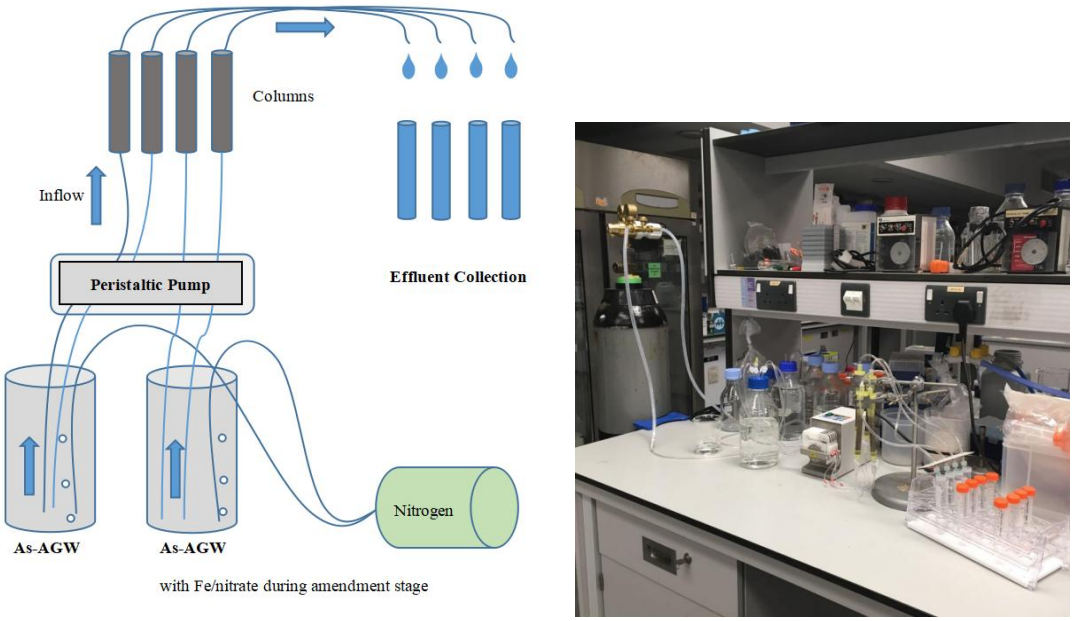

Figure 2.5 Laboratory column experiment set-up: The columns (BIO-RAD Econo-column 7371012) were 10 cm long glass tubes, with an inner diameter of 1 cm. The rest of the experimental system consisted of: PYREX bottles containing AGW, Fe(II)-AGW, and Nitrate-AGW, separately and continuously bubbled with nitrogen gas; high-precision tubing (X12 SC0049T 3-Stop LMT55, 0.19 mm ID) through peristaltic pump (ISM834C, Ismatec) to pump the solutions into the columns at a stable flow rate; iron stand to hold columns perpendicular to the bench board; effluent collector to collect effluents samples; apparatuses and tubing that connected things above. Tubing were replaced regularly in case of clogging by precipitation.

2.3.2 Experimental design

A total of 5 laboratory column experiments (**Table 2.4)**, were conducted, including 4 packed with fresh sediments, while an abiotic control column was packed with autoclaved sediments (**Figure 2.5**). Two columns, AGW+Fe+NO_3 a and b, were treated with Fe(II) and nitrate during the experiment, while fed with arsenic-containing artificial groundwater during the rest of the experiment period. Three additional columns, AGW a and b, and an abiotic control column Abio, were run in parallel with the 2 AGW+Fe+NO_3 columns in terms of flow rates and duration, but fed with only As-AGW during the whole experiment without any treatment.

Table 2.4 Laboratory-based column experiments

Experiment	Treatment
AGW+Fe+NO_3 a and b	10 mmol/L $NaNO_3$/$FeSO_4$
AGW a and b	non
Abio	non

In order to mimic the *in situ* remediation process (Sun, 2021), the column experiments went through 3 periods: **Pre-treatment**: 8 PV/day (1.0 mL/hour) for 6 days, then 4 PV/day for 6 days; AGW containing 3 μmol/L arsenite, 10 μmol/L phosphate and 1 mmol/L lactate. **Treatment**: 4 PV/day for 1 day, then 8 PV/day for 9 days; 10 alternative injection cycles (24 hours) of Fe-AGW (11:00-21:00) and Nitrate-AGW (21:00-11:00) for the AGW+Fe+NO_3 experiments, while the AGW experiments were continuously fed with only AGW without any treatment. **Post-treatment**: 8 PV/day for 58 days; AGW only.

2.3.3 Sample collection and analysis

During the experiment, effluents were collected with 15 mL centrifuge tubes. The pH of the most recently collected effluent sample was measured after the completion of collection of the sample. An arsenic test kit (ITS 481396 Water Quality Test Kit, Arsenic, Standard Range, 100/Pk) was applied daily during the post-treatment observation, to monitor arsenic concentration breakthrough. All effluents samples were acidified with 2% HCl (V/V), and further analyzed on an ICP-AES (Agilent Vista Pro) for element concentrations with limits of detection approximately 1 μg/L. Analytical methods are detailed in *2.4 Aqueous sample analysis* and *2.5 Solid sample analysis*.

2.4 Aqueous sample analysis

2.4.1 Field parameters

Groundwater, after being extracted from the anoxic subsurface, is typically transported to oxic environments with significantly different conditions. During sampling, storage and transportation, the parameters of the groundwater, including

temperature, dissolved oxygen, redox potential, and unstable chemical species, may undergo rapid transformations due exposure to air, light, and various other factors. This is particularly relevant in the context of the present study, which focuses on anoxic groundwater. Field investigations and experiments often occur at remote locations distant from the laboratory. Given the instability of certain parameters, it is imperative to conduct sample analyses on-site and in a timely manner.

Common parameters probed in the field during sampling include pH, redox potential (ORP), electrical conductivity (EC), salinity and dissolved oxygen (DO). Groundwater samples are measured on-site under overflowing conditions until the fluctuating readings reach stable, using multi-parameter devices (Thermo Orion 520M-01A, Hach Pocket Pro and Pro+ Testers) with calibrated probes. Effluents of column experiments, for its scarcity, were usually collected within a few hours and measured immediately after the collection completed. Effluent temperature, ORP and DO had changed dramatically during the collection period, therefore no longer representative of the actual conditions.

Further described in the following sections are concerning other common parameters, such as alkalinity, that require procedures more than just testing with ready-to-use probes and devices, as well as a couple of water constituents including nitrate, nitrite, arsenic, sulfide, ferrous and ferric iron that were analyzed on-site, using spectrophotometric or colorimetric methods. Some parameters and chemical compositions are stable for a certain long period of time if preserved well with appropriate methods, were analyzed in the laboratory.

2.4.2 Groundwater alkalinity

Alkalinity is a basic variable determining groundwater geochemistry. It measures the strength of a solution to resist acidification, usually calculated as the total concentration of dissolved bicarbonate and carbonate. Bicarbonate and carbonate can buffer groundwater against pH fluctuation, which is vital for the stabilization of groundwater system. In this study, alkalinity of groundwater and effluent samples was

determined by titration with standard 1 mol/L HCl solution (ANPEL Laboratory Technology, Shanghai) and a pH probe connected with a multi-parameter device (Thermo Orion 520M-01A), following the classic method of Gran titration (Gran, 1952; Stumm and Morgan, 1996). The samples for alkalinity determination were filtered immediately after collection and titrated within 12 hours.

The volume of acid addition is plotted against F, which is calculated by the Gran function as

$$F = (V_{\mathrm{HCl}} + V_0) \cdot 10^{-pH},$$

where V_{HCl}=acid addition volume and V_0=sample volume. By plotting F against V_{HCl}, the equivalence point was then determined at the turning point of the curve, indicating all HCO_3^- were converted to H_2CO_3, and the molar concentration of HCO_3^- is then calculated using the HCl molar concentration m_{HCl}, V_{HCl} and V_0 as

$$m_{HCO_3^-} = \frac{m_{HCl} \cdot V_{HCl}}{V_0}.$$

The carbonic acid is present primarily (99%) as HCO_3^- under a pH lower than 8.3, which is the case for all fresh groundwater and fresh effluent samples in this study. Alkalinity is then approximated as

$$Alk = m_{HCO_3^-} + 2m_{CO_3^{2-}} \approx m_{HCO_3^-}.$$

2.4.3 Spectrophotometry and colorimetry

During the field investigation and the field-based column experiments, a field spectrophotometer (HACH DR1900) and ready-to-use test kits are applied for the detection of unstable components in groundwater and effluent. Key species of sulfur, nitrogen and iron were analyzed, including:

Sulfide (Kit: HACH 2244500), using the USEPA approved Methylene Blue mothod (Hach Method 8131 protocol for the test kit), with a range of 5 - 800 μg/L S^{2-}. For 10

mL of sample, 0.5 mL Sulfide 1 reagent and 0.5 mL Sulfide 2 reagent were used, while a 10 mL Hach® test vial was applied. When the sample volume was scarce, for 2 mL of sample, 0.1 mL Sulfide 1 reagent and 0.1 mL Sulfide 2 reagent were used, while a Hach® Cuvette test tube was applied.

Nitrate Nitrogen (Kit: HACH 2605345), using Chromotropic Acid Test ’N Tube Method (Hach Method 10020), with a range of 0.2 - 30.0 mg/L NO_3-N. For each test, 1 mL of sample is required.

Nitrite Nitrogen (Kit: HACH 2608345-CN), using NitriVer® 3 Diazotization Test 'N Tube™ Method (Hach Method 10019), with a range of 0.002 - 0.500 mg/L NO_2-N. For each test, 1 mL of sample is required.

Ammonia (Kit: HACH 2604545), using the AmVer™ Salicylate Test 'N Tube™ Method (Hach Method 10023), with a range of 0.02 - 2.50 mg/L NH_3-N. For each test, 2 mL of sample is required.

Ferrous iron (Kit: HACH 103769), using the USEPA approved 1,10-phenanthroline method (Hach method 8146), with a range of 0.02 - 3.00 mg/L Fe^{2+}. For each test, 10 mL of sample is required.

Total soluble ferrous and ferric iron (Kit: HACH FERROVER 2105769), using the USEPA approved 1,10 phenanthroline method (Hach Method 8008), with a range of 0.02 to 3.00 mg/L Fe. For each test, 10 mL of sample is required.

For the above parameters, samples were collected and immediately filtered through 0.45 μm Polyethersulfone (PES) filters (ANPEL) to remove particles, preserved under 4 ℃, and analyzed without dilution within 6 hours.

Specifically, standard phenol red colorimetric method (Sollo et al., 1971; Stenger and Kolthoff, 2002) was applied for bromide detection in groundwater, with the standard curve shown below (**Figure 2.6**). The standard method requires 50 mL of sample. In the case of this study, effluent samples were scarce in volume while high in bromide concentration, hence to address these issues we revised the procedures by diluting 0.1

mL sample (containing at most 80 mg/L) 100 times with DIW to 10 mL (containing at most 0.80 mg/L Br). Standard solution was made with filtered source groundwater (no bromide detected in background) diluted with DIW to make the final solution for analysis all contain 1% of groundwater (the same dilution factor as the samples), hence eliminated the interference from background.

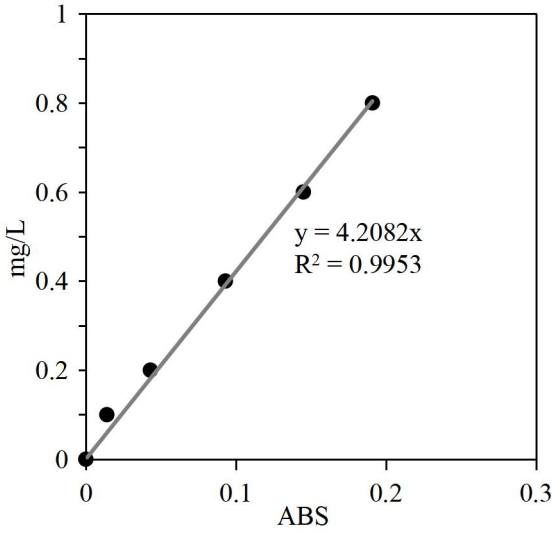

Figure 2.6 Standard curve for bromide detection: concentration versus absorbance (ABS): The standard curve (R^2 > 0.995) of bromide was prepared with analyzing standard solutions with 0.1 mg/L, 0.2 mg/L, 0.4 mg/L, 0.6 mg/L, and 0.8 mg/L Br, as well as a bromide-free blank. The absorbance was read at 590 nm and the detection limit was 0.1 mg/L.

2.4.4 Major ions and anions

To understand groundwater chemistry, groundwater and effluent samples were filtered (0.45 μm, PES membrane, ANPEL) and stored at 4 ℃ for major ion analysis. Analyses of major anions (F^-, Cl^-, Br^-, NO_2^-, NO_3^- and SO_4^{2-}) were performed on a Ion Chromatography (Dionex ICS, USA) with IonPac® AS15 Analytical/Capillary Column and AG15 Guard/Capillary Column, using KOH as eluent. Analysis of major ions (K^+, Na^+, Ca^{2+} and Mg^{2+}) were performed on an Ion Chromatography (Dionex ICS, USA) with IonPac® AS14 Analytical/Capillary Column and AG14 Guard/Capillary Column, using KOH as eluent. The detection limit of the IC for the anions and cations was 0.2 mg/L. Quality control samples were run once per 10-15

samples to ensure deviation from the standard curve lower than 5%.

2.4.5 Trace elements

To analyze arsenic and iron concentrations, groundwater and effluent samples were filtered (0.45 μm, PES membrane, ANPEL) and acidified with 1% HNO_3 (V/V) (GR, CNW technologies) for dissolved trace element analysis. Analyses of dissolved As, Fe, and Mn were performed on an ICP-MS (Thermo Fisher Scientific Element XR) using germanium (Ge) as internal standard. The detection limit for arsenic was 1 μg/L. Quality control standards were analyzed at least once per 15 samples. Standard reference materials NIST 1640a and NIST 1640f standards were repeatedly used during each measurement. The reference values of As concentration for 1640a and 1640f are 8.01 ± 0.067 μg/L and 60.45 μg/L, respectfully, while average measurement results are 8.58 μg/L and 58.94 μg/L, with relative standard deviations (RSDs) both lower than 4%.

2.4.6 Arsenic species: preservation and analysis

For inorganic arsenic species (arsenite and arsenate) analysis, groundwater and effluent samples were preserved by addition of EDTA stock (250 mmol/L), prepared by dissolving 46.53 g of EDTA ($C_{10}H_{14}N_2Na_2O_8 \cdot 2H_2O$, grade: for molecular biology, Sigma) in 500 mL ultra-pure water (18 MΩ), to a concentration of 20 mmol/L in filtered (0.45 μm, PES membrane, ANPEL) aqueous sample, and storage in dark at 4 ℃, with a lost of 0.4±1.6% (n=5) arsenite after 60 days based on our field tests on real groundwater samples from the same site and comparison with existing methods (Duan et al., 2024). Arsenic species were determined by an Ion Chromatography (IC) (Princen, Guangzhou, China) coupled with ICP-MS operated in KED mode, with As Spec anion exchange fast column and guard column (both 50 mm * 4.0 mm, PrinCen, Guangzhou, China), using gradient mobile phase A (0.23 mL HNO_3 and 1.8 mL ammonia to 500 mL with a pH around 10) and phase B (2.32 mL HNO3 and 4.6 mL ammonia to 500 mL with a pH around 9). The gradient protocol for mobile phases

was phase A for 85 s, then phase B for 120 s, followed by 125 s of phase A, at a flow rate of 1.2 mL/min.

2.4.7 Dissolved organic carbon (DOC)

For dissolved organic carbon analysis, groundwater and effluent samples were filtered (0.45 μm, Whatman) and collected in 22 ml brown vials (covered in aluminium foil and calcined under 500℃ for 5 hours to remove organic carbon residue), and acidified with phosphorus acid to 1% (V/V) in order to remove dissolved inorganic carbon. The samples were frozen before analysis. A TOC analyzer (Analytik Jena multi N/C 3100) was applied to measure DOC of filtered sample as TOC. The device was calibrated with newly diluted standards made with 1% (V/V) phosphorus acid solution and $CaCO_3$. For every 8 samples been run, we added a standard sample and a blank sample. The relative standard deviations are within 5%.

2.5 Solid sample analysis

2.5.1 Grain sizes

The grain sizes were classified and graded in a fining-downward sequence (**Table 2.5**), and plotted on the logarithmic scale.

Table 2.5 Grain size classification

Size (μm)	Classification
>2000	Pebbles & granule
1000-2000	Very coarse grained sand
600-1000	Coarse grained sand sand
200-600	Medium grained sand
125-200	Fine grained sand
62-125	Very fine grained sand
<62	Silt & clay

The particle sizes are expressed as diameter, traditionally classified according to the mesh sizes the particle could pass. The size ranges listed here are based on Brassington (1988).

The distribution of grain sizes were analyzed with a Malvern Mastersizer 3000,

capable of measuring particle size from 10 nm up to 3.5 mm. Grain sizes of sediment samples in this study all fell in the range of 20 nm to 2.0 mm. We treated 0.5 g of homogenized sediment as follows before analysis: (1) Remove organic matter with 40 mL 5% H_2O_2, water-bath at 85℃ for 1.5 hour, centrifuge at 4000 rpm for 10 min, and discard the supernatant, repeat with MilliQ water for 3 times to remove H_2O_2. (2) Remove carbonate by adding 40 mL 0.5 mol/L HCl and mix, water-bath at 85℃ for 1.5 hour. Centrifuge at 4000 rmp for 10 min and discard the supernatant, repeat with MilliQ water for 3 times to remove HCl. (3) Add 10 mL 0.5 mol/L sodium hexametaphosphate solution and ultrasonic-shake for 10 min.

2.5.2 Bulk chemistry

Bulk chemistry (element concentrations) of the sediment samples was determined by X-ray fluorescence spectroscopy (XRF) (S8 Tiger, Bruker). Samples were ground to powder and made into sample tablets (4 cm in diameter) with boric acid powder (to help coagulate sample powder particles) using a tablet press, before analysis with XRF instrument for bulk chemistry.

2.5.3 Environmental magnetism

Magnetic properties of initial and end-point sediments were measured to characterize the magnetic minerals in sediments. Low-frequency magnetic susceptibility (χ_{lf}) and high-frequency magnetic susceptibility (χ_{hf}) were obtained by firstly packing sediment samples (approximately 3.0 g) into 1 cm^3 non-magnetic plastic boxes, fixed with wool, then measured χ_{lf} and χ_{hf} with a 3-frequency Kappa-bridge (AGICO MFK1-FA) under 200 $A \cdot m^{-1}$ magnetic field, at low-frequency (976Hz) and high-frequency (15616 Hz), respectively. Anhysteretic remanent magnetization (ARM) was then obtained using an Alternating Field Demagnetizer (ASC Scientific D-2000) at 100 mT alternating field (AF) and 50 uT direct current (DC) field, and measured with a Spinner Magnetometer (AGICO JR-6A). Saturated isothermal remanent magnetization under room temperature (SIRM) were first measured as Isothermal remanent magnetization (IRM)

obtained at 1 T magnetic field. IRM imparted at -100 mT (IRM_{-100mT}) and at -300 mT (IRM_{-300mT}) were obtained by an Impulse Magnetizer (ASC Scientific IM-10-30).

To study magnetic hysteresis properties, first-order reversal curve (FORC) distributions were measured using a Lakeshore vibrating sample magnetometer (VSM 8604) at the Southern University of Science and Technology (SUSTech) Centre for Marine Magnetism (CM^2). Sediment samples are at first saturated in a positive magnetic field, and gradually decrease the field to a reversal field (H_a), then a partial hysteresis curve is measured as the applied field (H_b) increases from H_a back to saturation (Smirnov, 2006). FORCs data were obtained by repeating measurement of partial hysteresis curves (FORCs) for different values of reversal field, and processed using the FORCinel package with the variFORC protocol (Egli, 2013). Magnetically separated particles from sediments were characterized with a Desktop SEM (PHENOM XL) at the Heritage Lab, SUSTech.

For further analysis, megnetic particles were separated from sediments. Approximately 200 mg of sediment sample were first suspended in DIW with sodium hexametaphosphate as dispersant, and treated for 30 min with ultra-sonic to remove magnetic particles from the non-magnetic particles. Magnetic particles were then isolated with a bar magnet from the suspension, and repeatedly treated following the procedure. The final solution with suspended magnetic particles was cleaned with DIW before scanning.

2.5.4 Chemical extraction for acidic volatile sulfide (AVS) and somultaneously extracted metals (SEMs)

Sulfide in reducing sediments controls a large portion of metal concentrations in pore water. AVS represents a fraction of amorphous sulfide minerals, including FeS, in sediments. In this study we applied the HCl (2 mol/L) extraction method for AVS and SEMs (simultaneously extracted metals with AVS), and a colorimetric method for the analysis of sulfide concentration (Allen et al., 1993). SEMs concentrations were analyzed using ICP-MS. The limit of detection of AVS was approximately 0.01 μmol

per gram dry sediment, while recovery was normally above 90%. Extraction of AVS from sediments in frozen storage for as long as five months were detected as approximately 90% of initial level.

2.5.5 Chemical extraction for reactive iron and exchangeable arsenic

The HCl acid extraction aims to leach arsenic, manganese and especially reactive Fe(II)/Fe(III) associated with carbonates, oxides, amorphous and relatively labile crystalline oxyhydroxides. Reactive Fe(II) in minerals such as siderite, green rust, and lepidocrocite, has been found more reactive for NDFO than dissolved Fe(II) (Grabb et al., 2017; Liu et al., 2019; Rakshit et al., 2008; Sørensen and Thorling, 1991), characterization of the reactive phase of iron species in sediments are important in this study. The phosphate extraction aims for the exchangeable, strongly adsorbed arsenic fraction that is available for mobilization, through anion exchange of phosphate for arsenate and arsenite (Keon et al., 2001; Sun et al., 2021; van Geen et al., 2008).

Aliquot of 0.5 to 1 g of sediments was (a) extracted with 10 mL of 1 mol/L HCl (bubbled with nitrogen gas for over 10 hours) in 15-mL centrifuge tubes, (b) leached with 1 mol/L NaH_2PO_3 with 0.1 mol/L L-ascorbic acid (added NaOH pellets to reach a pH of 5, and bubbled with nitrogen gas for over 10 hours) in brown glass serum bottles (Jung and Zheng, 2006; Sun et al., 2021). The bottles of phosphate extraction were sealed and crimped before shaken for 24 hours, then extracted solutions were sampled with syringes. Both extracted solutions were filtered through 0.22 μm filters (ANPEL) before analysis with ICP-MS and LC-AFS for Fe, Mn, and As. Analytical results were expressed on a dry sediment basis. In parallel with the extraction, aliquot of 1 to 2 g of sediments was weighed, dried, and weighed again, in order to obtain the dry to wet ratio and calculate the dry weight of sediments for extraction. Chemical extractions of natural sediments were performed on site right after the sediment cores were sampled. After the column experiments, sediments were immediately taken out of the columns. The inlet and out let sediments were sampled and extracted separately, while the rest of the sediments were homogenized and extracted. These were all

performed in a glove bag filled with nitrogen gas, in order to minimize unwanted oxidation.

2.5.6 Total organic carbon (TOC)

Sediment TOC was analyzed using TOC HT1300 Module of multi N/C 3100. We used 0, 5, 10, 20 and 50 mg $CaCO_3$ as standards for calibration. Before analysis, the freeze-dried sediment samples were freeze-dried and grind to pass a 0.15 mm sieve, then removed of carbonate with 0.5 mol/L HCl and washed with MiliQ water, and freeze-dried again. For each test, 100 mg of treated sediment sample was used.

2.5.7 DNA extraction and 16s rRNA sequencing

Sediment samples were preserved at -80℃ before DNA extraction. DNA was extracted from 0.5 g of each sediment sample, using the MP FastDNA Spin Kit (MP Biomedicals LLC, Solon, USA) following the manufacturer's instructions. The extracted DNA samples were then amplified through polymerase chain reaction (PCR). Primer set PRK341F (5'-CCTAYGGGRBGCASCAG-3') and PRK806R (5'-GGACTACNNGGGTATCTAAT-3') were applied in order to amplify the V3-V4 hypervariable region (Yu et al., 2005). The PCR products were purified and subjected to 300 bp paired-end sequencing on a DNBSEQ-G400 platform at BGI (Shenzhen, China). Quality control, trimming, merging of paired ends, and error correction were performed in DADA2, which outputs the abundance of error-corrected amplicon sequence variants (ASVs) (Callahan et al., 2016). For taxonomic assignment of 16S rRNA genes, ASVs were compared with the SILVA SSU database v132 (Quast et al., 2012). Further analysis was carried out in R package phyloseq and ampvis2. The highest number of reads were 51,235 for initial sediment, while 39087, 38340, 36268, and 39123 for end-point sediments of experiments GW+Fe+NO3 a, GW+Fe+NO3 b, GW+Fe+NO3+ace, GW+Fe+NO3+lac, and 44828, 43716, 40276, and 42816 for end-point sediments of experiments GW a, GW b, GW+ace, GW+lac, respectively.

Chapter 3 Immobilizing arsenic by iron and nitrate treatment: divergence driven by reactive organic carbon

To investigate how ROC augmentation impact iron and sulfur cycling in carbon-poor anoxic groundwater systems, and its potential in improving the application of iron and nitrate treatment, this research chapter presents a study of 4 field-based column experiments on treatment with iron and nitrate, fed with freshly pumped natural groundwater, with and without the ROC augmentation as acetate or lactate amendment during the treatment. As has been detailed in *2.2 Field based column experiments*, the 4 experiments are:

Table 3.1 Experimental

Experiment	Treatment
GW+Fe+NO_3 a	5 mmol/L $FeCl_2$+$NaNO_3$
GW+Fe+NO_3 b	
GW+Fe+NO_3+ace	5 mmol/L $FeCl_2$+$NaNO_3$ 1 mmol/L acetate
GW+Fe+NO_3+lac	5 mmol/L $FeCl_2$+$NaNO_3$ 1 mmol/L lactate

Pre-treatment: 2.6 PV/day for 40 PV, equilibrium of experiments system with fresh groundwater. **Treatment**: 27 PV at 2.6 PV/day for 27 PV, iron and nitrate treatment by simultaneous injection of $FeCl_2$ and $NaNO_3$, with and without ROC augmentation. **Post-treatment**: 2.6 PV/day for 25 PV, flushing; 5.4 PV/day for 230 PV, long-term observation.

Results are presented in 4 sections: groundwater chemistry, sediment characterization, environmental magnetism of sediments, and sediment microbial ecology. Fe(II)-nitrate treatment successfully immobilized arsenic and significantly increased strongly absorbed arsenic phases in end-point sediment. Sulfide precipitation was less with ROC augmentation and especially with lactate amendment. Microbial communities changed dramatically after experiment, with iron and sulfur metabolizing genera enriched in relative abundances.

3.1 Aqueous chemistry

3.1.1 Initial site groundwater chemistry

Groundwater GW-AMS3-2 and sediment S-AMS3-7 (used for the experiments) were sampled from the same site, at the same depth, and during the same drilling. GW-AMS3-2 had a slightly alkaline pH value of 7.87 and a reducing oxidation-reduction potential (ORP) of -300 mV (**Table 3.2**). The dissolved oxygen (DO) of the freshly-pumped groundwater was 0.76 mg/L, although slightly higher than the usually applied 0.5 mg/L threshold for anoxic groundwater (Jurgens et al., 2009), still considered anoxic in this study, since water pumped from shallow Bangladesh aquifers were also occasionally detected with oxygen (Zheng et al., 2004). Electric conductivity (EC) was 1.932 mS/cm, much higher than the typical threshold of 0.15 mS/cm for fresh groundwater.

The initial site groundwater had a salinity of 0.95 ppt. Major ions were mostly sodium (9.482 mmol/L), followed by 2.304 mmol/L magnesium, and 1.921 mmol/L calcium. Major anions in groundwater were mostly chloride (6.798 mmol/L), followed by 2.719 mmol/L sulfate, and 1.357 mmol/L nitrate. Alkalinity as dissolved bicarbonate is usually considered a byproduct of iron oxyhydroxide reduction, hence high dissolved arsenic were always accompanied by it (Nickson et al., 1998; Zheng et al., 2004). The initial site groundwater had relatively high (> 4 mmol/L HCO_3^-) alkalinity of 5.81 mmol/L as dissolved bicarbonate.

Notably, the initial site groundwater contained 0.094 mmol/L sulfide, 0.028 mmol/L ammonia, and relatively low dissolved organic carbon (DOC) of 2.2 mg/L. Dissolved arsenic concentration was 119 μg/L and mostly (87%) arsenite. Dissolved iron (120 ug/L) were high in GW-AMS3-2, including 42% as ferrous iron.

Table 3.2 Groundwater chemistry

Parameters	Unit	GW-AMS3-2	YCB-MLW5
pH	\	7.87	7.77
Alkalinity	mmol/L HCO_3^-	5.81	9.51
ORP	mV	-300	-107
EC	mS/cm	1.932	1.470
TDS	ppt	1.33	0.99
Salinity	ppt	0.95	0.71
DO	mg/L	0.76	0.6
DOC	mg/L	2.2	6.0
Fe^{2+}	μg/L	50	90
Fe	μg/L	120	500
Mn	μg/L	282	316
As^{3+}	μg/L	104	89
As	μg/L	119	109
Li^+	mmol/L	0.010	0.007
NH_4^+	mmol/L	0.028	0.322
K^+	mmol/L	0.169	0.041
Mg^{2+}	mmol/L	2.304	1.074
Ca^{2+}	mmol/L	1.921	1.799
Na^+	mmol/L	9.482	8.264
F^-	mmol/L	0.011	0.024
Cl^-	mmol/L	6.798	3.695
NO_2^-	mmol/L	0.006	0.001
NO_3^-	mmol/L	1.357	0.149
SO_4^{2-}	mmol/L	2.719	0.807
S^{2-}	mmol/L	0.094	0.094

Water chemistry parameters were compared between initial site groundwater **GW-AMS3-2**, and influent groundwater **YCB-MLW5**. GW-AMS3-2 was collected from site AMS3 during core drilling, at a depth of 9 m where sediment S-AMS3-7 used for the experiments was sampled. YCB-MLW5 used for the column experiment was sampled from a multi-level observation well of 39.5 m depth.

3.1.2 Influent groundwater chemistry

The influent groundwater (YCB-MLW5) for the experiments was similar with initial site groundwater in terms of certain chemical characteristics critical to this study, such as pH, DO, and As/As(III) concentrations, although a few other parameters are inevitably different (**Table 3.2**). It had a pH value of 7.77 and a reducing ORP of -107 mV. Its DO was 0.60 mg/L, slightly lower than GW-AMS3-2, and close to the 0.50

mg/L threshold for anoxic groundwater. Groundwater EC was 1.470 mS/cm, lower than initial site groundwater. The influent groundwater had a salinity of 0.71 ppt. Major ions were mostly sodium (8.264 mmol/L) as well, followed by 1.799 mmol/L calcium, and 1.034 mmol/L magnesium. Major anions in groundwater were mostly chloride (3.695 mmol/L), followed by 0.807 mmol/L sulfate, and 0.149 mmol/L nitrate. The influent groundwater had relatively high alkalinity of 9.51 mmol/L as dissolved bicarbonate. Notably, the influent groundwater contained 0.094 mmol/L sulfide, 0.322 mmol/L ammonia, and 6.0 mg/L of DOC. Dissolved arsenic concentration was 109±9 μg/L (n=26) and mostly (82%) arsenite (89±6 μg/L, n=4), similar with initial site groundwater. While dissolved iron were high (500 μg/L), ferrous iron only accounted for 18% of total dissolved iron.

3.1.3 Effluent EC, pH, and alkalinity

Effluent pH were only slightly higher than influent pH before the treatment and almost indifferent during post-treatment observation (**Figure 3.1**). During the treatment, effluent pH of all 4 experiments experienced drops, to nearly 7 for GW+Fe+NO_3 a, GW+Fe+NO_3 b and GW+Fe+NO_3+lac, and to below 6 for GW+Fe+NO_3+ace. The two experiments, GW+Fe+NO_3 a and GW+Fe+NO_3 b, are reported individually for they were packed separately and run with individual tube lines. Noted that the effluent and influent pH were measured in laboratory after a period of collection under similar conditions, thus all appeared to be higher than the more frequently monitored fresh groundwater pH (**Figure 3.2**). The average groundwater pH (8.22 ± 0.10, n=7) measured in laboratory was 0.46 higher than groundwater samples (7.77 ± 0.03, n=64) measured on site when freshly pumped out. Effluent EC were always lower than influent EC before and after the treatment, while much higher during the treatment, resulted from the addition of $FeCl_2$ and $NaNO_3$ in influent. Effluent alkalinity was much lower than influent groundwater alkalinity during the pre-treatment equilibrium (**Figure 3.1**). During the treatment, effluent alkalinity was significantly lower to around 3 mmol/L. After the treatment, effluent

alkalinity increased but continued to be lower than the influent level.

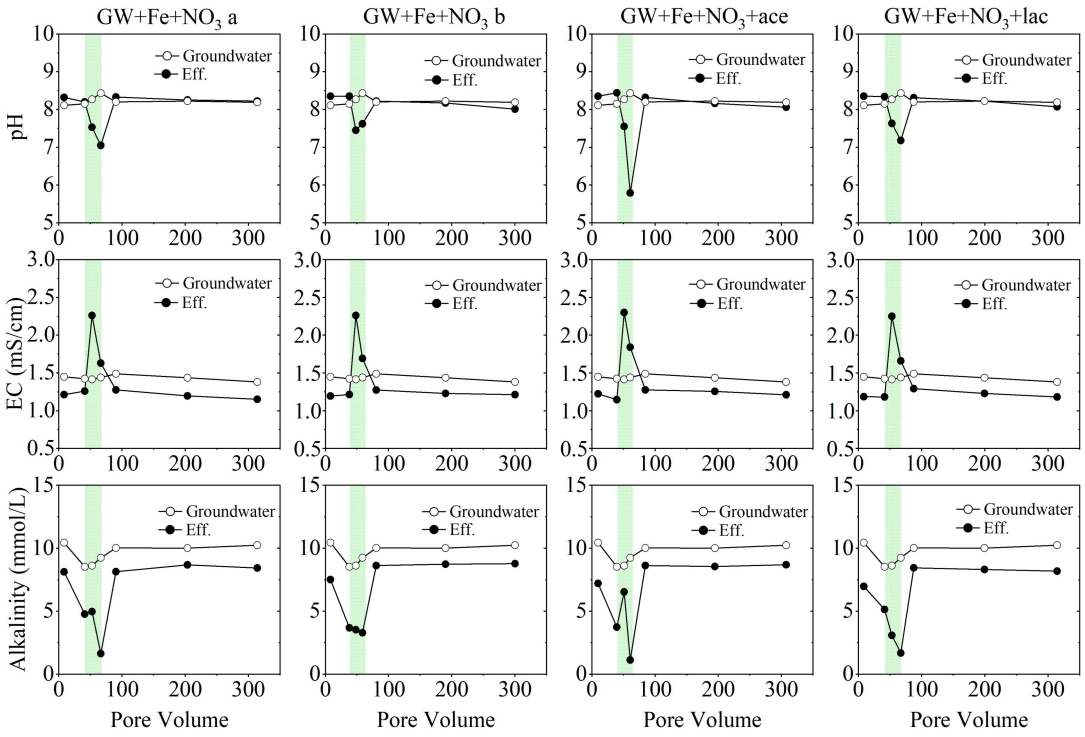

Figure 3.1 Effluent pH, EC, and alkalinity versus pore volume: Effluent data (**Eff.**, black dots) of the 4 column experiments are compared with groundwater data (black circles). The treatment period was emphasized with the green shade area, during which iron and nitrate treatment was performed for all 4 columns, while ROC (acetate or lactate) augmentation was performed for GW+Fe+NO_3+ace and GW+Fe+NO_3+lac, respectively. The groundwater and effluent samples were collected, preserved and measured the same, for data comparability.

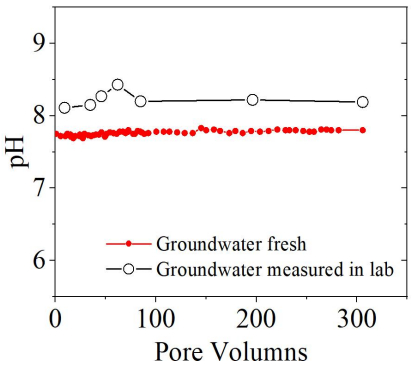

Figure 3.2 Groundwater pH versus pore volume: Groundwater pH (black circles) of samples collected by fraction collector and measured in lab (on site), following the same procedures as measuring effluent pH, are compared with groundwater pH (red dots) freshly probed during pumping.

3.1.4 Effluent fluoride, chloride and bromide

The groundwater samples (n=21) collected during the experiments contained negligible concentrations of fluoride (0.00±0.01 mmol/L) and bromide (0.00±0.00 mmol/L), but relatively high concentrations chloride (3.70±0.07 mmol/L) (**Figure 3.3**). The data are consistent with the groundwater chemistry previously reported (**Table 3.2**). The effluent data showed that fluoride concentrations increased during pre-treatment equilibrium and post-treatment observation, likely indicates dissolution and flushing of fluoride from the sediments by influent groundwater. However, during the treatment, effluent fluoride were much lower.

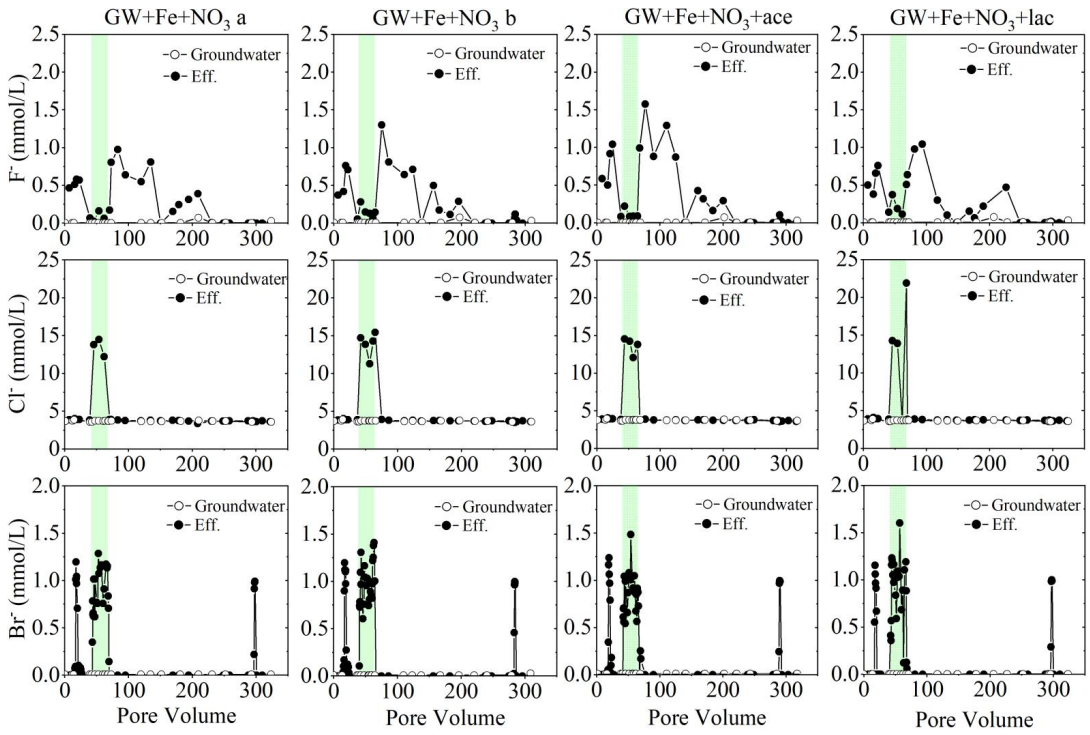

Figure 3.3 Effluent fluoride, chloride, and bromide versus pore volume: Effluent molar concentrations (**Eff.**, black dots) of the 4 column experiments are compared with groundwater concentrations (black circles). The treatment period was emphasized with the green shade area, during which iron and nitrate treatment was performed for all 4 columns, while ROC (acetate or lactate) augmentation was performed for GW+Fe+NO_3+ace and GW+Fe+NO_3+lac, respectively.

During the treatment, chloride and bromide were introduced through influent, their effluent concentrations, although fluctuated inevitably, are relatively stable around the theoretical influent concentrations, i.e. 1 mmol/L for bromide and 12.5 mmol/L for

chloride. The effluent bromide concentrations were 0.91±0.28 mmol/L (n=20), 0.97±0.29 mmol/L (n=25), 0.85±0.28 mmol/L (n=23), and 1.00±0.36 mmol/L (n=19) for experiments GW+Fe+NO_3 a, GW+Fe+NO_3 b, GW+Fe+NO_3+ace and GW+Fe+NO_3+lac, respectively, while their effluent chloride concentrations were 13.5±1.2 mmol/L (n=3), 13.9±1.6 mmol/L (n=5), 13.7±1.1 mmol/L (n=4), and 13.4±7.5 mmol/L (n=4). Although effluent chloride concentrations of GW+Fe+NO_3+lac fluctuated significantly for 2 data points, the more abundant bromide data supported our assumption that the mixing were relatively stable throughout the treatment period with inevitably fluctuations most likely due to infrequent tubing changing. Chloride and bromide, as conservative tracers in influent, were later used for calibrating influent concentrations during the mixing processes.

3.1.5 Effluent iron, nitrogen, arsenic and sulfate

The influent groundwater contained higher concentration (500 μg/L, or 8.95 μmol/L) of dissolved iron, mostly (82%) Fe^{3+}, than initial site groundwater (120 μg/L, or 2.15 μmol/L) (**Table 3.2**). During the experiment, influent iron concentrations fluctuated and gradually increased from around 10 to 20 μmol/L (**Figure 3.4**). Effluent iron concentrations (3.3±1.9 μmol/L, n=51) of the 4 experiments during pre-treatment equilibrium were much lower than influent iron concentrations (9.5±0.6 μmol/L, n=6). During the treatment, effluent iron concentrations were as low as 20 μmol/L at the beginning, then gradually increased towards but not exceeding influent level of 5000 μmol/L, then suddenly dropped to as low as 2.02 μmol/L after the stop of Fe(II)-nitrate feeding. During post-treatment observation, effluent iron concentrations gradually increased for columns GW+Fe+NO_3-a and -b but remained lower than influent level most of the time, although significantly higher effluent iron concentrations than influent level were observed for columns GW+Fe+NO_3+ace and GW+Fe+NO_3+lac between 200 to 300 PV.

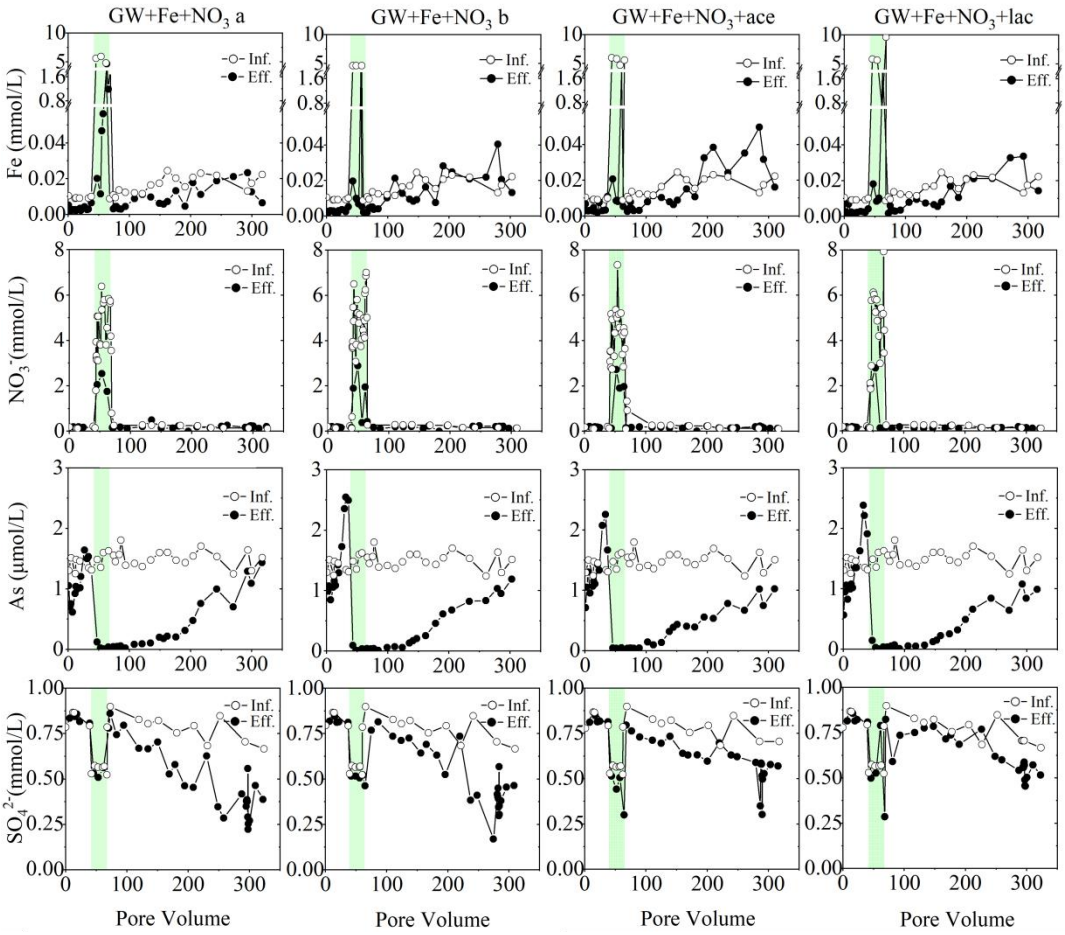

Figure 3.4 Effluent concentrations of iron (Fe), nitrate (NO_3^-), arsenic (As), and sulfate (SO_4^{2-}) versus pore volume: The effluent concentrations (**Eff.**) are expressed with black dots, while influent concentrations (**Inf.**) are expressed with black circles. The treatment period was emphasized with the green shade area, during which iron and nitrate treatment was performed for all 4 columns, while ROC (acetate or lactate) augmentation was performed for GW+Fe+NO_3+ace and GW+Fe+NO_3+lac, respectively. Influent concentrations were groundwater concentrations during pre-treatment equilibrium and post-treatment observation. During the treatment, influent concentrations were calibrated with measured tracers (chloride and bromide) data to represent the actual levels subject to inevitable fluctuations during mixing.

While influent groundwater nitrate concentrations were 0.183±0.056 mmol/L (n=21), before and after the treatment when additional nitrate was absent, effluent nitrate were 0.152±0.044 mmol/L (n=31) for GW+Fe+NO_3+ace, 0.143±0.029 mmol/L (n=30) for GW+Fe+NO_3+lac, 0.192±0.068 mmol/L (n=29) for GW+Fe+NO_3 a, and 0.189±0.058 mmol/L (n=29) for GW+Fe+NO_3 b (**Figure 3.4**). We analyzed nitrogen species during the treatment more frequently and promptly with spetrophotometer in the field. As the treatment began, effluent nitrate were at first similar to influent level (5 mmol/L

$NaNO_3$ treatment) for all 4 columns, then gradually decreased throughout the treatment to as low as 0.7 mmol/L (**Figure 3.5**). While effluent nitrite were negligible before and after the treatment, it quickly increased to around 0.6 mmol/L during the treatment for GW+Fe+NO_3 a and b, and to even higher for GW+Fe+NO_3+ace and GW+Fe+NO_3+lac, then gradually decreased along with effluent nitrate through the remaining period of the treatment. Effluent ammonia were 102, 97, 106 and 54 μmol/L for GW+Fe+NO_3 a, GW+Fe+NO_3 b, GW+Fe+NO_3+ace and GW+Fe+NO_3+lac at the start of the experiment, then gradually decreased to as low as 0.36 ± 0.41μmol/L (n=4) for all 4 experiments at around PV = 29. During the treatment, effluent ammonia of all 4 columns increased at first to as high as 29.3, 116, 89.2 and 11.4 μmol/L for GW+Fe+NO_3 a, GW+Fe+NO_3 b, GW+Fe+NO_3+ace and GW+Fe+NO_3+lac, then gradually decreased to around 10 μmol/L, and to even lower after the treatment.

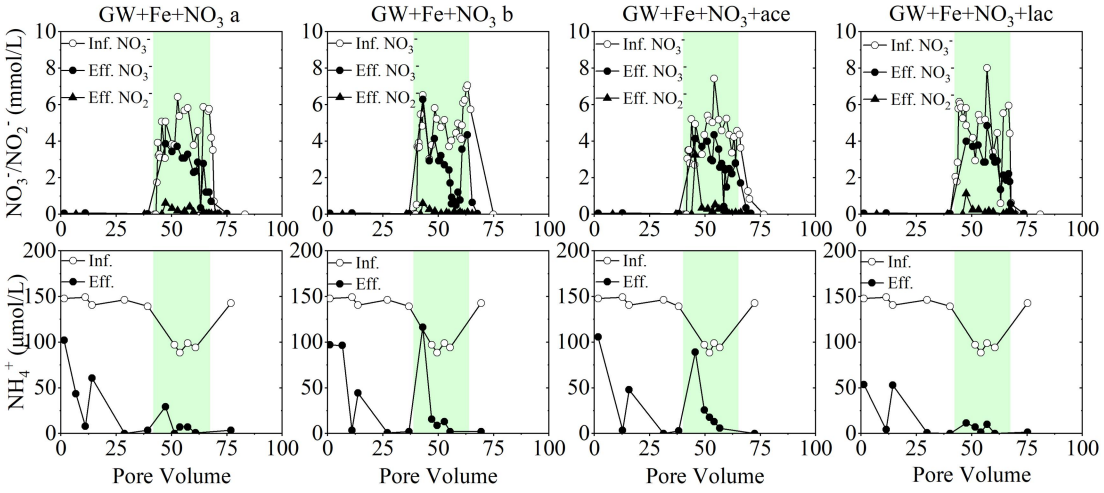

Figure 3.5 Effluent nitrate, nitrite and ammonia concentrations: Effluent nitrate (**Eff. NO_3^-**) and nitrite (**Eff. NO_2^-**) concentrations are compared with influent nitrate (**Inf. NO_3^-**) concentrations, while effluent ammonia (**Eff NH_4^+**) concentrations are compared with influent ammonia (**Inf NH_4^+**) concentrations. The treatment period was emphasized with the green shade area, during which iron and nitrate treatment was performed for all 4 columns, while ROC (acetate or lactate) augmentation was performed for GW+Fe+NO_3+ace and GW+Fe+NO_3+lac, respectively. Influent ammonia, as well as effluent ammonia, nitrate and nitrite, were analyzed on site using spectrophotometric methods. Influent concentrations were groundwater concentrations during pre-treatment equilibrium and post-treatment observation. During the treatment, influent concentrations were calibrated with measured tracers (chloride and bromide) data to represent the actual levels subject to inevitable fluctuations during mixing.

Effluent arsenic concentrations (**Figure 3.4**) were 1/2 to 2/3 the level of influent at the beginning of the experiment, but gradually recovered to influent level (approximately 1.5 μmol/L) before the treatment started. Effluent arsenic of column GW+Fe+NO_3 b increased to a level (2.5 μmol/L) much higher than the influent concentration. Columns GW+Fe+NO_3+ace and GW+Fe+NO_3+lac were observed with similar results. During the treatment, effluent concentrations of arsenic were reduced to lower than 10 μg/L, the WHO guideline level, for all 4 columns. Post experiment, effluent arsenic concentrations gradually recovered to close to influent level for all 4 columns at the end of the experiment, although the gaps between effluent and influent concentrations were slightly wider for the ROC-amended columns GW+Fe+NO_3+ace and GW+Fe+NO_3+lac.

Effluent sulfate concentrations (**Figure 3.4**) were stably the same level of influent sulfate from the start of the experiment until the treatment ended, for all 4 columns. Post treatment, however, effluent sulfate concentrations started to fall more significantly below the influent level. When the treatment was finished, the gaps between influent and effluent sulfate concentrations were narrow (< 0.1 mmol/L), they then gradually became wider throughout the remaining of the experiment, for GW+Fe+NO_3 a and b, to as wide as 0.50 mmol/L. Meanwhile, the gaps between influent and effluent sulfate concentrations for ROC-amended columns GW+Fe+NO_3+ace and GW+Fe+NO_3+lac remained relatively narrow (< 0.2 mmol/L), throughout the post-treatment observation.

3.2 Solid phase chemistry

As shown in **Figure 3.6**, the initial sediments were brown Holocene sands. By the end of the treatment, the sediments turned a little bit orange in GW+Fe+NO_3 a and b, while turned darker in ROC-amended GW+Fe+NO_3+ace and GW+Fe+NO_3+lac. By the end of the experiment, sediments in all Fe(II)-nitrate treated columns turned dark,

while in the ROC-amended columns GW+Fe+NO_3+ace and GW+Fe+NO_3+lac were less darker than in columns GW+Fe+NO_3 a and b, especially near the top (outlet) of the columns. This change in color likely indicates formation of sulfide minerals during the experiment and especially during the post-treatment period.

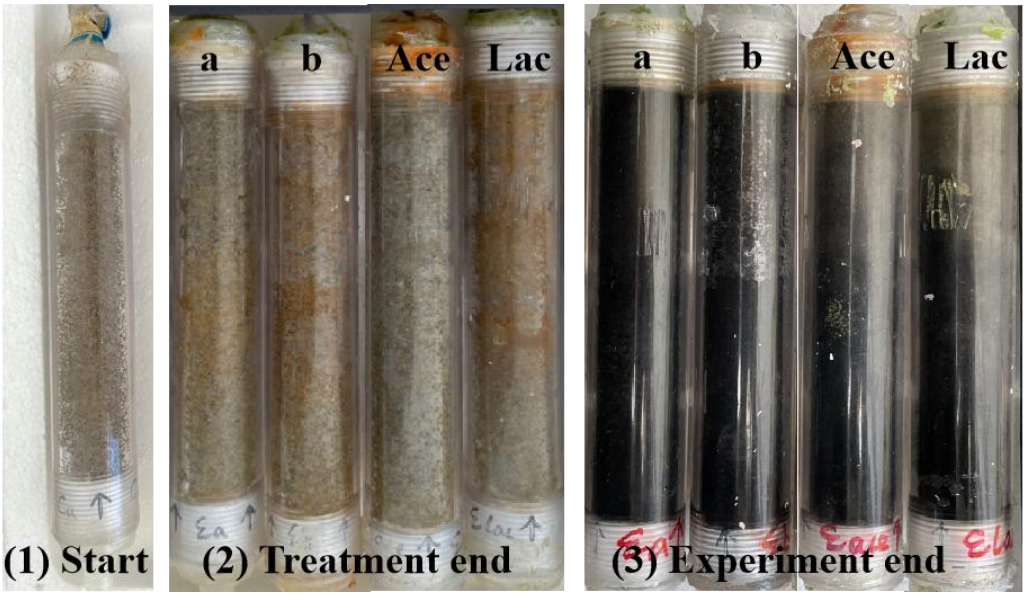

Figure 3.6 Columns at the (1) start, (2) treatment end, and (3) experiment end: Photos were taken for the columns at the (1) start of experiment, (2) end of the treatment, and (3) end of the experiment, of the 4 iron and nitrate treatment experiments GW+Fe+NO_3 a (**a**), GW+Fe+NO_3 b (**b**), GW+Fe+NO_3+ace (**Ace**) and GW+Fe+NO_3+lac (**Lac**). The photos were taken with the same device against a white board in the middle of the day for comparability.

3.2.1 Extractable arsenic and iron phases

The initial sediments contained 0.75 mg phosphate extractable arsenic per kilogram dry sediment. Phosphate extractable arsenic were higher than initial sediment in end-point sediments of columns GW+Fe+NO_3 a, GW+Fe+NO_3 b and GW+Fe+NO_3+lac, while lower for GW+Fe+NO_3+ace (**Table 3.3**). Phosphate extractable As^{5+} were 30% in initial sediments. After the experiment, Phosphate extractable As^{5+} mostly disappeared in sediments of columns GW+Fe+NO_3 a and GW+Fe+NO_3+ace, while remained 19% and 23% in sediments of columns GW+Fe+NO_3 b and GW+Fe+NO_3+lac. HCl extractable iron in initial sediments were 0.60 g/kg dry sediment, and mostly (0.52 g/kg) ferrous iron. These iron extracted

from amorphous to low-crystalline minerals more than doubled after the experiment, with the portion of Fe(III) almost all gone in sediments of columns GW+Fe+NO_3 a and GW+Fe+NO_3 b, while increased in sediments of ROC-amended columns GW+Fe+NO_3+ace and GW+Fe+NO_3+lac. While HCl extractable iron concentrations largely increased (by 0.79±0.23, n=4) in sediments of all 4 columns after the experiment, HCl extractable arsenic concentrations in end-point sediments varied among the columns: decreased in sediments of columns GW+Fe+NO_3 a and GW+Fe+NO_3+lac, while increased in sediments of columns GW+Fe+NO_3 b and GW+Fe+NO_3+ace, compared with initial sediment.

Table 3.3 Phosphate extractable arsenic and HCl extractable iron from sediment.

Parameters	Initial		GW+Fe+NO_3 a	GW+Fe+NO_3 b	GW+Fe+NO_3+ace	GW+Fe+NO_3+lac
P-ext As (mg/kg)	0.75	Outlet	0.40	0.53	0.70	0.50
		Middle	0.94	1.31	0.62	0.94
		Inlet	0.69	0.68	0.69	0.54
P-ext As(V) (mg/kg)	0.22	Outlet	0.00	0.20	0.14	0.00
		Middle	0.00	0.26	0.00	0.22
		Inlet	0.00	0.00	0.00	0.00
HCl-ext Fe (g/kg)	0.60	Outlet	1.15	1.02	0.75	0.88
		Middle	1.72	1.38	1.20	1.25
		Inlet	1.36	1.31	1.04	0.92
HCl-ext Fe(III) (g/kg)	0.08	Outlet	0.09	0.15	0.09	0.13
		Middle	0.00	0.00	0.16	0.13
		Inlet	0.05	0.04	0.03	0.00

Phosphate extractable total arsenic (**P-ext As**) and arsenate (**P-ext As^{5+}**), representing strongly-absorbed arsenic in sediments, as well as HCl extractable total iron (**HCl-ext Fe**) and ferric iron (**HCl-ext Fe^{3+}**), representing reactive iron from amorphous to low-crystalline iron minerals in sediments, are presented, for initial and end-point sediments of the 4 iron and nitrate treatment experiments. The end-point sediments analyzed including an aliquot each from the inlet and outlet of the column, and an aliquot from the rest of the sediments (middle) after mixed thoroughly. Chemical extractions were performed for approximately 0.5 g sediments with 1 mol/L HCl and 1 mol/L sodium phosphate (pH adjusted to 5), respectively.

3.2.2 Acidic volatile sulfide (AVS) and simultaneously extracted metal (SEM)

Although sulfide was detected in initial site groundwater, AVS in initial sediment was only 0.042 ± 0.01 μmol per gram dry sediment (n=2), with also low SEM-As (0.014 ± 0.001 μmol/g) and SEM-Fe (4.58 ± 0.760 μmol/g) (**Table 3.4**). AVS largely increased

in all end-point sediments (5.002, 1.708 and 1.613 μmol/g for GW+Fe+NO_3 a, GW+Fe+NO_3 b, and GW+Fe+NO_3+ace) except but column GW+Fe+NO_3+lac (0.031±0.42 μmol/g, n=2). SEM-As and SEM-Fe were the highest (96.53 μmol/g) in sediments of column GW+Fe+NO_3 a, followed by GW+Fe+NO_3+lac (61.9 ± 1.37 μmol/g, n=2) and GW+Fe+NO_3+ace (51.61 μmol/g), then column GW+Fe+NO_3 b (26.01 μmol/g).

Table 3.4 AVS, SEM-As, and SEM-Fe of initial and end-point sediments

Parameters	Unit	Initial (n=2)	GW+Fe+NO_3 a	GW+Fe+NO_3 b	GW+Fe+NO_3+ace	GW+Fe+NO_3+lac (n=2)
AVS	μmol/g	0.042±0.01	5.002	1.708	1.613	0.031±0.42
SEM-As	μmol/g	0.014±0.00	0.061	0.024	0.044	0.040±0.00
SEM-Fe	μmol/g	4.58±0.76	96.53	26.01	51.61	61.9±1.37

The concentrations of acidic volatile sulfides (**AVS**), simultaneously extracted arsenic (**SEM-As**) and iron (**SEM-Fe**) were all in terms of dry sediment weight. Initial and end-point sediment of GW+Fe+NO_3+lac were sampled and extracted twice.

3.2.3 Bulk chemistry

Table 3.5 Bulk chemistry of sediment: initial and after the experiment

Parameters	Unit	Initial	GW+Fe+NO_3 a	GW+Fe+NO_3 b	GW+Fe+NO_3+ace	GW+Fe+NO_3+lac
Al_2O_3	%	6.98	8.56	8.69	8.75	8.70
SiO_2	%	83.0	82.0	81.5	80.9	81.2
S	ppm	84	423	198	125	128
Fe_2O_3	%	2.02	2.02	2.07	2.06	2.06
Mn	ppm	345	266	271	266	256
As	ppm	10.6	8.20	8.20	7.50	9.20
As/Fe (molar)	10^{-4}	5.59	4.33	4.22	3.88	4.76
SiO_2/Al_2O_3 (molar)		20.2	16.3	16.0	15.7	15.9

The mass concentration units (% and ppm) are all in terms of dry sediment weight.

The SiO_2/Al_2O_3 ratio was 20.232 in initial sediment (**Table 3.5**), indicating that the sediment is mostly silica-based sand, consistent with grain size analysis of sample S-AMS3-7, as reported in *2.3.1 Materials*. The percentage of SiO_2 component slightly decreased in end-point sediment, while Al_2O_3 increased to a certain degree, resulting in the SiO_2/Al_2O_3 ratio of end-point sediments all lower than initial sediment. Bulk

arsenic were 8.2 ppm in end-point sediments of both GW+Fe+NO_3 a and b, while 7.5 ppm of column GW+Fe+NO_3+ace was the lowest, and 9.2 ppm of GW+Fe+NO_3+lac was the highest.

3.3 Environmental magnetism of sediment samples

3.3.1 Magnetic susceptibility

Low frequency magnetic susceptibility χ_{lf} were 30.75, 29.42, 26.34 and 29.89 (10-8 m3/kg) in end-point sediments of columns GW+Fe+NO_3 a, GW+Fe+NO_3 b, GW+Fe+NO_3+ace and GW+Fe+NO_3+lac, respectively, and all lower than 31.49 (10^{-8} m^3/kg) in initial sediment (**Table 3.6**). While χ_{lf} of GW+Fe+NO_3+ace was significantly lower than the others, χ_{lf} of GW+Fe+NO_3+lac was the highest and closest to initial sediment.

Table 3.6 Magnetic properties of initial and end-point sediment

Parameters	Unit	Initial	GW+Fe+NO_3 a	GW+Fe+NO_3 b	GW+Fe+NO_3+ace	GW+Fe+NO_3+lac
χ_{lf}	$10^{-8}m^3/kg$	31.49	30.75	29.42	26.34	29.89
χ_{hf}	$10^{-8}m^3/kg$	31.4	30.74	29.41	26.52	29.85
χ_{ARM}	$10^{-5}m^3/kg$	30.22	29.61	31.55	29.97	31.94
$SIRM_{-1T}$	Am^2/kg	2.44	2.28	2.29	2.18	2.32
IRM_{-100mT}	Am^2/kg	1.4	1.35	1.39	1.27	1.35
IRM_{-300mT}	Am^2/kg	1.95	1.82	1.86	1.74	1.87
S-ratio		79.70%	79.80%	80.90%	79.80%	80.70%
HIRM	Am^2/kg	2.2	2.05	2.08	1.96	2.1
SIRM/χ	10^3 $A \cdot m^{-1}$	7.75	7.41	7.78	8.28	7.76

Magnetic properties of initial and end-point sediments include: low frequency magnetic susceptibility (**χ_{lf}**) under 200 $A \cdot m^{-1}$ magnetic field and at low-frequency (976Hz), high frequency magnetic susceptibility (**χ_{lf}**) under 200 $A \cdot m^{-1}$ magnetic field at and high-frequency (15616 Hz), Anhysteretic remanent magnetization (**χ_{ARM}**) at 100 mT alternating field (AF) and 50 μT direct current (DC) field, Saturated isothermal remanent magnetization at 1 T under room temperature (**$SIRM_{-1T}$**), isothermal remanent magnetization (IRM) imparted at -100 mT (**IRM_{-100mT}**) and at -300 mT (**IRM_{-300mT}**), **S-ratio** (IRM_{-300mT}/SIRM), hard isothermal remanent magnetization (**HIRM**), and **SIRM/χ** ratio.

The frequency-dependent susceptibility $\chi_{fd} = (\chi_{lf} - \chi_{hf}) / \chi_{lf}$ represents magnetic particles near the SP/stable SD boundary that can change from SP to stable SD state

when increasing observation frequency from low to high. The χ_{fd} results were all lower than 2% (in fact close to zero), indicating no or only very small super-paramagnetic (SP) particles exist in initial and end-point sediment. The results are consistent with the study on YCA and YCB sites, where χ_{fd} were also close to zero for all depths of sediment samples been tested (Sun, 2021).

IRM_{-300mT} represents the remanent magnetization after saturated in a high magnetic field and then a back-field of -300 mT to reverse the magnetite/maghemite contributed SIRM. Hard isothermal remanent magnetization (HIRM) is calculated as $HIRM=0.5\cdot(SIRM+IRM_{-300mT})$ to isolate the magnetic signal of weakly magnetic antiferromagnetic minerals with high coercivity (such as hematite and goethite), from ferrimagnetic minerals (such as magnetite and maghemite) (Liu et al., 2012).

The S ratio (IRM_{-300mT}/SIRM, measures the relative abundance of high coercivity minerals (hematite/goethite) mixed with ferrimagnetic minerals (magnetite/maghmite). S ratios were 80.37±0.68% (n=4) for end-point sediments and 79.92% for initial sediments, indicating that hematite and goethite are relatively abundant in initial and end-point sediments.

The SIRM/χ ratio qualitatively identifies mineral compositions. The highest SIRM/χ ratio was 8.28 (10^3 $A\cdot m^{-1}$) for GW+Fe+NO_3+ace sediment, compared with 7.41, 7.78, 7.76 (10^3 $A\cdot m^{-1}$) for GW+Fe+NO_3 a, GW+Fe+NO_3 b, GW+Fe+NO_3+lac, and 7.75 (10^3 $A\cdot m^{-1}$) for initial sediment, indicating hematite and/or goethite minerals are more abundant in end-point sediment of GW+Fe+NO_3+ace than the rest.

3.3.2 Temperature dependence of magnetic property

Duing the heating (temperature increasing), he magnetic susceptibility (10^{-7} m^3/kg) increased significantly after the temperature exceeded 400°C and rapidly decreased when exceeding 560°C, and reached the lowest level at around 580°C, the curie temperature of magnetite, indicating that magnetite may be the dominant ferrimagnetic minerals in sediments (**Figure 3.7**). When heating was finished and

temperature decreased, the magnetic susceptibility reached its highest at around 440°C. While magnetic susceptibility slowly decreased as the temperature decreased to room temperature, it was still several times higher than during heating. The cooling (temperature decreasing) curve signals enhanced significantly, indicating the signals were mostly from magnetite minerals formed during heating > 580°C. The production of strongly magnetic particles may be a result of transformation from poorly crystalline nano-phase goethite (weakly magnetic) during heating.

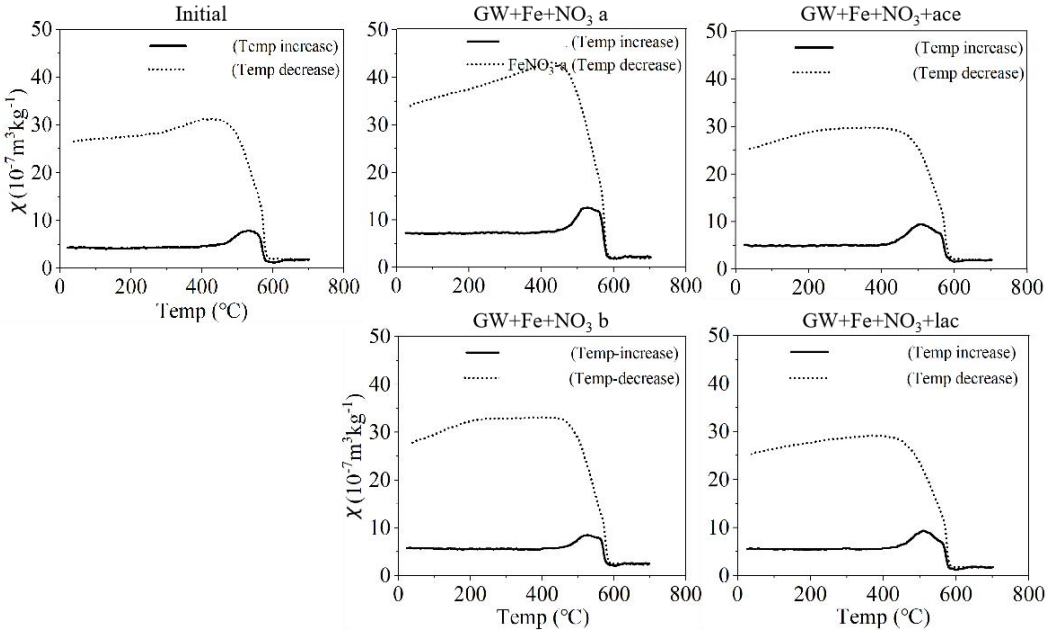

Figure 3.7 χ-T curves: temperature dependence of magnetic susceptibility: The χ-T curves consisted of a black solid line (**Temp increase**), recording the magnetic susceptibility of the sediment sample in response to increasing temperature from room temperature to 700°C, and a black dotted line (**Temp decrease**), recording the magnetic susceptibility of the sediment sample in response to decreasing temperature from 700°C to room temperature.

3.3.3 First order reversal curve (FORC) diagram

A FORC diagram is a coutour plot of the distribution of of a series of FORCs, which are measured after firstly saturating the sample in a large and positive magnetic field H_{sat}, then decreasing the field to a reversal field H_a, and as the magnetization curve while the field is increased back from H_a to H_{sat} in a series of regular field steps H_b (Acton et al., 2007; Pike et al., 2001a; Pike et al., 2001b). By plotting (B_C, B_U) as B_C

= (H_b - H_a)/2 and B_U = (H_b + H_a)/2, the FORC diagram can map the coercivity distributions of the magnetic grains in sample, and the interactions between the grains (Acton et al., 2007; Muxworthy and Dunlop, 2002; Pike et al., 1999; Roberts et al., 2000).

Figure 3.8 exhibits the FORC diagrams of initial sediment and the 4 end-point sediments to trace the variation in the magnetic domain state of samples. They are all triangular type-K FORC distributions (Acton et al., 2007) showing a continuum of interactions between grains of different coercivities. FORC distributions are all broad and characterized by concentric and elongated contour, suggesting that the magnetic particles in initial and end-point sediments all exhibit mixed vortex state to multi-domain (MD) type of behaviour. The contour plots of end-point sediments showed significant peaks at around B_C = 10 mT, comparing with initial sediment, suggesting the likely formation of smaller particles of magnetite during the experiment.

For all 5 diagrams, the contours intersecting the B_U axis with very low magnetic coercivity (B_C) represent super paramagnetic (SP) particles with high interactions, which are fine particles below a critical size with high thermal energy (Pike et al., 2001b). The closed contours with primary peaks between B_C = 10 mT and B_C = 20 mT represent single domain (SD) magnetite particles (Roberts et al., 2006). The interactions between grains significantly decrease between B_C = 20 mT and B_C = 40 mT, while contours extend to over B_C = 100 mT along the coercivity B_C axis shows much higher magnetic coercivity than SP particles and the compressing along the interaction B_U axis (negligible vertical spread from B_C = 40 mT) indicates very low magnetic interaction between particles, suggesting the likely presence of MD particles and goethite (Roberts et al., 2006).

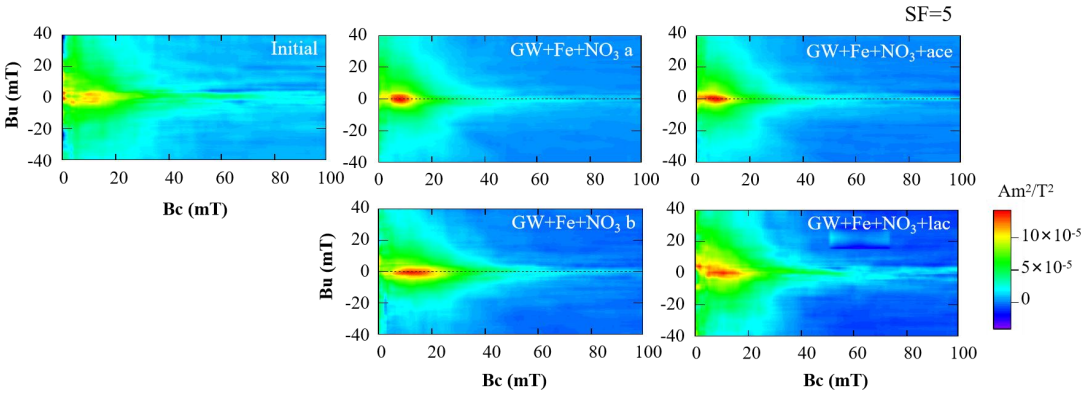

Figure 3.8 First-order reversal curve (FORC): before χ-T heating: The FORC diagrams of initial and end-point sediments, are plotted and represented in (B_C, B_U) coordinates, with B_C as the magnetic coercivity and B_U corresponds to the distribution of interaction fields, where the blue indicates negative regions that are a fundamental component of the magnetic response of SD particle systems (Newell, 2005).

Figure 3.9 exhibits the FORC diagrams of sediments after heating. Initial and end-point sediments experienced significant changes in magnetic properties after being heated to 700°C during the χ-T analysis, and became similar in FORC distributions, which suggest the likely transformation of goethite to SD particles of magnetite (B_C > 20 mT), while smaller particles with high magnetic interactions remained.

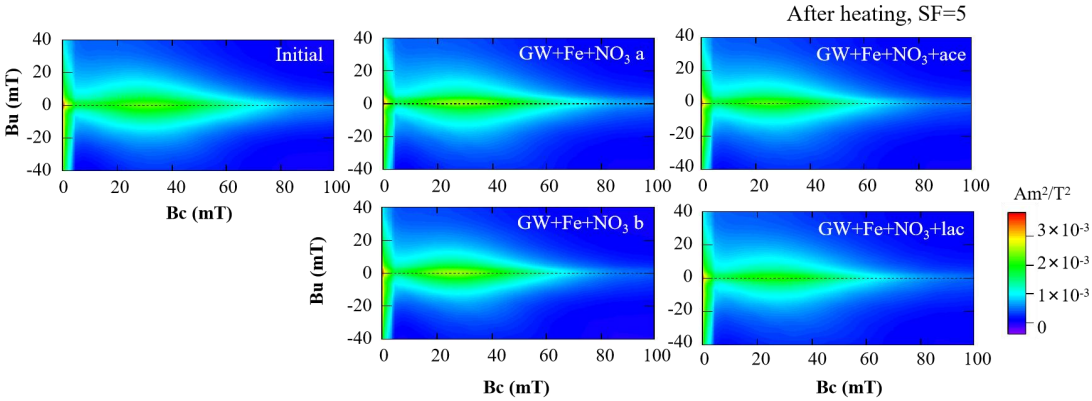

Figure 3.9 First-order reversal curve (FORC): after χ-T heating: The FORC diagrams of initial and end-point sediments after being heated from room temperature to 700°C as in *3.3.2*, are plotted and represented in (B_C, B_U) coordinates, with B_C as the magnetic coercivity and B_U corresponds to the distribution of interaction fields, where the blue indicates negative regions that are a fundamental component of the magnetic response of SD particle systems (Newell, 2005).

3.3.4 Scanning magnetic particles

We noticed there were magnetic particles in initial and end-point sediments (**Figure 3.10**), so we separated these particles and investigated their composition using SEM-EDS. Magnetically separated particles from initial sediment were relatively large grains (> 200 μm) with irregular shapes, consist of mostly O (48.70 to 54.62%, atomic concentration) and Si (16.63 to 25.57%), with 2.08 to 2.53 % Fe, likely SiO2 grains coated with iron minerals (**Figure 3.11a, b**). Smaller grains (< 20 μm) were found with mostly O (37.94%, atomic concentration), Si (18.54%), Fe (13.37%) and Mg (12.08%) (**Figure 3.11c**). Magnetically separated particles from GW+Fe+NO_3 a sediments were found with twisted aggregate of small particles and flakes ranging from nano to micro scales, consist of mostly Fe (54.4%) and O (27.12%) (**Figure 3.12a**), while some part also contain higher Fe (83.81%) (**Figure 3.12b**). Larger particles (>100 μm) were found with 48.36% Fe and 40.48% O (**Figure 3.12c**) while smaller flakes with 100% Fe detected (**Figure 3.12d**).

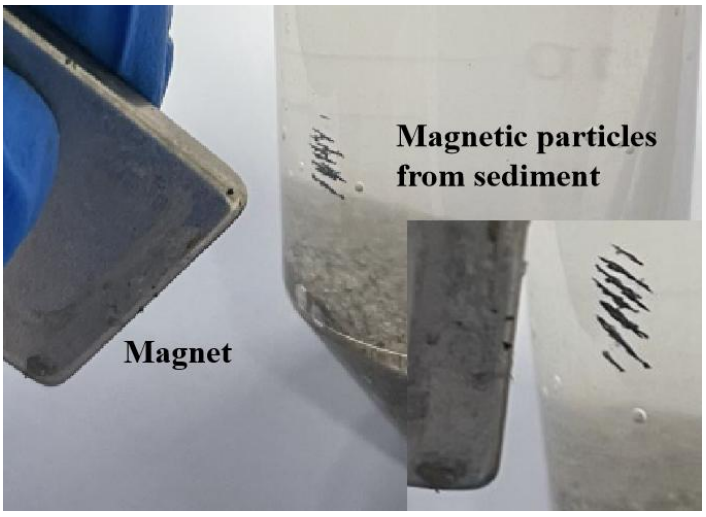

Figure 3.10 Magnetic particles from end-point sediments of column GW+Fe+NO_3 a: The magnetic particles were detected with a magnet and later isolated from sediments.

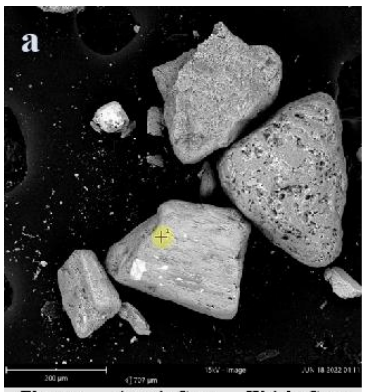

Element	Atomic Conc.	Weight Conc.
O	48.70	31.53
Si	25.57	29.05
Mg	15.59	15.33
Sr	2.25	7.96
Ca	4.60	7.45
Fe	2.08	4.70
Br	1.23	3.97

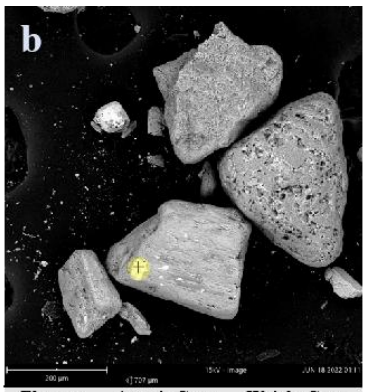

Element	Atomic Conc.	Weight Conc.
O	54.62	31.37
Ti	11.06	19.00
Ca	12.00	17.27
Si	16.03	16.16
Br	2.50	7.16
Fe	2.53	5.07
Sr	1.26	3.97

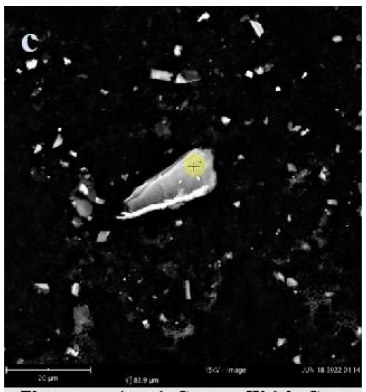

Element	Atomic Conc.	Weight Conc.
Fe	13.37	24.95
O	37.94	20.27
Si	18.54	17.39
Br	5.57	14.87
Mg	12.08	9.81
Sr	1.15	3.36
Ti	1.84	2.93
K	2.04	2.67
C	6.51	2.61
Cl	0.95	1.13

Figure 3.11 Magnetically separated particles from initial sediment: The figure shows 2 spots (**a** and **b**)on a large grain (< 250 μm) and a flake (**c**) (< 25 μm) of the separated magnetic particles, with black crosses in yellow circle indicating the point detected with SEM-EDS for element concentrations.

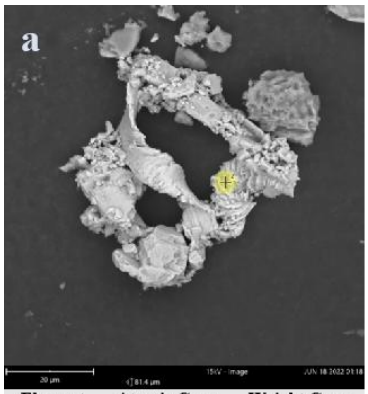

Element	Atomic Conc.	Weight Conc.
Fe	54.40	71.26
O	27.12	10.18
Ti	7.91	8.88
Cr	5.98	7.30
P	1.47	1.06
Si	1.17	0.77
C	1.95	0.55

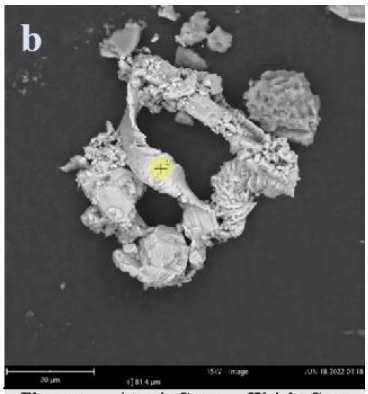

Element	Atomic Conc.	Weight Conc.
Fe	83.31	90.13
Cr	6.57	6.62
O	6.92	2.14
Si	1.17	0.64

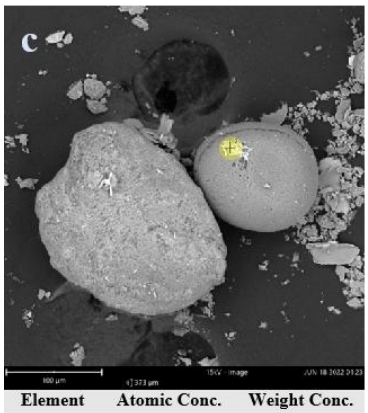

Element	Atomic Conc.	Weight Conc.
Fe	48.36	74.14
O	40.48	17.78
Al	3.92	2.90
Mg	3.89	2.59
Si	3.35	2.59

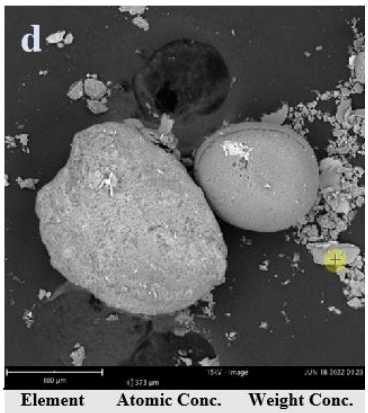

Element	Atomic Conc.	Weight Conc.
Fe	100.00	100.00

Figure 3.12 Magnetically separated particles from end-point sediment of GW+Fe+NO_3 a: The figure shows 2 spots (**a** and **b**) on twisted aggregate of nano- to micro-scale particles and flakes, a flake (**c**) on a large grain (~100 μm), and a flake (**d**) of the scattered, from the separated magnetic particles, with black crosses in yellow circle indicating the point detected with SEM-EDS for element concentrations.

3.4 Sediment microbial ecology

Analysis of the groundwater and sediments have shown evidence of iron oxidation, iron reduction and sulfate reduction, to ascertain if these processes are mediated by microorganisms, we further analyzed the microbial communities in sediments before and after the experiment. **Figure 3.13** presents the relative abundances of dominant

(relative abundances > 10%) microbes in initial and end-point sediments. The microbial communities in initial sediments were dominant by *Burkholderia* (39.3%), *Acinetobacter* (16.5%), and *Enterobacteriaceae* (10.82%). *Burkholderia* was also found prominent in aquifer sediments of high arsenic regions in India and Bangladesh (Das et al., 2017; Layton et al., 2014). It was demonstrated as playing key roles in microbial mineral weathering and arsenic mobilization (Mailloux et al., 2009). In addition, *Acinetobacter* was also found abundant (16.5%), which was reported to be commonly dominant in typical high arsenic sediments in Hetao Plain (Wang et al., 2014), and *Enterobacteriaceae* (10.82%) as well, which is known for arsenic-resistance in various arsenic-contaminated environments (Sultana et al., 2011; Turpeinen et al., 2004).

The genus *Burkholderia*, one of a predominant genus found in arsenic contaminated groundwater of the Ganges Brahmaputra Delta aquifer system (Das et al., 2017), were found with the highest relative abundance (>39%) in initial sediments (**Figure 3.13**). After the experiment, abundances of *Acetobacterium*, *Rhodopseudomonas*, *Azospira*, *Acidovorax* and *Dechloromonas* were found largely enriched in sediments of iron and nitrate treated columns, while relative abundance of *Burkholderia* was rendered negligible. The most abundant genera were similar among sediments of all four iron and nitrate treated columns, except that *Acidovorax* was not detected in sediments of lactate-amended column GW+Fe+NO_3+lac. Members of the *Rhodopseudomonas* were reported to be phototrophic Fe(II)-oxidizing bacteria, while also possess the capability to switch between four different types of metabolism: photoautotrophy, photoheterotrophy, chemoautotrophy, and chemoheterotrophy.

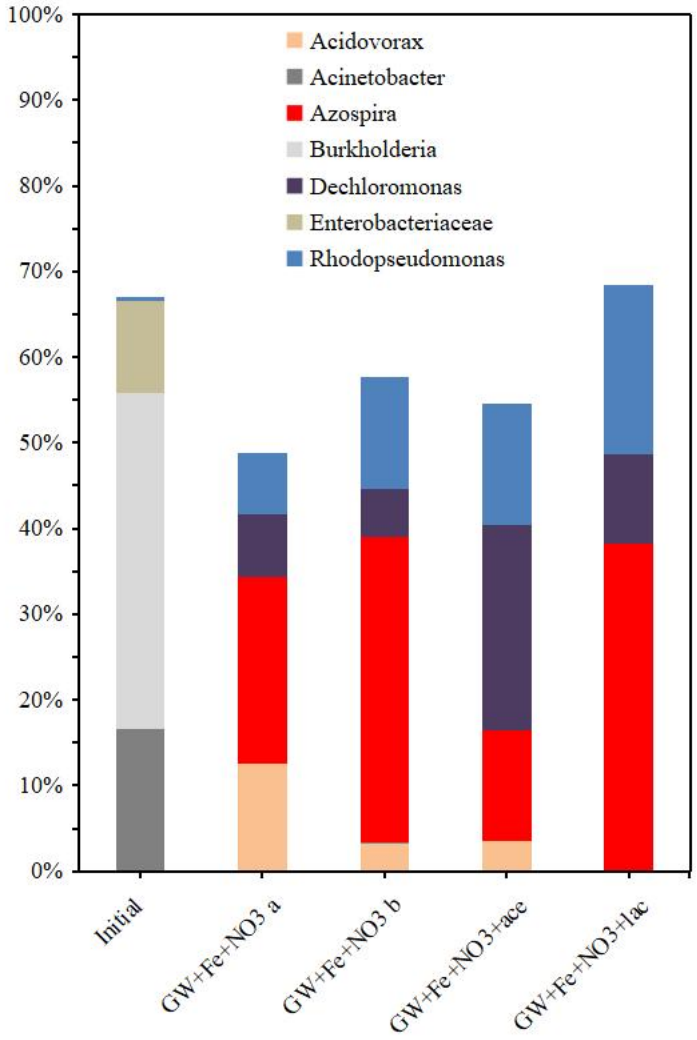

Figure 3.13 Dominant bacteria (relative abundances > 10%), at the genus level, in initial and end-point sediments: Panels from left to right show the initial and end-point sediments of the 4 experiments with iron and nitrate treatment, including GW+Fe+NO_3+ace with acetate augmentation and GW+Fe+NO_3+lac with lactate augmentation. The dominant bacteria are identified as genera with relative abundances above 10% in any of of the 5 sediments. The relative abundances were acquired by DNA extraction from 0.5 g of sediments, 16S rRNA gene sequencing and analysis.

3.4.1 Iron metabolizing microbes largely enriched during the experiment

Bacteria capable of nitrate-dependent Fe(II) oxidation, *Azospira*, *Dechloromonas*, *Acidovorax* were found relatively abundant in end-point sediments of all 4 experiments, while negligible in initial sediments (**Figure 3.14a**). Among them, *Azospira* species were reported as capable of perchlorate reduction, anaerobic oxidation of humic substances, and sulfide oxidation, and likely capable of carrying

coupled nitrate reduction and anaerobic Fe(II) oxidization (Mehta-Kolte et al., 2017; Zecchin et al., 2019). Species of the perchlorate- and nitrate-reducing genus *Dechloromonas* was also reported to couple nitrate reduction and Fe(II) oxidation during anoxic batch incubation with concentrations of nitrate, Fe(II), and acetate similar to this study (Chakraborty and Picardal, 2013). The more well-studied nitrate reducing iron oxidizer *Acidovorax* was also found relatively abundant in end-point sediments of all columns except for column GW+Fe+NO_3+lac, confirming the coupled process likely happened during the experiment, while suggesting lactate might favor other genera to perform it. Meanwhile, the classic FRB genus *Geobacter* was found as the most abundant FRB among all end-point sediments (**Figure 3.14b**).

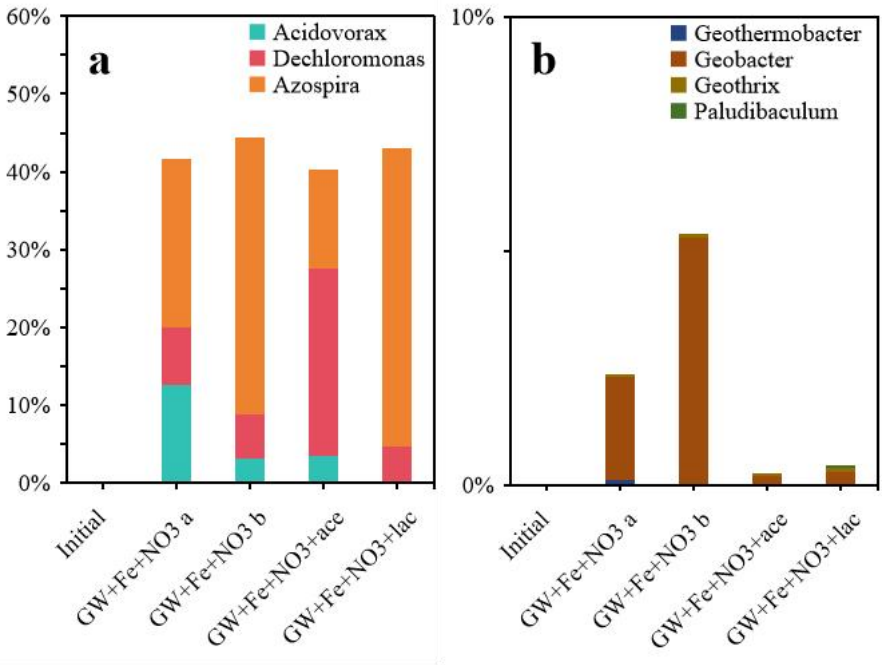

Figure 3.14 Relative abundances of (a) NDFO bacteria and (b) FRB, at the genus level, in initial and end-point sediments: Panels from left to right show the initial and end-point sediments of the 4 experiments with iron and nitrate treatment, including GW+Fe+NO_3+ace with acetate augmentation and GW+Fe+NO_3+lac with lactate augmentation. The relative abundances were acquired by DNA extraction from 0.5 g of sediments, 16S rRNA gene sequencing and analysis.

3.4.2 Sulfate and sulfur reducers largely enriched during the experiment

Possible sulfate and sulfur reducing microbes including genera *Desulfomicrobium, Desulfobulbus, Desulfuromonas, Desulfatiferula, Desulfovibrio, Desulfobacterium*,

Desulforhopalus and *Geothermobacter* were found relatively abundant in end-point sediments of all 4 columns, although negligible in initial sediments (**Figure 3.15**). The compositions in end-point sediments were similar among the 4 iron and nitrate treated columns, except that *Desulfobulbaceae* spp. (such as *Desulfobulbus* and *Desulforhopalus*) was found more abundant in GW+Fe+NO_3 a and b. While potential sulfate and sulfur reducing genera were relatively abundant in end-point sediments of GW+Fe+NO_3 a (>20%) and b (>10%), they were found relatively less abundant in end-point sediments of GW+Fe+NO_3+ace and GW+Fe+NO_3+lac (both <10%). For end-point sediments of GW+Fe+NO_3+lac, SRB capable of completely degrading acetate were found the most abundant among 4 experiments, while SRB incapable of completely degrading acetate were found the least abundant.

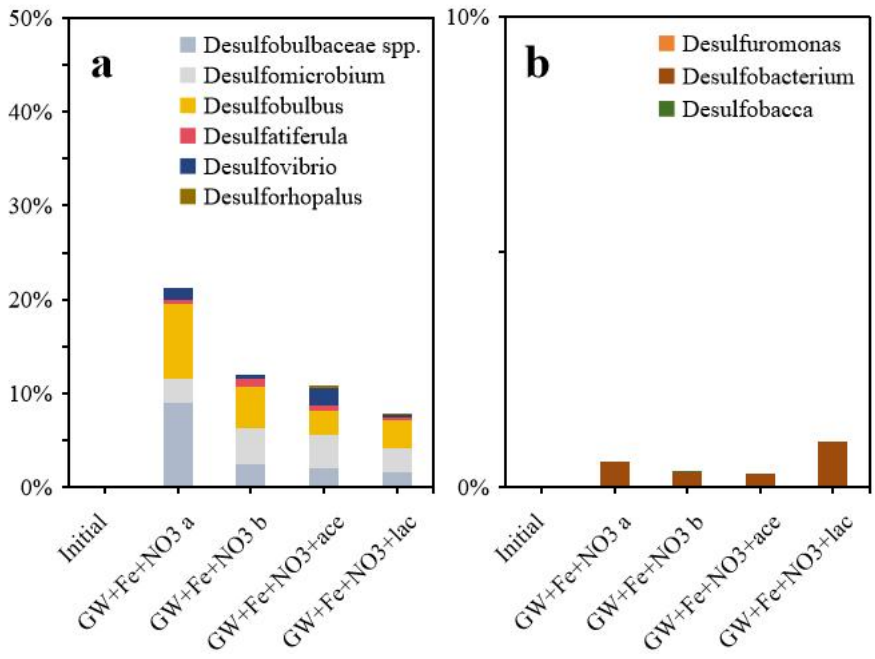

Figure 3.15 Relative abundances of SRB (a) incapable and (b) capable of completely degrading acetate, at the genus level, in initial and end-point sediments: Panels from left to right show the initial and end-point sediments of the 4 experiments with iron and nitrate treatment, including GW+Fe+NO_3+ace with acetate augmentation and GW+Fe+NO_3+lac with lactate augmentation. The relative abundances were acquired by DNA extraction from 0.5 g of sediments, 16S rRNA gene sequencing and analysis.

3.5 Discussion

3.5.1 Transformation of iron minerals and arsenic species during the experiment

The primary purpose of ferrous iron and nitrate treatment is to achieve long-term arsenic immobilization through *in situ* formation of mixed valence iron minerals such as magnetite (Sun et al., 2016a). However, with the presence of sulfate in the anoxic groundwater system, sulfate reduction can produce sulfide minerals with iron and arsenic. In the field experiment (Sun, 2021) at YCB site (depth 39.5 m, the same as influent groundwater YCB-MLW4), As XANES results revealed that arsenic appeared 29% as orpiment (while 42% as arsenate and 29% as arsenite) in sediment before the experiment, and increased to 48% as orpiment (while 52% as arsenate and 0% as arsenite) after the experiment, while Fe XANES results showed that magnetite increased from 0% to 7% and pyrite increased from 0% to 6%.

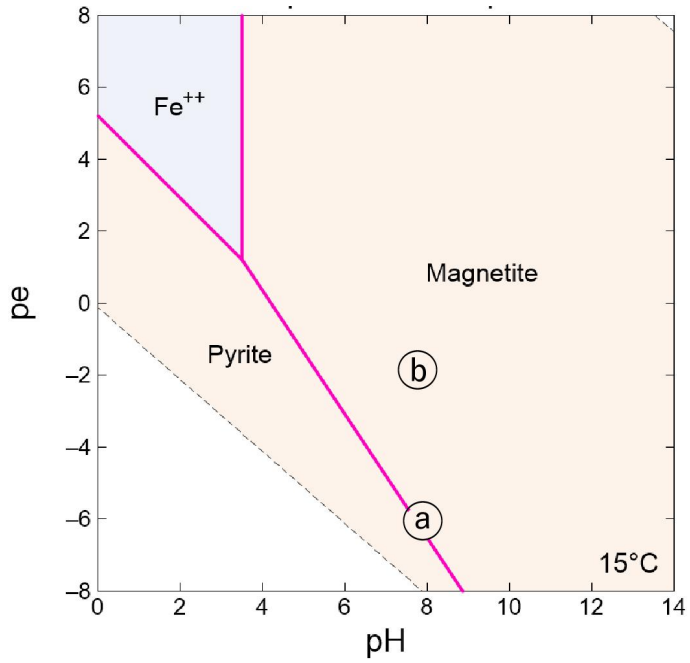

Figure 3.16 The pE/pH diagram for iron in the presence of sulfate: Groundwater redox versus pH data of groundwater ⓐ AMS3-2 where the initial sediments were sampled, and ⓑ YCB-MLW5, the influent groundwater, were plotted. The diagram, characterized by the following conditions: temperature of 15°C, 2 μmol/L Fe(II), 8 μmol/L Fe(III), 1 mmol/L sulfate, 8 mmol/L bicarbonate, was constructed using Geochemist's Workbench (Rockware Inc., Golden, CO) with the Lawrence Livermore National Laboratories (LLNL) combined database thermo.V8.R6.230 (Delany and Lundeen, 1991).

In **Figure 3.16** we plotted groundwater AMS3-2 of the initial site, and groundwater YCB-MLW5 as influentin the experiment, in a simplified pE/pH diagram, which indicates that YCB-MLW5 favors the formation of mixed valence Fe(II/III) oxides (magnetite) over iron sulfide (pyrite), while our initial site has no significant preference.

Experiment results has shown that sulfate consumption and sulfide precipitation were significant during the experiment. The presence of nitrate and nitrite potentially stimulates sulfate reducing ammonium oxidation (Zhang et al., 2019), although nitrate and particularly nitrite has been found capable of effectively inhibiting sulfate reduction and preventing sulfide accumulation (Kaster et al., 2007; Londry and Suflita, 1999). Potential sulfate/sulfur reducers were notably enriched in relative abundance after the experiment. The *Desulfobulbaceae* spp. was found particularly abundant in sediment columns GW+Fe+NO_3 a and b, known for utilizing nitrate, and sulfur disproportionation using $FeCl_2$ or $Fe(OH)_3$ as sulfide scavengers (Müller et al., 2016; Müller et al., 2020). The amount of acidic volatile sulfide formation only accounts for part of the sulfate consumed during the experiment. Immobilization of arsenic by sulfide precipitation is impossible to ignore, and will be discussed further with more experiment results in *Chapter 4*.

It is worth noting that our analysis of sediment samples were after relatively long term observation after the treatment, aiming to examine the stability of newly formed minerals in the longer run. In the end, newly formed sulfide still likely constitute a major sink in this study. Nonetheless, the largely increase of relative abundance in iron oxidizers *Dechloromonas* and *Azospira*, associated to iron (hydr)oxide (Zecchin et al., 2019), and more classic nitrate reducing Fe(II) oxidizer *Acidovorax* (Liu et al., 2019; Pantke et al., 2012; Straub et al., 1996; Straub et al., 2004) evidenced the possible formation and transformation of mixed valence Fe(II/III) minerals during the experiment.

The relatively low net increase of HCl extractable iron in the end-point sediments,

comparing with the amount of iron precipitated during the experiment, could indicate that iron and nitrate treatment eventually formed more stable minerals in the sediments that were not easily leached by acid. Increased amount of strongly absorbed arsenic in the sediments suggests that ferric iron might have transformed into more stable phases, possibly as mixed-valence iron minerals, as biological transformation between Fe(III) and Fe(II) were potentially active during the experiment, with both Fe(II) oxidizers and Fe(III) reducers being found increasingly abundant in end-point sediments of all 4 columns.

Among the HCl extractable iron, extracted from carbonate and amorphous to low-crystalline (hydr)oxide forms, ferrous iron largely increased in sediments of all columns, while ferric iron decreased. Carbonates and amorphous to low crystalline iron (hydr)oxides largely formed during the experiments possibly due to the precipitation of soluble iron from influent, supported by the much lower dissolved iron concentrations in effluents than in influent groundwater throughout most of the experiment period. HCl extractable ferric iron was barely found in the end-point sediments (only tiny amount in the inlet and outlet sediments) of columns GW+Fe+NO_3 a and b. ROC amendment likely favored the formation of mixed valence iron minerals, or at least the preservation of ferric iron in amorphous to low crystalline iron hydroxides.

Did iron and nitrate treatment actually form magnetite in this study? We tried to examine this by environmental magnetism approaches, which has been widely applied for heavy metal monitoring in soil for its sensitiveness and non-destructiveness. In an earlier field push-pull test of Fe(II)-nitrate treatment (Sun, 2021), a significant shift from low coercivity to high coercivity in FORC diagram was observed, from Bc around 10 mT (magnetite) to Bc around 40-60 mT (likely greigite), indicating the formation of sulfide minerals, and was confirmed by XAS analysis of the sediments. Analyzing magnetic properties of sediment provided us a special perspective on arsenic contamination in the groundwater system. In this study, magnetite transforming into smaller particle was significant, according to FORC diagrams, the

response could be resulted from neo-formd nano-particulate magnetite or the dissolution of the existing larger-grain magnetite particles. Specifically, end-point sediments of column GW+Fe+NO_3+ace has significantly lower χ_{lf} while higher SIRM/χ ratio, indicating lower abundance in magnetite while more abundant in higher coercity minerals, such as hematite and goethite.

The presence of As(V) and Fe(III) minerals in initial sediments is likely due to limited quantity and quality (low bio-availability) of dissolved organic carbon in the initial groundwater system, according to DOM study and high resolution profiling at the same research site (Dai, 2022; Sun et al., 2021), and in this study further supported by the low TOC in initial site groundwater (**Table 3.2**), and relatively low abundance of iron metabolizing microbes in initial sediments (**Figure 3.14**).

The pH of influent groundwater is above the optimal pH for arsenate adsorption to Fe oxides (Chowdhury et al., 2011; Dixit and Hering, 2003), although Fe(II)-nitrate treatment lowered the pH of influent and subsequently lowered the pH of effluent during the treatment (**Figure 3.1**). Phosphate extractable arsenic (exchangeable, strongly absorbed fraction) in end-point sediments largely increased, while HCl extractable arsenic (associated with amorphous to low crystalline iron minerals) in end-point sediments were all As(III) for all columns. Phosphate extractable arsenic in sediment, considered a mobilizable fraction bound to particle surface rather than embedded within crystalline minerals, has been found a key factor controlling arsenic concentrations in groundwater (Keon et al., 2001; van Geen et al., 2004; Zheng et al., 2005). The presence of phosphate extractable arsenate in end-point sediments of column GW+Fe+NO_3+lac may be a result of re-oxidation of arsenite by Fe(III) (hydr)oxides after the depletion of lactate.

3.5.2 Impact of ROC augmentation on mineral transformation and arsenic immobilization

Groundwater systems, often considered as oligotrophic, usually contain very low organic carbon itself. This study tried to investigate whether and how ROC

augmentation impact the transformation of iron mineral and immobilization of arsenic by iron and nitrate treatment. Previous work have suggested that arsenic mobilization in our study site was likely attributed to preferential utilization of low molecular weight DOM that has higher bio-availability (Sun, 2021). However, the shallow aquifer of the study site is characterized by low DOC concentrations (2.4±0.95 mg/L), and the DOM bio-availability has been found very low (0-10%) according to 28-day incubation experiments (Dai, 2022). Less abundance in labile microbially derived DOM was also found in typical aquifers with high concentrations of arsenic in Bangladesh, where dissolved iron (mostly ferrous iron) and arsenic are high (Mladenov et al., 2010). The groundwater system most likely had entered a steady state where reductive dissolution of iron minerals and mobilization of arsenic were much less active due to the low abundance of bio-available organic substrate, hence the high portion of Fe(III) among dissolved total iron in groundwater.

Simple and labile ROC, such as acetate and lactate, can stimulate microbial activities in aquifer and, for its high bio-availability, achieve faster rate of ferric iron reduction, comparing *in situ* natural organic matter extracted from local aquifer sediments (Glodowska et al., 2020). In this study, end-point sediments of both acetate- and lactate-amended experiments contained less reactive iron minerals but with higher portion of ferric iron. Sulfide precipitation were also lower with ROC augmentation. End-point sediment of actate-amended GW+Fe+NO_3+ace were most abundant in nitrate-dependent Fe(II)-oxidizing *Azospira*, while least abundant in sulfate/sulfur reducing bacteria. End-point sediment of acetate-amended GW+Fe+NO_3+ace were relatively more abundant in another possible denitrification contributor *Decholoromonas*. These evidences suggest that ROC augmentation stimulated NDFO while suppressed sulfate reduction, resulting in the formation of more mixed-valence iron minerals and less sulfides for arsenic immobilization. While the lactate-amended experiment sequestered slightly more arsenic, comparing with not-amendment experiments, arsenic associated with reactive iron minerals and strongly absorbed mobilizable arsenic were both lower with ROC augmentation, suggesting arsenic was

more stably immobilized with ROC augmentation. The small amount and period of ROC, especially lactate, augmentation might have enhanced the formation of more stable iron minerals in sediment, and immobilized arsenic more stably.

3.5.3 Inhibiting sulfate reduction while promoting NDFO: lactate versus acetate

The augmentations with acetate and lactate came up with different results. Acetate augmentation inhibited sulfate reduction, but did not promote arsenic immobilization with iron and nitrate treatment. With acetate augmentation, iron and nitrate treatment didn't trap more arsenic than without. In fact, strongly-absorbed mobilizable (phosphate extractable) arsenic in end-point sediments of GW+Fe+NO_3+ace was only 57% that of the no-augmentation experiments. Meanwhile, stimulation of arsenic immobilization was insignificant. Batch experiment has found Fe(III) was preferably reduced than sulfate when coexist (Xia et al., 2019). It is likely than acetate amendment promoted Fe(II) oxidation in the presence of nitrate, and subsequently suppressed sulfate reduction by elevating Fe(III) concentration in groundwater.

Lactate augmentation inhibited sulfate reduction and stimulated arsenic immobilization by iron and nitrate treatment. With lactate amendment, sulfate reduction was largely inhibited, with only 172 μmol sulfate consumed during the experiment GW+Fe+NO_3+lac, comparing with 354 μmol on average during GW+Fe+NO_3 a and b. Neo-formed AVS was also the lowest in GW+Fe+NO_3+lac among all experiments, only 11 μmol, compared with 83.7 μmol on average for GW+Fe+NO_3 a and b. While phosphate extractable arsenic increased in GW+Fe+NO_3+lac sediments was low, total trapped arsenic during the experiment was the highest among all columns.

After iron and nitrate treatment with lactate amendment, not only the most arsenic was immobilized, but also the least arsenic immobilized were associated with sulfate reduction and sulfide precipitation. Sulfide is known as an intermediate in nitrate-dependent oxidation of ROC such as lactate (Hubert and Voordouw, 2007). ROC amendment hence might have decreased the available dissolved sulfide for

precipitation.

Incubation of subsurface sediments with lactate amendment observed that ferrihydrite was reduced firstly without sulfate reduction when Fe(III) was present as excess electron sink, followed by a second phase of sulfate and iron reduction (Kwon et al., 2016). Batch incubation of river sediments also found that ferric iron reduction happens first when ferric iron and sulfate co-exist, while sulfate reduction only starts after ferrous iron concentration stabilized (Xia et al., 2019). The presence of HCl extractable ferric iron in end-point sediments of lactate- and acetate-amended columns GW+Fe+NO_3+ace and GW+Fe+NO_3+lac could answer how sulfate reduction was inhibited in these ROC-amended columns, since the HCl extractable poorly crystalline iron (hydr)oxides are critical for iron and sulfate reduction (Mark Jensen et al., 2003; Vandieken, 2005). Ferric iron in amorphous to low crystalline minerals, especially those coating on clay, are more biologically available to reduce, hence can more effectively inhibit sulfate reduction (Lovley and Phillips, 1987). The inhibition of sulfate reduction can be achieved in the presence of readily reduceable ferric iron, in which case the FRB out-competed the SRB, leaving electron donor concentrations too low for sulfate reducers to metabolize (Lovley and Phillips, 1987). The less abundance in sulfate reducers in the end-point sediments of ROC amended columns could be the result of this effect. With ROC amendment, more amorphous to low crystalline forms of ferric iron was preserved, probably because ROC amendment enhanced the dissolution of more crystalline ferric iron minerals and excess dissolved ferric iron subsequently precipitated.

It was reported that nitrate reducing iron oxidizers depend on organic substrates and isolation of lithotrophic species turned out to be difficult (Straub et al., 2004). In the original laboratory experiments applying Fe(II)-nitrate treatment, lactate was amended in the artificial groundwater influent throughout the experiment to stimulate reducing conditions (Sun et al., 2016a; Sun et al., 2016b).

While laboratory studies overwhelmingly favor the formation of mixed Fe(II)-Fe(III)

oxides such as magnetite for aresenic immobilization, field observations suggest the likely significant role of sulfide minerals (Sun, 2021). In addition to confirm the role of sulfide minerals, our experiments emphasized the importance of reactive organic carbon for forming mixed-valence iron minerals, inhibiting sulfate reduction and subsequent sulfide mineral precipitation, during Fe(II)-nitrate treatment in anoxic groundwater, especially in systems with low bio-available organic carbon. Since sulfide and (hydr)oxide minerals are primary arsenic sinks in groundwater systems, ROC amendment may be able to stimulate certain mineral (trans)fomation selectively for remediation purposes, which certainly worth more research in future studies.

Chapter 4 Immobilizing arsenic by sulfide precipitation: divergence driven by reactive organic carbon

The previous chapter has found sulfide precipitation after the iron and nitrate treatment likely served a major role in arsenic immobilization. To further examine the impact of sulfate reduction and sulfide precipitation on iron mineral transformation and arsenic immobilization in anoxic groundwater aquifers, as well as the likely divergence driven by ROC, this research chapter presents a study of 4 field-based column experiments of blank treatment without iron and nitrate, fed with freshly pumped natural groundwater, with and without the ROC augmentation as acetate or lactate amendment during the treatment, as has been detailed in *2.2 Field based column experiments*. The 4 experiments are:

Table 4.1 Experimental

Experiment	Treatment
GW a	blank
GW b	
GW+ace	blank
	1 mmol/L acetate
GW+lac	blank
	1 mmol/L lactate

Pre-treatment: 2.6 PV/day for 40 PV, equilibrium of experiments system with fresh groundwater. **Treatment**: 27 PV at 2.6 PV/day for 27 PV, blank treatment without iron and nitrate, with or without ROC augmentation. **Post-treatment**: 2.6 PV/day for 25 PV, flushing; 5.4 PV/day for 230 PV, long-term observation.

Results are presented in 4 sections: groundwater chemistry, sediment characterization, environmental magnetism of sediments, and sediment microbial ecology. While the treatment was without iron and nitrate, arsenic immobilization was also achieved, likely due to sulfide precipitation, as sulfate consumption and sulfide precipitation were significant. Microbial communities changed dramatically after the experiment, with potential iron and sulfur metabolizing genera enriched in relative abundances.

4.1 Aqueous chemistry

Influent and initial site groundwater chemistry has been reported in **Table 3.2**.

4.1.1 Effluent EC, pH, alkalinity

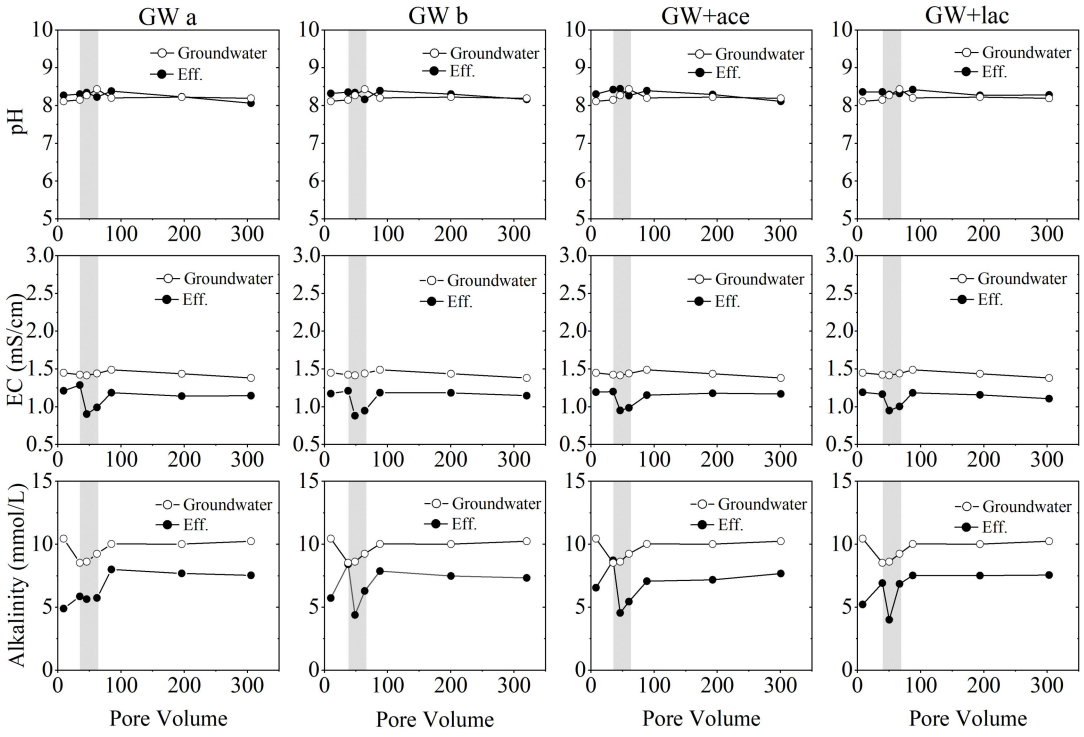

Figure 4.1 Effluent and groundwater pH, EC, and alkalinity: Groundwater samples were collected, preserved and measured according to the effluent samples, their average pH (8.22, n=7) was 0.46 higher than groundwater samples (7.77, n=64) measured on site when freshly pumped out (**Figure 3.2**). The treatment periods are emphasized with gray shade area, during which blank treatment without iron and nitrate was performed for all 4 columns, while ROC (acetate or lactate) augmentation was performed for GW+ace and GW+lac, respectively.

Effluent pH were between 8 and 8.5, almost indifferent from influent pH measured following the same procedures, throughout the experiment, for all 4 experiments (**Figure 4.1**). The two experiments, GW a and GW b, are reported individually for they were packed separately and run with individual tube lines. Effluent EC were always lower than influent EC throughout the experiment, especially during the treatment, when the influent was groundwater diluted with DI water. Effluent alkalinity was much lower than influent groundwater alkalinity during the pre-treatment equilibrium, while recovered to influent level by the start of the treatment, for columns GW b and

GW+ace. During the treatment, effluent alkalinity was much lower than groundwater alkalinity. Post treatment, effluent alkalinity remained lower than influent level, but higher than effluent alkalinity pre-treatment.

4.1.2 Effluent fluoride, chloride, and bromide

The groundwater samples (n=21) collected during the experiments contained negligible concentrations of fluoride (0.00±0.01 mmol/L) and bromide (0.00±0.00 mmol/L), but relatively high concentrations chloride (3.70±0.07 mmol/L) (**Figure 4.2**). The data are consistent with the groundwater chemistry previously reported (**Table 3.2**).

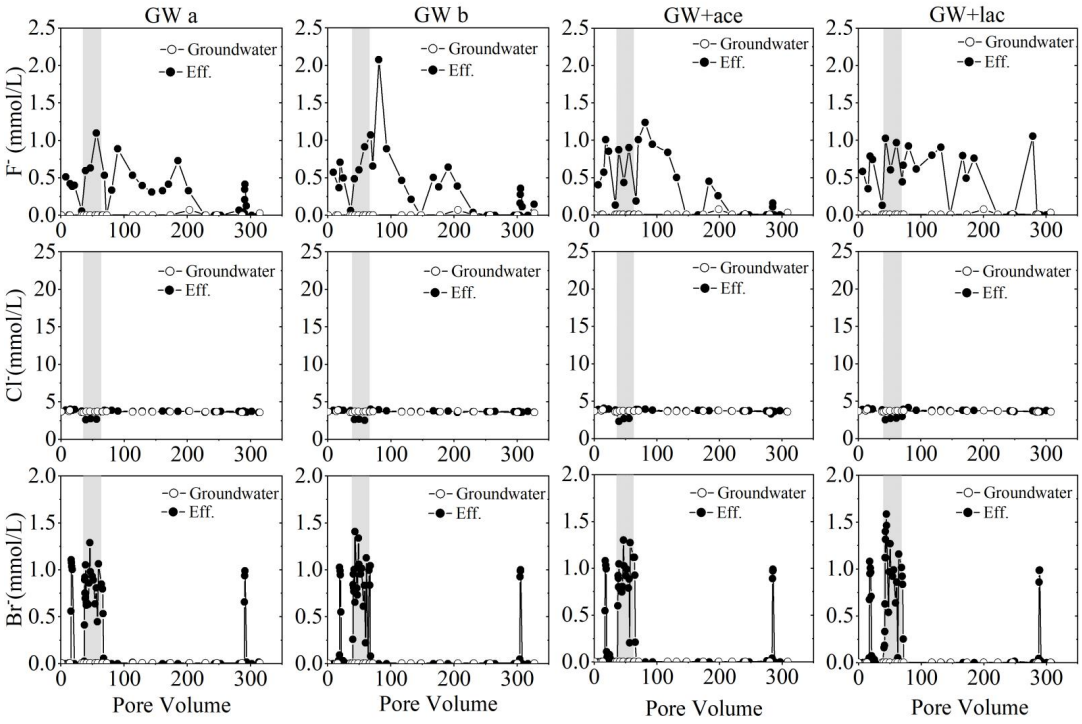

Figure 4.2 Effluent fluoride (F^-), chloride (Cl^-), and bromide (Br^-) versus pore volume: Effluent concentrations are compared with groundwater concentrations. The treatment periods are emphasized with gray shade area, during which blank treatment without iron and nitrate was performed for all 4 columns, while ROC (acetate or lactate) augmentation was performed for GW+ace and GW+lac, respectively. Groundwater (n=21) concentrations were 0.00±0.01 mmol/L for fluoride, 3.70±0.07 mmol/L for chloride, and 0.00±0.00 mmol/L for bromide.

The effluent data showed that fluoride concentrations fluctuated above groundwater level during the experiment, likely indicates dissolution and flushing of fluoride from

the sediments by influent groundwater. Although effluent fluoride concentrations went down to groundwater level after 200 PV, a sudden elevation were observed at around 300 PV, during the short period of bromide injection. Such elevation, however, was not observed for experiments reported in *Chapter 3*.

During the treatment, bromide was introduced through influent, their effluent concentrations, although fluctuated inevitably, are relatively stable around the theoretical influent concentration of 1 mmol/L. The effluent bromide concentrations were 0.83±0.19 mmol/L (n=19), 0.86±0.32 mmol/L (n=21), 0.91±0.24 mmol/L (n=19), and 1.02±0.36 mmol/L (n=18) for experiments GW a, GW b, GW+ace and GW+lac, respectively, while their effluent chloride concentrations were 2.69±0.08 mmol/L (n=3), 2.62±0.07 mmol/L (n=3), 2.57±0.22 mmol/L (n=3), and 2.74±0.18 mmol/L (n=4), accounting for 73%,71%, 69%, and 74% of the groundwater level. The theoretical ratio, according to the mixing and dilution by DIW, should be 67%. The results showed that the mixing processes were relatively stable throughout the treatment.

4.1.3 Effluent iron, nitrogen, arsenic and sulfur

Effluent iron concentrations were significantly lower than influent levels, for all 4 columns, throughout the pre-treatment equilibrium, and remained low during the treatment (**Figure 4.3**). During post-treatment observation, effluent iron increased gradually as influent iron increased, but remained much lower than the influent level for all 4 columns during most of the time.

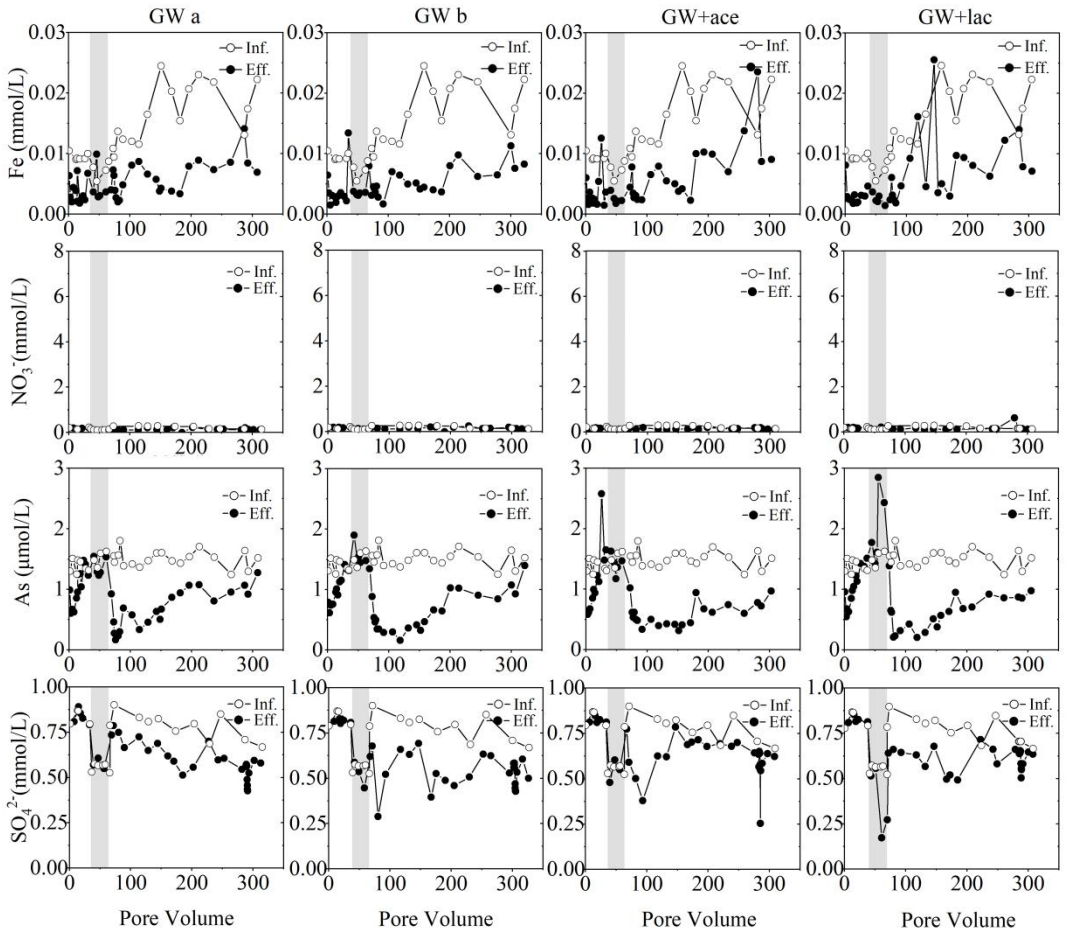

Figure 4.3 Effluent concentrations of iron (Fe), nitrate (NO_3^-), arsenic (As), and sulfate (SO_4^{2-}) versus pore volume: The effluent concentrations (**Eff.**) are expressed with black dots, while influent concentrations (**Inf.**) are expressed with black circles. The treatment periods are emphasized with gray shade area, during which blank treatment without iron and nitrate was performed for all 4 columns, while ROC (acetate or lactate) augmentation was performed for GW+ace and GW+lac, respectively. Influent concentrations were groundwater concentrations during pre-treatment equilibrium and post-treatment observation. During the treatment, influent concentrations were calibrated with measured tracers (chloride and bromide) data to represent the actual levels subject to inevitable fluctuations during mixing.

While influent groundwater nitrate concentrations were 0.183±0.056 mmol/L (n=21), effluent nitrate were stably below influent levels: 0.138±0.037 mmol/L (n=34) for GW a, 0.149±0.039 mmol/L (n=33) for GW b, 0.138±0.035 mmol/L (n=35) for GW+ace, and 0.143±0.035 mmol/L (n=33) for GW+lac, throughout the experiment. Effluent nitrite were always negligible during the experiment. Effluent ammonia (**Figure 4.4**) were 71, 53, 106, 66 μmol/L for columns GW a, GW b, GW+ace and GW+lac, respectively, at the start of pre-treatment equilibrium, then gradually

decreased to as low as 0.89±0.68 μmol/L (n=4) for all 4 columns at around PV=27. During the treatment and until early post-treatment, effluent ammonia for all 4 columns remained lower than 13 μmol/L, much below the influent levels of 144±4 μmol/L (n=6) and 95±5 μmol/L (n=4) during the treatment.

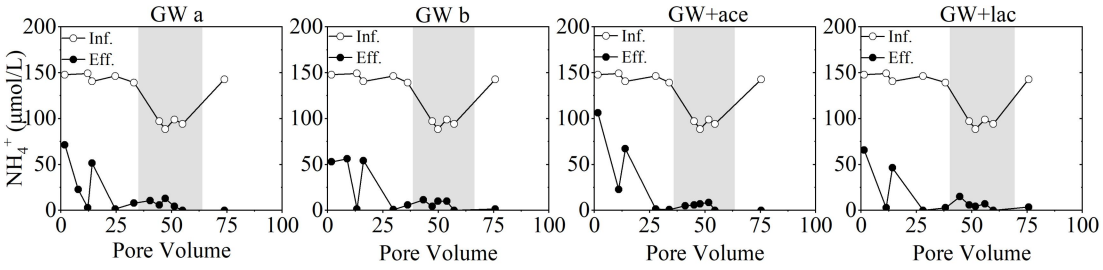

Figure 4.4 Effluent ammonia concentrations (μmol/L): Concentrations of effluent and influent ammonia were measured on site with spetrophotometric methods. The treatment periods are emphasized with gray shade area, during which blank treatment without iron and nitrate was performed for all 4 columns, while ROC (acetate or lactate) augmentation was performed for GW+ace and GW+lac, respectively. Influent concentrations were groundwater concentrations during pre-treatment equilibrium and post-treatment observation. During the treatment, influent concentrations were calibrated with measured tracers (chloride and bromide) data to represent the actual levels subject to inevitable fluctuations during mixing.

Effluent arsenic concentrations (**Figure 4.3**) at the beginning of the experiment were roughly 1/2 to 2/3 the level of influent, but gradually recovered to influent level before the treatment started. During the treatment, mobilization of arsenic was observed for all 4 columns. For columns GW a and b, effluent concentrations of arsenic increased to around 1.5 μmol/L in effluent, which is around 1.5 times the mixed influent concentration. For ROC amended columns GW+ace and especially the lactate amended GW+lac, the effluent concentrations of arsenic increased to higher than the level of columns GW a and GW b. By integrating the area between effluent and influent curves, we estimated that 0.07, 0.10, 0.12 and 0.22 μmol arsenic were mobilized for columns GW a, GW b, GW+ace, and GW+lac, respectively. After the treatment, immediately after switching the influent back from diluted to natural groundwater, all 4 columns experienced a sudden drop in effluent arsenic concentrations, to as low as 0.1 μmol/L, then slowly recovered to concentrations close to the influent level at the end of the experiment. During post-treatment observation,

we sampled effluents twice closely, and analyzed the arsenic speciation in influent and effluent as detailed in **Table 4.2**. The influent contained 100±7 μg/L (n=2) arsenic, among which 88±1% were As(III), consistent with the early field sampling results reported in **Table 3.2**. On average, effluent As(III) percentages were 70±28%, 86±4%, 87±13% and 85±11% for columns GW a, GW b, GW+ace, GW+lac, respectively.

Table 4.2 Post-treatment effluent arsenic (μg/L) speciation

Sample	Species	Influent	GW a	GW b	GW+ace	GW+lac
112	As(III)	91.98	3.73	12.60	15.97	9.32
2021.08.24	As(V)	12.73	3.60	2.53	0.54	2.44
	$As(III)/As_{total}$	88%	51%	83%	97%	79%
115	As(III)	82.50	5.89	10.67	15.38	6.04
2021.08.25	As(V)	12.79	0.58	1.29	4.27	0.33
	$As(III)/As_{total}$	87%	91%	89%	78%	95%
Average	$As(III)/As_{total}$	88±1%	70±28%	86±4%	87±13%	85±11%

Arsenic species, As(III) (arsenite) and As(V) (arsenate), of the 2 sets (112 and 115) of samples (influent groundwater, and effluent of the 4 experiments) are presented, with approximated total arsenic calculated as As_{total} = As(III) + As(V) given that no other species was detected.

Effluent sulfate concentrations (**Figure 4.3**) were stably the same level of influent groundwater sulfate from the start of the experiment till the treatment finished, regardless of the dilution with DI water in the mixed influent during the treatment, except that the effluent sulfate concentration dropped significantly for GW+lac. Post treatment, however, effluent sulfate concentrations started to fall below the influent level for all 4 columns. The gap between influent and effluent sulfate concentrations of columns GW+Fe+NO_3 a and b remained rather stable around 0.18 mmol/L during post treatment period. For the ROC augmentation experiments, and especially the acetate amended column GW+ace, the gap between influent and effluent sulfate became significantly narrower than other columns from around PV=150 till the end of the experiment.

4.2 Solid phase chemistry

During the experiments, the color of sediments turned dark (**Figure 4.5**). It appears

that GW+lac sediments had the darkest color among 4 experiments at the end of treatment, yet by the end of the experiments, its color, although turned darker, was much lighter (especially near the top) than the sediments without ROC augmentation. The dark color indicated the likely formation of sulfide minerals, which was further supported by the distinct odor of hydrogen sulfide, and confirmed by AVS extraction results. We analyzed the sediments before and after the experiments for their characteristics, and reported in detail in the following sections.

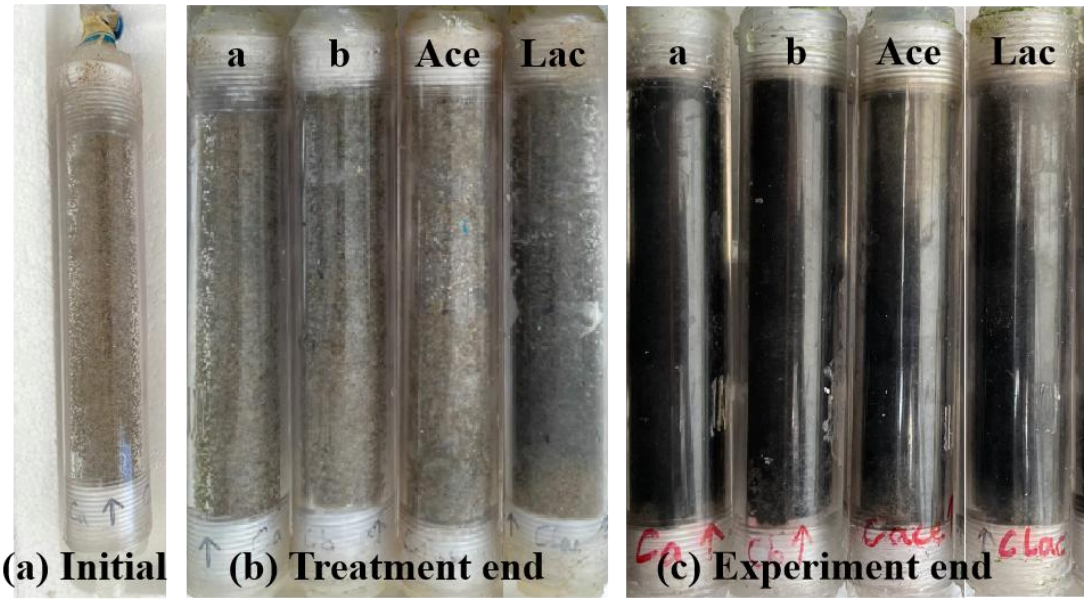

Figure 4.5 Columns at the (1) start, (2) treatment end, and (3) experiment end: Photos were taken for the columns of the experiments GW+Fe+NO_3 a (**a**), GW+Fe+NO_3 b (b), GW+Fe+NO_3+ace (**Ace**) and GW+Fe+NO_3+lac (**Lac**), at the (1) start of experiment, (2) end of the treatment, and (3) end of the experiment. The photos were taken with the same device against a white board in the middle of the day for better comparability.

4.2.1 Extractable arsenic and iron phases

The initial sediments contained 0.75 mg/kg phosphate extractable arsenic per kilogram dry sediment, the concentration decreased in the end-point sediments for GW a and b by 0.27±0.19 mg/kg, after the experiment (**Table 4.3**). Phosphate extractable As(V) in end-point sediments were negligible for all 4 experiments, although a little remained in the tiny amount of outlet sediments for GW b, GW+ace, and GW+lac, and inlet sediment for GW+ace.

HCl extractable iron in the initial sediments were 0.60 g/kg dry sediment, and mostly (0.52 g/kg) ferrous iron. These iron of amorphous to low crystalline minerals more than doubled after the experiment, with very small portion left as ferric iron. While HCl extractable iron largely increased (by 0.79±0.15 mg/kg, n=4) for all 4 columns during the experiment, Fe(III) didn't significantly change in concentration, comparing with the initial sediment (**Table 4.3**). The acetate-amended column GW+ace retained significantly more HCl extractable Fe(III) in sediments after the experiment, especially in the column inlet, while the lactate-amended column GW+lac was the only column that no HCl extractable Fe(III) was found in its inlet sediment after the experiment.

Table 4.3 Phosphate extractable As(V)/As and HCl extractable Fe(II)/Fe of initial and end-point sediments

Parameters	Initial		GW a	GW b	GW+ace	GW+lac
P-ext As (mg/kg)	0.75	Outlet	0.39	0.76	0.74	0.54
		Middle	0.61	0.38	0.60	0.46
		Inlet	0.91	0.69	0.76	0.66
P-ext As(V) (mg/kg)	0.22	Outlet	0.00	0.21	0.25	0.19
		Middle	0.00	0.00	0.00	0.00
		Inlet	0.00	0.00	0.15	0.00
HCl-ext Fe (g/kg)	0.60	Outlet	0.85	0.86	0.54	0.56
		Middle	1.39	1.57	1.22	1.35
		Inlet	1.18	1.06	0.65	0.85
HCl-ext Fe(III) (g/kg)	0.08	Outlet	0.10	0.08	0.06	0.08
		Middle	0.04	0.03	0.09	0.02
		Inlet	0.07	0.00	0.15	0.00

Phosphate extractable total arsenic (**P-ext As**) and arsenate (**P-ext As^{5+}**), representing strongly-absorbed arsenic in sediments, as well as HCl extractable total iron (**HCl-ext Fe**) and ferric iron (**HCl-ext Fe^{3+}**), representing reactive iron from amorphous to low-crystalline iron minerals in sediments, are presented, for initial and end-point sediments of the 4 iron and nitrate treatment experiments. The end-point sediments analyzed including an aliquot each from the inlet and outlet of the column, and an aliquot from the rest of the sediments (middle) after mixed thoroughly. Chemical extractions were performed for approximately 0.5 g sediments with 1 mol/L HCl and 1 mol/L sodium phosphate (pH adjusted to 5), respectively.

4.2.2 Acidic volatile sulfide (AVS) and simultaneously extracted metal (SEM)

AVS largely increased in end-point sediments for all 4 experiments (**Table 4.4**),

comparing with only 0.042 ± 0.01 μmol per gram dry sediment (n=2) in the initial sediment. Meanwhile, SEM-As in end-point sediment of GW a (0.03 μmol/g) and GW b (0.049±0.012 μmol/g) were not higher than those of columns GW+ace (0.05 μmol/g) or GW+lac (0.048 μmol/g). SEM-Fe also significantly increased in end-point sediments, with GW b the highest.

Table 4.4 AVS, SEM-As, and SEM-Fe of initial and end-point sediments

Parameters	**Unit**	**Initial** (n=2)	**GW a**	**GW b** (n=2)	**GW+ace**	**GW+lac**
AVS	μmol/g	0.042±0.01	1.480	4.53±0.27	2.353	2.576
SEM-As	μmol/g	0.014±0.001	0.030	0.049±0.012	0.050	0.048
SEM-Fe	μmol/g	4.58±0.76	27.19	67.24±36.2	49.95	68.97

The concentrations of acidic volatile sulfides (**AVS**), simultaneously extracted arsenic (**SEM-As**) and iron (**SEM-Fe**) were all in terms of dry sediment weight. Initial and end-point sediment of GW b were sampled and extracted twice.

4.2.3 Bulk Chemistry

Table 4.5 Bulk chemistry of initial and end-point sediments

Parameters	**Unit**	**Initial**	**GW a**	**GW b**	**GW+ace**	**GW+lac**
Al_2O_3	%	6.98	8.62	8.66	8.71	8.74
SiO_2	%	83	81.2	80.4	80.8	81.3
S	ppm	84	304	349	156	274
Fe_2O_3	%	2.02	1.99	2	2.03	2.02
Mn	ppm	345	272	258	271	268
As	ppm	10.6	7.5	8	7.9	8.7
As/Fe (molar)	10^{-4}	5.59	4.02	4.26	4.15	4.59
SiO_2/Al_2O_3 (molar)		20.23	16.02	15.78	15.78	15.81

The mass concentration units (% and ppm) are all in terms of dry sediment weight.

The bulk chemistry (**Table 4.5**) showed that the SiO_2/Al_2O_3 ratio was 20.232 in initial sediment, indicating that the sediment is mostly silica-based sand, consistent with grain size distribution of sample S-AMS3-7 reported in *2.2.1 Materials*. The percentage of SiO_2 component slightly decreased in end-point sediment, while Al_2O_3 increased to a certain degree, resulting in the SiO_2/Al_2O_3 ratio of end-point sediments of all 4 experiments lower than initial sediment. This is likely due to the transport of finer grains through groundwater pumping and injection into the columns, since the fresh groundwater was directly pumped from the well without filtering. Bulk arsenic

were 7.5 and 8 ppm in end-point sediments of GW a and GW b, 7.9 ppm in sediments of column GW+ace, while 8.7 ppm in sediments of GW+lac was the highest.

4.3 Sediment magnetism

4.3.1 Magnetic susceptibility

Magnetic properties of initial and end-point sediment samples are presented in **Table 4.6**. Low frequency magnetic susceptibility χ_{lf} were 28.40, 28.17, 28.86 and 29.44 (10^{-8} m^3/kg) for end-point sediments of experiments GW a, GW b, GW+ace and GW+lac, respectively, all lower than 31.49 (10^{-8} m^3/kg) of the initial sediment. The frequency-dependent susceptibility χ_{fd} results were all lower than 2% (in fact close to zero), indicating no or only very small super-paramagnetic (SP) particles exist in initial and end-point sediment.

Table 4.6 Magnetic properties of initial and end-point sediments

Parameters	Unit	Initial	GW a	GW b	GW+ace	GW+lac
χ_{lf}	$10^{-8}m^3/kg$	31.49	28.4	28.17	28.86	29.44
χ_{hf}	$10^{-8}m^3/kg$	31.4	28.73	28.13	28.88	29.45
χ_{ARM}	$10^{-5}m^3/kg$	30.22	32.03	31.73	30.84	33.6
SIRM$_{-1T}$	Am^2/kg	2.44	2.26	2.11	2.2	2.23
IRM$_{-100mT}$	Am^2/kg	1.4	1.34	1.24	1.31	1.32
IRM$_{-300mT}$	Am^2/kg	1.95	1.82	1.69	1.77	1.78
S-ratio		79.70%	80.60%	80.10%	80.40%	79.70%
HIRM	Am^2/kg	2.2	2.04	1.9	1.99	2.01
SIRM/χ	10^3 $A\cdot m^{-1}$	7.75	7.96	7.49	7.62	7.57

Magnetic properties of initial and end-point sediments include: low frequency magnetic susceptibility (**χ_{lf}**) under 200 $A\cdot m^{-1}$ magnetic field and at low-frequency (976Hz), high frequency magnetic susceptibility (**χ_{lf}**) under 200 $A\cdot m^{-1}$ magnetic field at and high-frequency (15616 Hz), Anhysteretic remanent magnetization (**χ_{ARM}**) at 100 mT alternating field (AF) and 50 μT direct current (DC) field, Saturated isothermal remanent magnetization at 1 T under room temperature (**SIRM$_{-1T}$**), isothermal remanent magnetization (IRM) imparted at -100 mT (**IRM$_{-100mT}$**) and at -300 mT (**IRM$_{-300mT}$**), **S-ratio** (IRM_{-300mT}/SIRM), hard isothermal remanent magnetization (**HIRM**), and **SIRM/χ** ratio.

IRM_{-300mT} represents the remanent magnetization after saturated in a high magnetic field and then a back-field of -300 mT to reverse the magnetite/maghemite

contributed SIRM. Hard isothermal remanent magnetization (HIRM) is calculated as HIRM = 0.5 · (SIRM + IRM_{-300mT}) to isolate the magnetic signal of weakly magnetic antiferromagnetic minerals with high coercivity (such as hematite and goethite), from ferrimagnetic minerals (such as magnetite and maghemite) (Liu et al., 2012).

The S ratio (IRM_{-300mT}/SIRM) measures the relative abundance of high coercivity minerals (hematite and/or goethite) mixed with ferrimagnetic minerals (magnetite and/or maghemite). S ratios were 80.23±0.33% (n=4) for sediments of the 4 columns, and 79.92% for the initial sediments, indicating that ferrimagnetic and antiferromagnetic minerals (hematite and/or goethite) are relatively abundant in both initial and end-point sediments.

The SIRM/χ ratios qualitatively identifying mineral compositions, were 7.96, 7.49, 7.62, 7.57 (10^3 $A \cdot m^{-1}$) for end-point sediments of experiments GW a, GW b, GW+ace, and GW+lac, respectively, while 7.75 (10^3 $A \cdot m^{-1}$) for initial sediment. The χ_{ARM}/SIRM ratios were 14.2, 15.0, 14.0 and 15.1 for end-point sediments of experiments GW a, GW b, GW+ace, and GW+lac, respectively, while 12.4 for initial sediments. The higher ratios for end-point sediments implied that SD particles formed or been transported into the column sediments during the experiment.

4.3.2 Temperature dependence of magnetic property

As **Figure 4.6** shows, the heating curves of initial sediments and end-point sediments were similarly smooth and flat under 400℃, then gradually increased as they became paramagnetic, and experienced a sudden drop at round 580℃, the curie temperature (T_C) of magnetite, indicating the presence of magnetite in both initial and end-point sediments. The flat curve before the peaking indicate the absence of certain sulfide minerals such as greigite (T_C ~ 320-400℃) and pyrrhotite (T_C ~ 320℃), which were found in end-point sediments of a previous field push-pull (Sun, 2021). The cooling curve signals enhanced significantly, likely from the newly formed magnetite as a result of transformation from poorly crystalline minerals such as goethite during heating > 580℃.

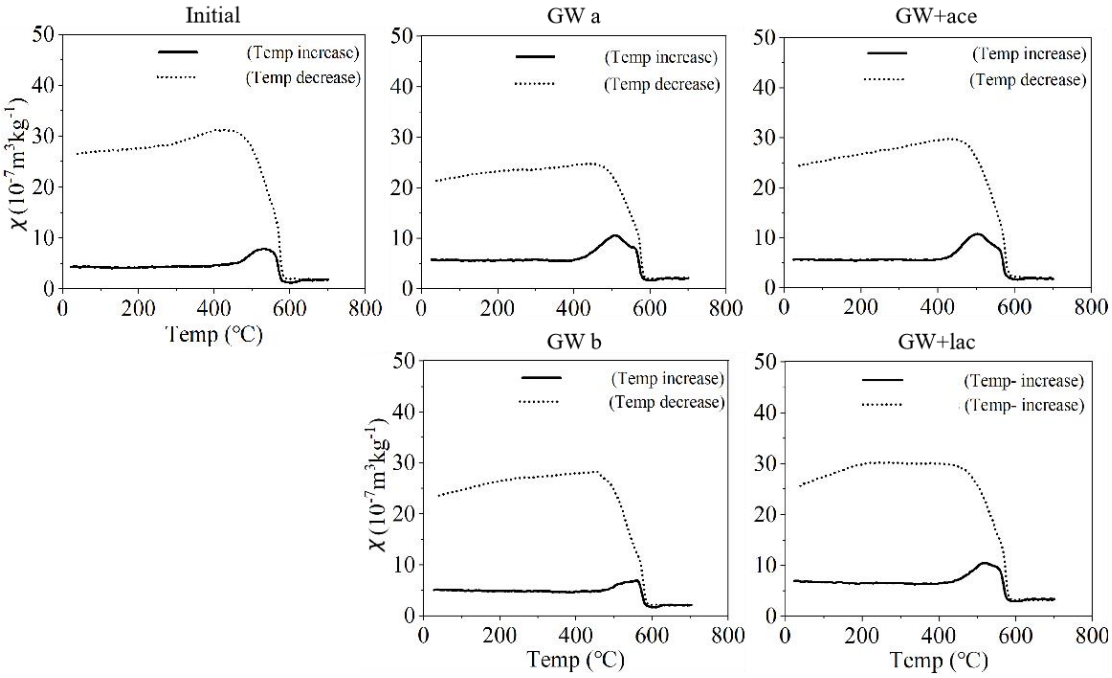

Figure 4.6 χ-T curves: temperature dependence of magnetic susceptibility: The χ-T curves consisted of a black solid line (**Temp increase**), recording the magnetic susceptibility of the sediment sample in response to increasing temperature from room temperature to 700°C, and a black dotted line (**Temp decrease**), recording the magnetic susceptibility of the sediment sample in response to decreasing temperature from 700°C to room temperature.

4.3.3 First order reversal curve (FORC) diagram

The FORC distributions (**Figure 4.7**) are all broad and characterized by concentric and elongated contour, suggesting that the magnetic particles in initial and end-point sediments all exhibit mixed vortex state to multi-domain (MD) type of behaviour. The contour plots of end-point sediments, especially of the 2 experiments with ROC augmentation, GW+ace and GW+lac, showed significant peaks at around B_C = 10 mT, suggesting the likely formation of smaller particles of magnetite during the experiment. For all 5 diagrams, the contours intersecting the B_U axis with very low magnetic coercivity (B_C) represent super paramagnetic (SP) particles with high interactions, while the closed contours with peaks around 10 mT and vertical spread represent interactive single domain (SD) particles. The elongated contours extending to over 100 mT along the B_C axis showed much higher magnetic coercivity than SP particles, while compressing along the B_U axis indicating very low magnetic

interaction, suggesting the likely presence of goethite.

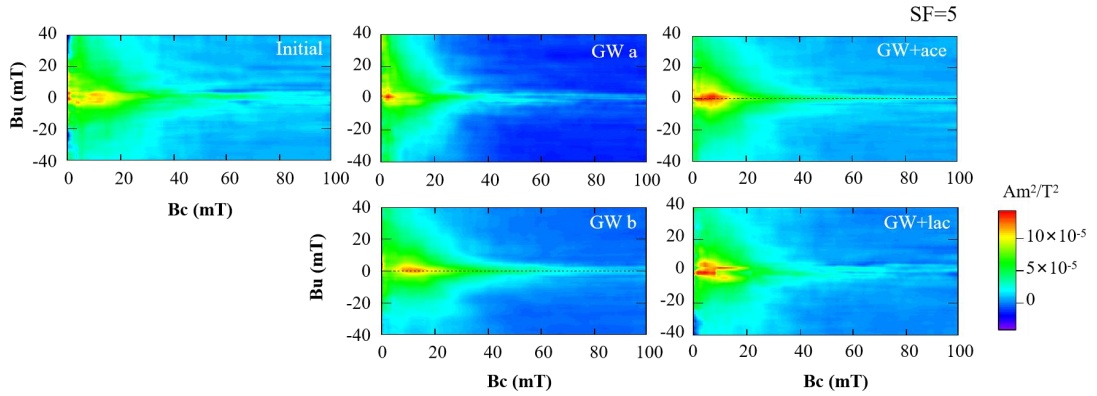

Figure 4.7 FORC diagrams of initial and end-point sediment samples: The FORC diagrams of initial and end-point sediments, are plotted and represented in (B_C, B_U) coordinates, with B_C as the magnetic coercivity and B_U corresponds to the distribution of interaction fields, where the blue indicates negative regions that are a fundamental component of the magnetic response of SD particle systems (Newell, 2005).

After being heated to 700°C during the χ-T analysis, the mineral composition significantly changed, and exhibited similar FORC distribution (**Figure 4.8**) for all sediments, suggesting the likely transformation from goethite to SD particles of magnetite, while smaller particles with high magnetic interactions remained.

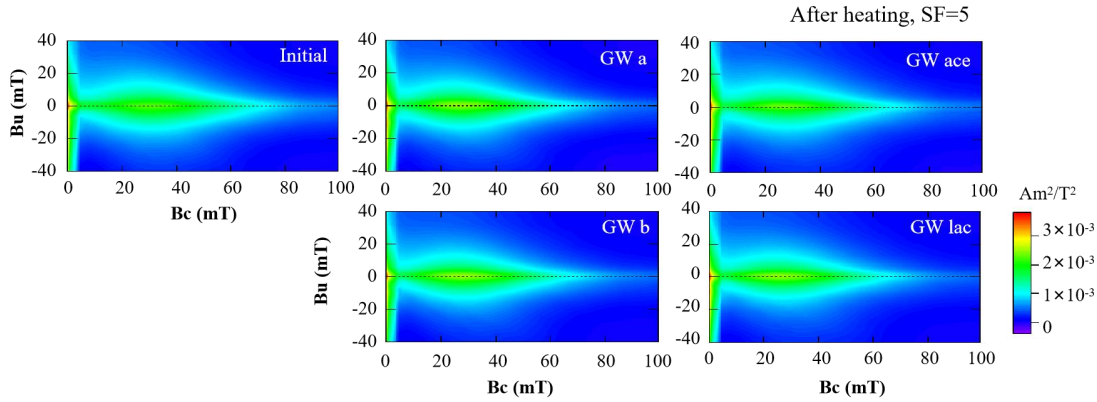

Figure 4.8 FORC diagrams of samples after χ-T heating: The FORC diagrams of initial and end-point sediments after being heated from room temperature to 700°C as in *3.3.2*, are plotted and represented in (B_C, B_U) coordinates, with B_C as the magnetic coercivity and B_U corresponds to the distribution of interaction fields, where the blue indicates negative regions that are a fundamental component of the magnetic response of SD particle systems (Newell, 2005).

4.3.4 Scanning magnetic particles

Magnetically separated particles from end-point sediments of GW a were found with large quantity of small grains (< 20 μm) consist of mostly Fe (75.85%, atomic concentration), followed by Cr (18.75%) and Ni (5.73%) (**Figure 4.9a**). Larger flakes were also found consisted of mostly O (34.67%,), Si (25.03%), Mg (10.18%) (**Figure 4.9b**) or O (38.09%), Si (20.56%), Fe (18.73%) (**Figure 4.9c**).

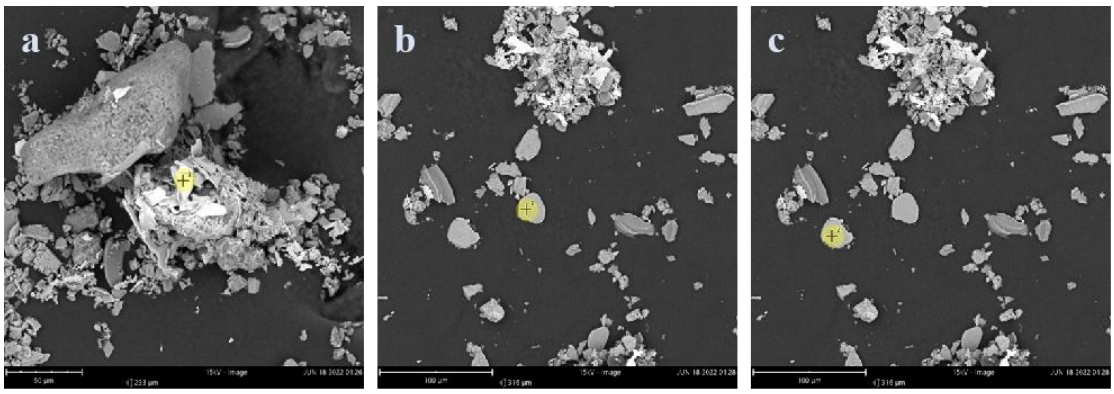

Element	Atomic Conc.	Weight Conc.
Fe	75.85	76.63
Cr	18.75	17.64
Ni	5.40	5.73

Element	Atomic Conc.	Weight Conc.
Si	25.03	21.34
Br	8.52	20.65
Fe	9.96	16.87
O	34.67	16.83
K	8.50	10.08
Mg	10.18	7.51
Sr	1.77	4.72

Element	Atomic Conc.	Weight Conc.
Fe	18.73	31.58
Br	9.51	22.94
O	38.09	18.41
Si	20.56	17.44
Mg	13.11	9.63

Figure 4.9 Magnetically separated particles from end-point sediment of GW a: The figure shows 3 flakes (< 50 μm) of the magnetically separated particles, with black crosses in yellow circle indicating the point detected with SEM-EDS for element concentrations.

4.4 Sediment microbial ecology

Analysis of the groundwater and sediments have shown evidence of iron oxidation, iron reduction and sulfate reduction, to ascertain if these processes are mediated by microorganisms, we further analyzed the microbial communities in sediments before and after the experiment. **Figure 4.10** presents the relative abundances of dominant (elative abundances > 10%) microbes in initial and end-point sediments. The microbial communities in initial sediments were dominant by *Burkholderia* (39.3%), *Acinetobacter* (16.5%), and *Enterobacteriaceae* spp. (10.82%). *Burkholderia* was also

found prominent in aquifer sediments of high arsenic regions in India and Bangladesh (Das et al., 2017; Layton et al., 2014). It was demonstrated as playing key roles in microbial mineral weathering and arsenic mobilization (Mailloux et al., 2009). In addition, *Acinetobacter* was also found abundant (16.5%), which was reported to be commonly dominant in typical high arsenic sediments in Hetao Plain (Wang et al., 2014), and *Enterobacteriaceae* spp. (10.82%) as well. *Enterobacteriaceae* is known for arsenic-resistance in various arsenic-contaminated environments, together with *Pseudomonadaceae* (Sultana et al., 2011; Turpeinen et al., 2004). In end-point sediments, however, *Enterobacteriaceae* spp. was not found, while relative abundance of *Pseudomonadaceae* spp. increased from 0 in initial sediments to as high as 10.16% (GW+ace).

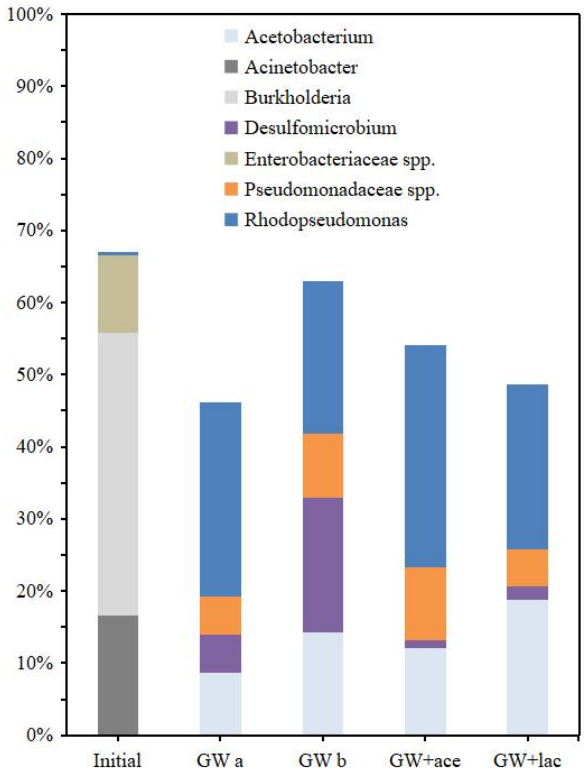

Figure 4.10 Dominant bacteria (relative abundances > 10%), at the genus level, in initial and end-point sediments: Panels from left to right show the initial and end-point sediments of the 4 experiments with blank treatment, including GW+ace with acetate augmentation and GW+lac with lactate augmentation. The dominant bacteria are identified as genera with relative abundances above 10% in any of of the 5 sediments. The relative abundances were acquired by DNA extraction from 0.5 g of sediments, 16S rRNA gene sequencing and analysis.

The genus with the highest relative abundance (>39%) in initial sediments, *Burkholderia*, were also rendered negligible in end-point sediments of all 4 columns, leaving *Acetobacterium* and *Rhodopseudomonas* relatively the most abundant genera.

4.4.1 Iron metabolizing bacteria enriched during the experiment

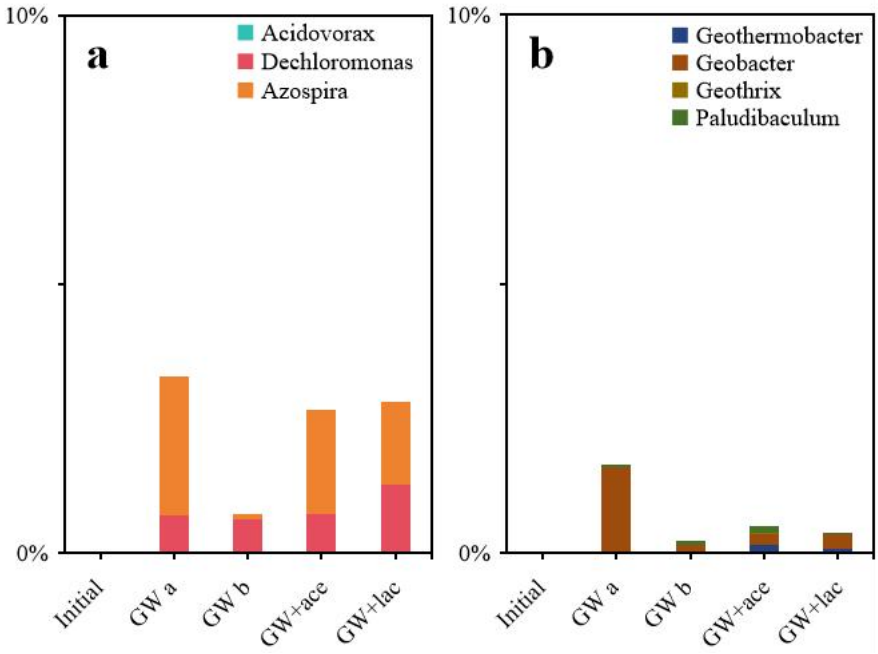

Figure 4.11 Relative abundances of (a) NDFO bacteria and (b) FRB, at the genus level, in initial and end-point sediments: Panels from left to right show the initial and end-point sediments of the 4 experiments with blank treatment, including GW+ace with acetate augmentation and GW+lac with lactate augmentation. The relative abundances were acquired by DNA extraction from 0.5 g of sediments, 16S rRNA gene sequencing and analysis.

Although the 4 experiments were not treated with iron and nitrate, NDFO bacteria *Dechloromonas* and *Azospira* were still found in the end-point sediments, although abundance of *Azospira* was particularly low (0.12%) for GW b, compared with the rest 3 experiments (2.0±0.5%) (**Figure 4.11a**). Among all possible FRB, the genus *Geobacter* were found with the highest relative abundance in all end-point sediments, whereas typical FRB were negligible in initial sediments (**Figure 4.11b**). With acetate amendment, the increase in relative abundances of *Geothermobacter* and *Paludibaculum* were relatively significant in column GW+ace, comparing with columns GW a and GW b, while with lactate amendment, only *Geothermobacter* increased evidently in column GW+lac.

4.4.2 Enrichment of SRB during the experiment

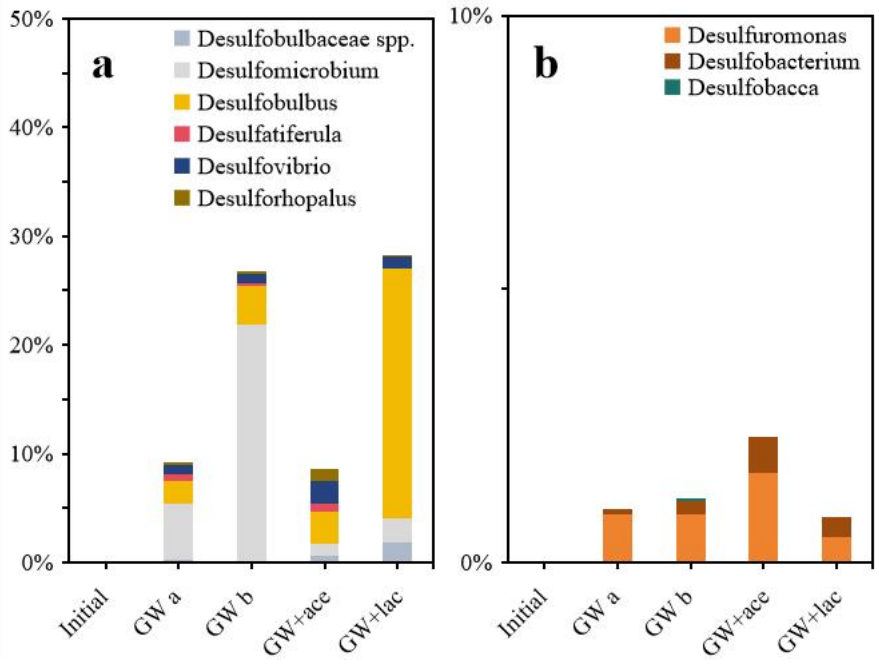

Figure 4.12 Relative abundances of SRB (a) incapable and (b) capable of completely degrading acetate, at the genus level, in initial and end-point sediments: Panels from left to right show the initial and end-point sediments of the 4 experiments with blank treatment, including GW+ace with acetate augmentation and GW+lac with lactate augmentation. The relative abundances were acquired by DNA extraction from 0.5 g of sediments, 16S rRNA gene sequencing and analysis.

We found in end-point sediments various possible SRB enrichment, including *Desulfomicrobium*, *Desulfobulbus*, *Desulfatiferula* (Hakil et al., 2014), *Desulfovibrio*, *Desulforhopalus*, *Desulfobulbaceae* spp., capable of incomplete oxidation of organic carbon to acetate, while also *Desulfobacterium* (Zhang et al., 2022), *Desulfobacca* and *Desulfuromonas* (Gebhardt et al., 1985) that are capable of completely oxidizing organic compounds (**Figure 4.12**). None of these genera was found in initial sediment. Particularly, *Desulfomicrobium* in end-point sediments of column GW b, and *Desulfobulbus* in end-point sediments of column GW+lac were found significantly enriched in relative abundance. In end-point sediment of GW+ace, with acetate augmentation, SRB incapable of completely degrading organic carbon were less abundant but more diverse among genera, while SRB capable of complete degradation were found more abundant.

4.5 Discussion

4.5.1 Arsenic mobilization, immobilization and speciation

Mobilization of arsenic were observed during the treatment, in not only ROC amended experiments, but all, most likely due to the dilution of influent with DI water, the similar reason held accountable for arsenic mobilization in some previous incubation experiments (van Geen et al., 2004). The disturbance of redox conditions by dilution, however, is most likely responsible for the abrupt drop of effluent arsenic concentrations after we resumed influent as sole fresh groundwater after the the treatment finished.

Existing push-pull tests conducted in Central Bangladesh, injecting shallow groundwater containing elevated concentration of arsenic to oxidized brown sediments of deeper aquifer containing lower concentration of arsenic, found adsorption of arsenic much more significant than potential release through reduction of iron oxyhydroxides (Radloff et al., 2011). In this study, we introduced a less reducing deeper groundwater as influent to sediments from a shallower aquifer with similar level of arsenic, and achieved arsenic immobilization as well.

Arsenic speciation transformation provides a critical perspective. The reduction of As(V) to As(III), rather than the reductive dissolution of iron oxides, was arguably responsible for arsenic mobilization under anaerobic conditions with the presence of arsenic reducers (Ahmann et al., 1997). After the experiment, strongly absorbed arsenic phases largely decreased in sediment, with strongly absorbed As(V) almost disappeared. Meanwhile, effluent As(III) : As(V) ratio was not so different comparing with the influent, further supported the reduction of As(V) to As(III).

4.5.2 Sulfides as plausible sinks for arsenic

Arsenic immobilization could be stimulated by sulfate reduction, by precipitating as sulfide minerals, being adsorbed or incorporated into iron sulfide minerals, or bound to organic carbon via sulfur (Planer-Friedrich, 2023). In this study, sulfate reduction

turned out to be significant in every column experiment, resulted in precipitation of newly formed sulfide minerals. This was first evidenced by the widening gap between effluent and influent sulfate concentrations (**Figure 3.4, Figure 4.3**), sediment color turning blackish in all columns at the end of the experiment (**Figure 3.6, Figure 4.5**) and the strong H_2S odour during HCl extraction, then confirmed by results of AVS extraction (**Table 3.4, Table 4.4**). With relatively low dissolved Fe(III), it is not likely that Fe(III) reduction out-competed sulfate reduction, as suggested by Kirk et al. (2004) and Xia et al. (2019). The significant increase of sulfate reducers in relative abundance in sediments also indicate that these enriched microorganisms had most likely participated in the sulfate reduction processes (**Figure 3.15, Figure 4.12**). The enrichment of SRB could be a result of less salinity stress from influent groundwater, of which the salinity was lower than initial site groundwater, since high salinity can inhibit SRB activities in sulfate-rich systems (Wang et al., 2022). Sulfate reduction can promote the transformation of Fe(III) minerals to amorphous FeS in the presence of abundant iron hydroxides while low dissolved sulfide, or promote arsenic sulfide precipitation with excess dissolved sulfide and limited dissolved iron (Kocar et al., 2010).

Based on influent and effluent concentrations, the estimated total arsenic trapped were 1.1 μmol during experiments GW a and b, while 1.7 μmol during experiments GW+Fe+NO_3 a and b, on average. Meanwhile, total sulfate consumed were 51 mmol during experiments GW a and b, on average, while 57 mmol during experiments GW+Fe+NO_3 a and b, on average. Although arsenic in shallow groundwater usually remains mobile under sulfate- and iron-reducing conditions, it was likely due to the low sulfate level in groundwater, hence insufficient sulfide to precipitate and to immobilize arsenic (Zheng et al., 2004). In this study, influent groundwater sulfate was higher than initial site, hence providing excess sulfate to the experimental system. While sulfate reduction was strong, effluent dissolved sulfide was undetectable with spectrophotometry throughout the experiment, indicating authigenic sulfides were mostly consumed or precipitated, as sulfide (proved by AVS extraction) or sulfur

(evidence from microbial analysis). Lowered As in effluent probably resulted from continuing sulfide precipitation.

Ammonia was significantly lowered in effluent (**Figure 4.4**), indicating that ammonia could have served as an electron donor in this study. Apart from influent DOC (6.0 mg/L) and Fe(II), sulfate reduction could also have been supported by ammonium oxidation through sulfate dependent ammonium oxidation (SRAO, or Sulfammox), although the mechanism and kinetics of the process, as well as the identification of related microorganisms are not well known (Liu et al., 2021; Makinia et al., 2021).

4.5.3 Mass balance reveals arsenic trapped with sulfide precipitation

To overview arsenic trapped with sulfide precipitation more quantitatively, we did mass balance estimation on arsenic, iron and sulfur during experiment in molar amounts (**Table 4.7**). The molar ratio of trapped As : Fe during the experiment were 1 : 326 for GW+Fe+NO_3 a and b, while 1 : 20 for GW a and b, all without ROC amendment. To examine the impact of Fe(II) and nitrate treatment solely, we estimated the net trapped As : Fe to be 1 : 918, by subtracting the amount trapped (average) during experiments GW a and b columns from the amount trapped (average) during experiments GW+Fe+NO_3 a and b. To compare, the trapped As : Fe molar ratios were 1 : 22 (at YCA site) and 1 : 210 (at YCB site) in previous field push-pull experiments (Sun, 2021), and approximately 1 : 2000 in the laboratory column experiment (Sun et al., 2016a). Other column experiments, mimicking similar (high sulfate, dry climate, high alkalinity and salinity) environment, found that arsenic can be immobilized in the form of As(III)-S precipitation when S : Fe > 1 and S : As > 100 (Kumar et al., 2020). Sun (2021) in the single well push-pull tests found As_2S_3 increased significantly in end-point sediments in both sites, also indicated that sulfate reduction and sulfide precipitation could have played a significant role in arsenic immobilization.

In this study, experiments GW+Fe+NO_3 a and b did trapped more sulfate, among which 24% transformed into AVS, compared to 19% for GW a and b. Trapped arsenic

in end-point sediments of GW+Fe+NO_3 a and b were less associated with AVS, compared with GW a and b, indicating reduced sulfate most likely had transformed into more stable sulfide minerals or solid sulfur that was not easily extractable. Meanwhile, 61% of net trapped sulfate eventually formed AVS, estimated by subtracting results of GW a and b from GW+Fe+NO_3 a and b. Simultaneously extracted iron and arsenic results showed that AVS associated arsenic represented 39% (average) of total trapped arsenic during experiments GW a and b, and 33% (average) during GW+Fe+NO_3 a and b, while only 25% of the net trapped arsenic by Fe(II)-nitrate treatment were AVS associated. This indicates that the net effect of Fe(II)-nitrate treatment might have significantly reduced the tendency (by 42%) of immobilizing arsenic by sulfide precipitation.

Table 4.7 Mass balance estimation during experiment in molar amounts.

Parameters	Unit	GW+Fe+NO_3 a	GW+Fe+NO_3 b	GW+Fe+NO_3+ace	GW+Fe+NO_3+lac	GW a	GW b	GW+ace	GW+lac	GW_{avg}	GW+Fe+NO_{3avg}	Net_{avg}
Trapped As	µmol	1.7	1.66	1.68	1.75	1.02	1.19	1.26	1.07	1.11	1.68	0.57
Trapped Fe	µmol	567	527	727	759	18.4	20.6	16.2	15.9	19.5	547	528
Trapped SO_4^{2-}	µmol	383	325	236	172	239	389	218	291	314	354	40
New P-ext As	µmol	0.05	0.18	-0.04	0.05	-0.04	-0.1	-0.04	-0.08	-0.07	0.11	0.18
New Cl-ext Fe	µmol	389	326	243	221	274	367	243	292	320	357	36.9
New AVS	µmol	96.7	70.7	35.4	11	27.7	90.9	50.9	55.2	59.3	83.7	24.4
New SEM-Fe	µmol	1792	499	1059	1109	437	784	999	1404	611	1145	534
New SEM-As	µmol	0.9	0.22	0.66	0.52	0.31	0.56	0.78	0.74	0.43	0.56	0.13
AVS/trapped-SO_4^{2-}		0.25	0.22	0.15	0.06	0.12	0.23	0.23	0.19	0.19	0.24	0.61
SEM-As/AVS		0.01	0.00	0.02	0.05	0.01	0.01	0.02	0.01	0.01	0.01	0.01
SEM-As/trapped-As		0.53	0.13	0.39	0.30	0.30	0.47	0.62	0.69	0.39	0.33	0.23

For mass balance estimation, the following parameters were calculated. Trapped As, Fe and sulfate amounts were estimated by integrating the area between effluent and influent data curves. New extractable As and Fe were estimated by deducting initial sediment extractables from end-point results, as: [$conc_{end\text{-}point}$ - $conc_{initial}$] · [sediment weight] ÷ [molar weight]. New AVS and simultaneously extracted metal (SEM) were estimated by subtracting initial sediment AVS and AVS-SEM from end-point results, as: [$conc_{end\text{-}point}$ - $conc_{initial}$] · [sediment weight] ÷ [molar weight]. Molar ratios were calculated using the aforementioned data. GW_{avg} = average(GW a, GW b), GW+Fe+NO_{3avg} = average(GW+Fe+NO_3 a, GW+Fe+NO_3 b). Net_{avg} = GW+Fe+NO_{3avg} - GW_{avg}, estimates the net impact of Fe(II)-nitrate treatment.

The mass balance with our assumptions reveals that feeding with high sulfate reducing groundwater will lead to arsenic immobilization mostly through sulfate reduction and sulfide precipitation, while Fe(II)-nitrate treatment resulted in less As trapped by sulfide precipitation. Sulfur maybe formed during the process, as sulfur-reducing *Desulforomonas* was found relatively abundant in all columns, and especially in ferrous iron and nitrate treated ones.

By calculating the stoichiometry with total trapped iron, arsenic and sulfate, we came up with the newly formed minerals as $Fe_{326}AsS_{211}$, $Fe_{433}AsS_{140}$, $Fe_{433}AsS_{98}$ for GW+Fe+NO_3 a, GW+Fe+NO_3 b, GW+Fe+NO_3+ace and GW+Fe+NO_3+lac, respectively, and $Fe_{18}AsS_{283}$, $Fe_{13}AsS_{173}$, $Fe_{15}AsS_{272}$ for columns GW a, GW b, GW+ace and GW+lac, respectively. Comparing arsenic trapped and newly formed iron minerals, Fe : As molar ratios were 22 : 1 and 210 : 1 for the field experiments at site YCA and YCB, respectively (Sun, 2021) and 2000:1 for laboratory column experiment (Sun et al., 2018). The Fe : As ratios of the GW column series are closer to the ratio 4.5 : 1 in newly formed As-magnetite by microbial mediated reduction of iron oxide (Rawson et al., 2016).

If we assume iron and sulfate consumed primarily precipitated as FeS, then we can have:

$Fe_{115}As$·211FeS for columns GW+Fe+NO_3 a and b (average)

$Fe_{293}As$·140FeS for column GW+Fe+NO_3+ace, and

$Fe_{335}As$·98FeS for column GW+Fe+NO_3+lac

respectively, and

18FeS·AsS_{265} for columns GW a and b (average)

13FeS·AsS_{160} for column GW+ace, and

15FeS·AsS_{257} for column GW+lac,

respectively.

We can reveal from this more clearly that although the 4 column experiments without iron and nitrate treatment all immobilized considerable amount of arsenic, it was most likely the result of sulfide precipitation with arsenic. Meanwhile, ROC amendment seemed to have inhibited sulfide precipitation significantly. Lactate amendment strongly inhibited sulfide precipitation in the Fe(II)-nitrate treatment experiments, while had almost no such impact during the GW experiments. Acetate amendment didn't inhibit sulfide precipitation as effectively as lactate amendment in the Fe(II)-nitrate treatment experiments, yet significantly impacted the GW experiments. We now turn to the different ROC amendment and their impact.

4.5.4 Acetate amendment significantly inhibited sulfate reduction

With acetate amendment, total sulfate trapped in column GW+ace during the experiment was 218 μmol, much lower than 291 μmol in lactate amended column GW+lac, and 314 μmol (on average) in non-amended columns GW a and b. Even more, column GW+ace immobilized more arsenic and has higher phosphate extractable (strongly-absorbed) arsenic in its sediments after the experiment than non-amended columns. From microbial community analysis, we know that most of the SRB present were of the type capable of only incomplete oxidation of organic carbon to acetate, hence acetate amendment did not stimulate the growth of SRB. The more balanced SRB community in end-point sediments of GW+ace could also be a result of this, with *Desulfobacteria* and *Desulforomonas*, the few SRB capable of completely oxidizing acetate to CO_2 (Gebhardt et al., 1985), found more abundant than in others. Qian et al. (2015) found that different SRB exhibit distinct preferences or dependencies on specific sulfur sources in bioreactors. Notably, *Desulfomicrobium* prefers sulfite, whereas *Desulfobulbus* favors sulfate.

Nitrate can inhibit sulfide formation from sulfate reduction in the water system (Sørensen, 1987), while ROC, such as acetate and lactate, has been widely known for

stimulating sulfate reduction. In this study we observed that only lactate amendment enhanced sulfate consumption during the amendment, but in the long run ROC amendment inhibited sulfate reduction, especially with acetate amendment. Meanwhile, sulfate consumption was relatively stable during GW experiments with inevitable long-term exposure of nitrate from groundwater. It is possible that ROC enhanced other processes that also consume sulfide, reducing available sulfide for precipitation. This is possible since sulfide is known as an intermediate in nitrate dependent oxidation of ROC such as lactate (Hubert and Voordouw, 2007). In deed, almost no dissolved sulfide was detected in effluent during the experiment. Some chemolithoautotrophic denitrifying bacteria are capable of oxidizing sulfide to sulfate anaerobically using nitrate. Culture enrichment study suggest that acetate can be utilized by chemolithotrophic denitrifiers, and enhance denitrification and complete oxidation of sulfide to sulfate (Cardoso et al., 2006). Acetate might have not directly affect sulfate reduction process, but inhibited sulfide precipitation through enhancing sulfide utilization and re-oxidation to sulfate, hence an likely answer to the lower net trapped sulfate for column GW+ace.

Tufano and Fendorf (2008) in column experiments inoculated with dissimilatory iron reducing *Shewanella putrefaciens*, found the transformation of ferrihydrite to secondary biogenic goethite or magnetite increased arsenic retention, with 0.8 mmol/L lactate amendment achieved the highest magnetite composition in solid phases. This directly emphasized the important role of ROC in enhancing microbial dissimilatory iron reduction in carbon-poor groundwater system, and especially in forming mixed valence iron minerals such as magnetite.

Since sulfide and oxyhydroxide minerals are primary arsenic sinks in groundwater systems, ROC amendment may be the key to stimulating certain mineral (trans)fomation selectively for remediation purposes.

Chapter 5 Immobilizing arsenic by iron and nitrate treatment: interference from phosphate

This chapter presents a study of laboratory column experiments on immobilizing arsenic by iron and nitrate treatment with phosphate interference from (artificial) groundwater, for phosphate can compete with arsenic during immobilization by adsorption, to investigate possible mineral transformation and the impact of phosphate interference. As detailed in *2.3 Laboratory based column experiments*. The experiments are:

Table 5.1 Experimental

Experiment	Treatment
AGW+Fe+NO_3 a & b	10 mmol/L $NaNO_3$/$FeSO_4$
AGW a & b	non
AGW abio	non

In order to mimic the *in situ* remediation process (Sun, 2021), the column experiment went through 3 periods: **Pre-treatment**: 8 PV/day (1.0 mL/hour) for 6 days, then 4 PV/day for 6 days; AGW containing 3 μmol/L arsenite, 10 μmol/L phosphate and 1 mmol/L lactate. **Treatment**: 4 PV/day for 1 day, then 8 PV/day for 9 days; 10 alternative injection cycles (24 hours) of Fe-AGW (11:00-21:00) and Nitrate-AGW (21:00-11:00) for the AGW+Fe+NO_3 experiments, while the AGW experiments were continuously fed with only AGW without any treatment. **Post-treatment**: 8 PV/day for 58 days; AGW only.

Results are presented in 3 sections: effluent pH monitoring, effluent arsenic and phosphorus,effluent iron and sulfur. The presence of sulfate and lactate in influent AGW led to the likely formation of sulfide minerals, although with iron and nitrate treatment no significant sulfate consumption and sulfide precipitation was observed. Phosphorus competed with arsenic for adsorption sites, with concurrent arsenic mobilization and phosphorus immobilization observed after a long period of stable arsenic immobilization. The process was likely controlled by the transformation of minerals and arsenic species.

5.1 Effluent pH monitoring

Effluent pH of AGW experiment stayed around 7.6, slightly above the influent level of 7.5, for more than 300 PV, before went up to 8 at the end of the experiment (**Figure 5.1**). For the AGW+Fe+NO_3 experiment, effluent pH stayed around the influent level of 7.5 during the pre-treatment equilibrium.

During the treatment, fluctuation of effluent pH during the treatment was observed, since the iron and nitrate were injected alternatively instead of simultaneously. The pH of effluents went down to around 7.1 during Fe-AGW injection, and to around 7.3 during Nitrate-AGW injection. Noted that the pH of the initial AGW was around 7.5, of the Fe-AGW solution (and its residue) was between 5.4 and 5.5, and of the nitrate-AGW solution (and its residue) was around 6.0. After the treatment, the effluent pH of AGW+Fe+NO_3 went up to around 7.9 and lasted about 40 PVs, then went down to around 7.5, the influent level, for nearly 200 PV, before went up again to 8.

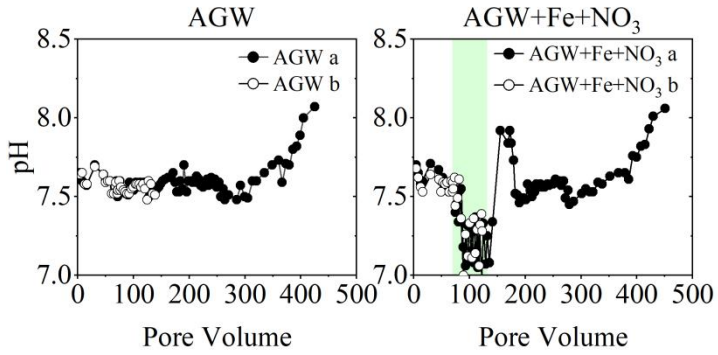

Figure 5.1 Effluent pH versus pore volume: Effluent pH of AGW a and AGW b, experiments fed with only AGW, and AGW+Fe+NO_3 a and AGW+Fe+NO_3 b, experiments with iron and nitrate treatment, are plotted against pore volume. The treatment period was emphasized with the light green shade area, during which Fe-AGW and Nitrate-AGW were alternatively injected into the columns. The pH of the influent AGW was around 7.5, of the Fe-AGW was from 5.4 to 5.5, and of the Nitrate-AGW was around 6.0.

5.2 Arsenic and phosphorus immobilization

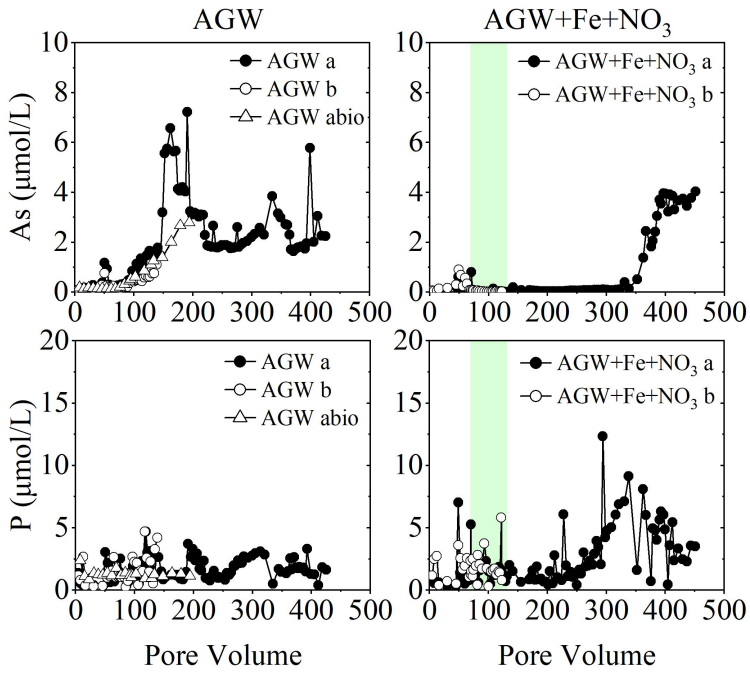

Figure 5.2 Effluent arsenic and phosphorus versus pore volume: Effluent arsenic (As) and phosphorus (P) of AGW a, AGW b, and abiotic (autoclaved sediments) AGW abio, experiments fed with only AGW, and AGW+Fe+NO3 a and AGW+Fe+NO3 b, experiments with iron and nitrate treatment, are plotted against pore volume. The treatment period was emphasized with the light green shade area, during which Fe-AGW and Nitrate-AGW were alternatively injected into the columns. The influent levels are 3 µmol/L for arsenic (as arsenite) and 10 µmol/L for phosphorus (as phosphate), throughout the experiment.

Effluent arsenic of AGW a, b and abio stayed low for around 100 PV during the early stage of equilibrium, then experienced a similar trend of recovery between 100 and 150 PV (**Figure 5.2**). Effluent arsenic of AGW a exceeded influent level of 3 µmol/L at around 150 PV and lasted for nearly 50 PV, then lowered to around 2 µmol/L with fluctuations and gradual rise to above 3 µmol/L again after 300 PV, indicating mobilization of arsenic from sediments. Although AGW abio were terminated early, we could still see that AGW abio experienced a slower recovery (about 200 PV) of effluent arsenic, and did not exceed the influent level, likely resulted from the mineral transformation during sterilization. It was terminated due to clogging, a problem similarly observed on sterilized abiotic column in previous experiments (Li, 2018).

Effluent phosphorus concentrations of the AGW experiments experienced drops when effluent arsenic quickly rose from around PV 150. After effluent arsenic peaked and started to drop, effluent phosphorus concentration rose and peaked, then fluctuated more or less in step with effluent arsenic.

With iron and nitrate treatment, breakthrough of effluent arsenic of experiments AGW+Fe+NO_3 was significantly delayed, comparing with the AGW experiments, accompanied with rather stable and low level of re-mobilization near the end of the experiment. At first. effluent arsenic concentrations experienced a similar equilibrium process before the treatment, with a slow recovery to 1 μmol/L before the treatment started. During the treatment, effluent arsenic concentrations were always lower than 10 μg/L, the WHO guideline level, and lasted for about 200 PV after the iron and nitrate treatment. Then, effluent arsenic concentrations gradually recovered to influent level in approximately 50 PV, rose further to slightly above the influent level and lasted for the rest of the experiment. The effluent arsenic concentrations started to rise at around 350 PV, reached the influent level of 3 μmol/L in about 50 PV, then kept rising to as high as 4 μmol/L, and remained between 3 and 4 μmol/L for the rest of the experiment, with fluctuations. The effluent arsenic concentrations elevated above influent level indicates re-mobilization of the once sequestered arsenic.

The effluent phosphorus concentrations of AGW+Fe+NO_3 experiments were kept low from the start of the experiment and started to rise at around 250 PV (about 100 PV ahead of the rise of arsenic concentrations), and reached the highest level, close to the influent concentration of 10 μmol/L, at around 350 PV. It was exactly when effluent arsenic concentrations started to rise, the effluent phosphorus concentrations peaked and started to drop, then remained a relatively low level about 1/3 of the influent concentration, till the end of the experiment.

5.3 Iron and sulfur utilization

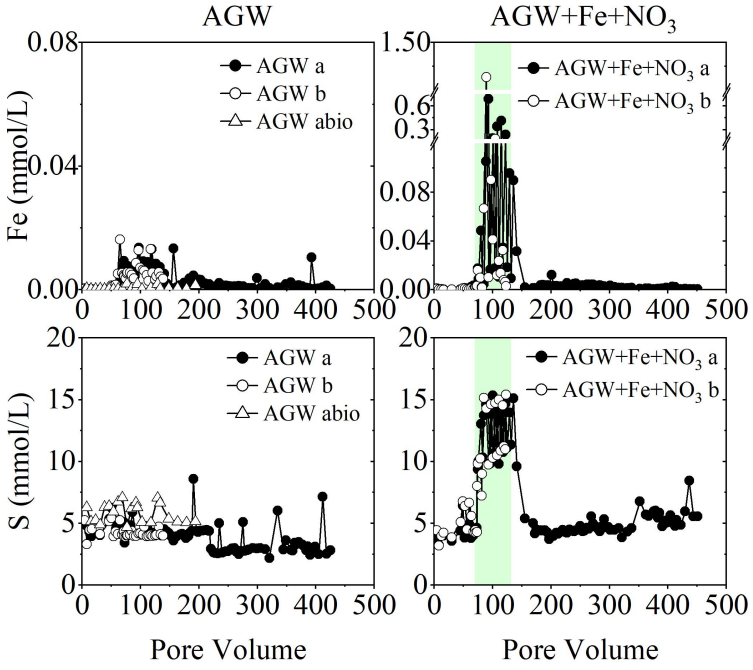

Figure 5.3 Effluent iron and sulfur concentrations versus pore volume: Effluent iron (Fe) and sulfur (S) of AGW a, AGW b, and abiotic AGW abio, experiments fed with only AGW, and AGW+Fe+NO_3 a and AGW+Fe+NO_3 b, experiments with iron and nitrate treatment (emphasized with the light green shade area), are plotted against pore volume. The influent levels are 0 mmol/L of iron and 5 mmol/L of sulfur (as sulfate), throughout the experiment for AGW a and b, while before and after the treatment (during nitrate treatment as well) for AGW+Fe+NO_3 a and b, but 10 mmol/L of iron (as ferric iron) and 15 mmol/L of sulfur (as sulfate) during the iron treatment.

Effluent iron concentrations were 0.003±0.003 mmol/L for AGW a (n=99), 0.005±0.004 mmol/L for AGW b (n=35), and 0.0005±0.0006 mmol/L for AGW abio (n=21) (**Figure 5.3**). The stable and low effluent iron concentrations indicating no significant dissolution of iron minerals or dissolved iron re-precipitated rapidly. Meanwhile, effluent sulfur concentrations were 3.9±1.1 mmol/L for AGW a (n=99), 4.3±0.4 mmol/L for AGW b (n=35), and 5.8±0.8 mmol/L for AGW abio (n=21). Comparing with influent level of 5 mmol/L, we see AGW a, the longest-run experiment consumed the most sulfate from influent. Effluent sulfur concentrations of AGW a started to be much lower (3.2±0.9 mmol/L, n=44), compared with effluent sulfur concentrations before 220 PV (4.5±0.8 mmol/L, n=45), indicating the likely

enhanced sulfate utilization.

For AGW+Fe+NO_3 experiments, effluent iron concentrations were 0.016±0.015 mmol/L for AGW+Fe+NO_3 a (n=16) and 0.001±0.001 mmol/L for AGW+Fe+NO_3 b (n=16) during pre-treatment equilibrium, while 0.026±0.018 mmol/L for AGW+Fe+NO_3 a (n=63) during post-treatment observation, indicating no significant dissolution of iron minerals, or dissolved iron just re-precipitated rapidly. During the treatment, effluent iron concentrations were over ten times lower than the influent level of 10 mmol/L, and fluctuated frequently, resulted from the alternative injection between Fe-AGW and NO_3-AGW. The trend of lowering effluent iron concentration during the treatment likely indicates increasing rate of iron utilization. Meanwhile, effluent sulfur fluctuated as well and always within the range of influent levels, i.e. 15 mmol/L during Fe-AGW injection and 5 mmol/L during NO_3-AGW injection. Effluent sulfur concentrations were: 4.3±0.7 mmol/L for AGW+Fe+NO_3 a (n=16) and 4.8±1.0 mmol/L for AGW+Fe+NO_3 b (n=16), during the pre-treatment equilibrium; 12.3±2.1 mmol/L for AGW+Fe+NO_3 a (n=20) and 11.8±2.7 mmol/L for AGW+Fe+NO_3 b (n=18), during the treatment; while 4.9±0.8 mmol/L for AGW+Fe+NO_3 a (n=63) during the post-treatment observation.

5.4 Discussion

5.4.1 Iron and nitrate treatment restrained lactate-fueled sulfate reduction

Sulfide precipitation likely served as a significant sink for arsenic, at least for the AGW experiments. Although extraction for AVS was not performed for the end-point sediments, the dark precipitation formed during the experiment (**Figure 5.4**) and the hydrogen sulfide odor from the end-point sediment both supported the formation of sulfide. The initial aquifer sediments under the condition of simulated groundwater flow was capable of immobilizing considerable amount of arsenic during

pre-treatment equilibrium, indicating the likely presence of iron oxides with available adsorption sites. Although no dissolved iron was fed to columns without treatment, iron mineral transformation was still possible, as the sediment itself contained considerable amount of iron. The significantly lower effluent sulfur than influent, indicating utilization of aqueous sulfate, starting from 200 PV when effluent arsenic started almost simultaneously decreasing from 2 times the influent concentration to below the influent level. Since the artificial groundwater contained sulfate and lactate, the reducing conditions very likely have facilitated the both sulfate reduction and reductive dissolution of iron oxides, resulting in precipitation of iron sulfide minerals given the fact that almost no dissolved iron was found in effluent. Iron sulfides are natural arsenic sinks found in many natural aquifers, capable of immobilizing a considerable amount of arsenic. Meanwhile, excess sulfide could also precipitate with arsenic.

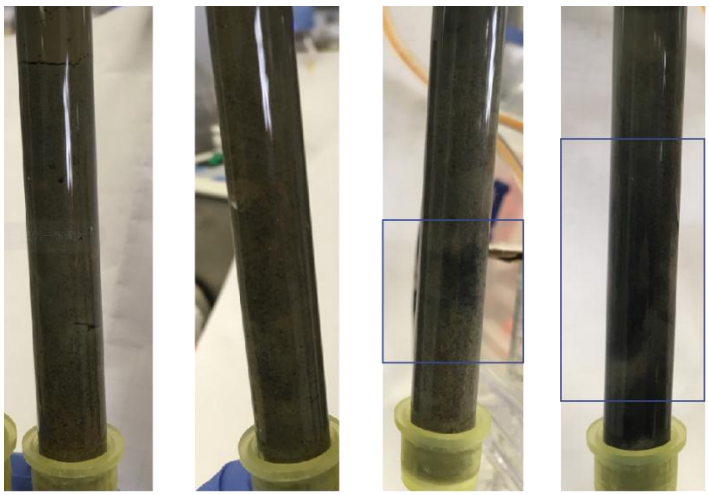

Figure 5.4 Photo of the columns at the end of the treatment: Photos were taken by the end of the iron and nitrate treatment for AGW+Fe+NO_3 experiments, at around 135 PV, 123 PV, 141 PV, and 138 PV for experiments AGW+Fe+NO_3 a, AGW+Fe+NO_3 b, AGW a and AGW b, respectively.

As for the iron and nitrate treatment experiments, it is highly likely that iron hydroxide precipitated as the pH going down during the treatment. Without

mineralogical analysis, we could only assume that some of the hydroxides then likely transformed into more crystalline minerals such as magnetite as the pH went up for a period after the treatment, as in laboratory experiments with similar settings (Sun et al., 2016a). The effluent iron concentrations during the alternate injection of Fe(II) and nitrate behaved very differently from those of the simultaneous injection experiments (Li, 2018; Sun et al., 2016a): almost all injected iron were consumed during the alternate injection, while only about half were consumed during simultaneous injection experiments with the same or lower influent concentration and column settings. The alternative injection switching between Fe-AGW and nitrate-AGW was to simulate the field experiments, based on the assumption that iron travels slower than nitrate in porous media, although the field push-pull test also recovered 57% and 62% of the total injected iron from the two research site during the pulling (Sun, 2021). Although sulfide precipitation was weaker for the iron and nitrate treated experiments, we still observed dark precipitation in later stage of post-experiment observation and odor of hydrogen sulfide at the end of the experiment. The increase of effluent sulfur could be related to the arsenic release and phosphorus immobilization at about the same time during the experiments, suggesting the possible transformation or dissolution of arsenic-bearing sulfide minerals.

Influenced by the transformation of minerals in sediments, the preferential immobilization of arsenic versus phosphorus during different stages may have exhibited distinct patterns. The behavior of arsenic concentration recovery during the first 150 PVs was similar for the AGW experiment and the abiotic column treated with only AGW containing arsenic, indicating that microbial communities may had little influence on mineral transformation and arsenic immobilization during this period. However, the abiotic sediments were achieved by autoclave, which could have changed the mineral composition in the sediments, hence a questionable sterilization method (Radloff et al., 2008).

5.4.2 Phosphate interferes both iron mineral transformation and arsenic immobilization

The competition for adsorption sites was likely re-balanced due to transformation of minerals, with effluent phosphorus concentrations peaked when effluent arsenic started breakthrough. Amorphous iron oxides are usually highly aggregated small particles with large surface area, hence the high capacity for adsorption (Schwertmann and Taylor, 1989). Amorphous iron oxides or hydroxides, can gradually increase in the degree of crystallinity over time (Schwertmann and Taylor, 1989), and transform into more thermodynamically stable minerals such as magnetite under reducing conditions (Sun et al., 2016a). The formation of goethite requires dissolution of ferrihydrite, while the formation of hematite requires the aggregation of ferrihydrite. Phosphate interference usually leads to adsorption onto ferrihydrite, hence inhibiting ferrihydrite dissolution and reducing goethite formation. Phosphate adsorption onto ferrihydrite may also inhibit ferrihydrite accumulation and transformation to hematite. The transformation of these minerals changes their capacity for arsenic adsorption, and sometimes releases incorporated arsenic, resulting the re-mobilization of initially immobilized arsenic. While the presence of phosphate competes with arsenic for adsorption sites, it could also interfered the mineral transformation processes that governed the mobilization and immobilization of arsenic.

In addition to the transformation of amorphous iron minerals formed during the iron and nitrate treatment to more crystalline minerals, arsenic species transformation could be a primary reason, although preservation and speciation analysis of was not accessible at the time. The adsorption of arsenic species is highly dependent on pH. Higher pH (> 7.5) and concentrations are in significant favor of the adsorption of arsenite over arsenate on ferrihydrite (Raven et al., 1998). Although arsenate was found with higher affinity for soil overall, when Fe(III) oxide is rich, arsenite can also display a higher affinity (Manning and Goldberg, 1997). Raven et al. (1998) also reported the high affinity of arsenite for amorphous iron oxides in pure solid phases.

Even in the presence of 0.5 mmol/L phosphate, the most effective extraction for arsenic, at most 18% arsenite were extractable from amorphous iron oxides (Jackson and Miller, 2000). While interference from influent sulfate likely resulted in precipitation of sulfides and immobilization of arsenic, the interference from influent phosphate competed with arsenic for sorption sites during immobilization due to its similar ionic radius and acid dissociation constant with arsenate (O'reilly et al., 2001). Phosphate can out-compete arsenate for sorption sites more effectively at higher pH, while out-compete arsenite more at lower pH, since a pH > 7.5 favors more arsenite adsorption over arsenate (Jackson and Miller, 2000). Adsorption experiments also found that the competitive effect of phosphate is stronger for arsenate than for arsenite, especially under alkaline conditions (Deng et al., 2018). The adsorption of phosphate on Fe(III) (hydro)oxides is stronger than that of arsenic, while the presence of high sulfide contents, especially those newly formed could have impact on the competitive adsorption between phosphate and arsenic species.

In laboratory column experiment performing simultaneous treatment of iron and nitrate, with an lower influent arsenic concentration of 100 μg/L, effluent arsenic started to recover only 50 PV after the treatment, and exceeded 10 μg/L after 100 PV (Sun et al., 2016). This study tried to mimic a field experiment that actually performed alternative injection of iron and nitrate by Sun (2021), and used the sediments from the same depth of the same research site. The alternative, instead of simultaneous, iron and nitrate treatment successfully kept effluents arsenic concentrations below or around 10 μg/L for about 200 PV. After all, the later arsenic concentration in effluents recovers, the better this strategy performs in arsenic immobilization. However, phosphate likely interfered both mineral transformation and arsenic adsorption, raised questions on the efficiency and stability of the iron and nitrate treatment approach on arsenic immobilization in anoxic groundwater. We also have no direct evidence to support the possible mineral transformation during the experiments that immobilized or mobilized arsenic, for lacking sediment

characterization. We suggest for future studies more parallel experiments to sacrifice during the process, with timing guided by monitoring effluent concentrations more timely, in order to provide cross-sectional information of the mineral transformation during the experiment, and to figure out the trigger for these processes.

Chapter 6 Conclusion

6.1 Revisiting research objectives

This study on immobilizing arsenic in anoxic groundwater by iron and nitrate treatment investigated (a) the divergence driven by reactive organic carbon augmentation on mineral transformation and arsenic immobilization in a carbon-poor groundwater system, (b) the impact of sulfate reduction and sulfide precipitation on arsenic immobilization, and (c) phosphate interference from the environment on mineral transformation and arsenic immobilization, in experimental systems balanced between artificial (laboratory) and natural (field) conditions, by conducting field investigations and performing long term field-based column experiments under anoxic conditions, as well as laboratory column experiment, in order to guide the development and improvement of future mitigation strategies for groundwater arsenic problem.

6.2 Overview of the main findings

- Retention of arsenic by iron and nitrate treatment is a complex process not only through mixed-valence iron mineral formation enhanced by NDFO, but also significantly by precipitation of sulfide produced from sulfate reduction.
- While sulfide precipitation presumably served as a major sink of arsenic, iron and nitrate treatment did immobilized more arsenic from groundwater, and increased the strongly absorbed arsenic phases in sediments.
- Iron and nitrate treatment significantly changes the microbial communities in aquifer sediments. ROC influenced the relative abundances of NDFO bacteria and SRB, which likely mediated iron and sulfur mineral (trans)formation in oligotrophic groundwater.

- ROC augmentation alone enhanced sulfate reduction and arsenic mobilization, yet when coupled to iron and nitrate treatment, it could stimulate NDFO while suppress sulfate reduction, resulting in lower sulfide precipitation and more mixed-valence iron mineral formation.
- Specifically, lactate enhanced arsenic immobilization by iron and nitrate treatment, by increased reactive Fe(III) and strongly absorbed As(V) phases in sediments. Acetate, on the other hand, inhibited microbial sulfate reduction and sulfide precipitation when amended alone.

6.3 Implications

Iron and nitrate treatment has been proved by this and many previous researches to be capable of enhancing iron mineral (trans)formation in anoxic aquifer sediments for stable arsenic sequestration. Groundwater arsenic can be successfully immobilized by newly formed iron and sulfur minerals.

This study has implications for both field and laboratory researches on mitigating groundwater contamination, by furthering our understanding on the controlling mechanisms of iron and sulfur mineral transformation in anoxic groundwater systems for arsenic immobilization. Stable immobilization of groundwater arsenic can be achieved through iron mineral (trans)formation and sulfide precipitation. Fe(II)-nitrate treatment successfully immobilized arsenic by increasingly forming more stable iron minerals and subsequent strong absorption. ROC augmentation, by providing labile carbon source addition to the carbon-poor groundwater system, favored microbial activities crucial to the transformation of iron minerals, while suppressed sulfide precipitation. The application of ROC augmentation demonstrated the potential to enhance the desired biogeochemical reactions during the remediation of anoxic groundwater with limited bio-available carbon. The findings are vital for the

development of effective *in situ* mitigation technology by shedding light on coupled biogeochemical cycles of arsenic, iron and sulfur in anoxic groundwater systems, which calls for augmentation of ROC together with iron and nitrate.

6.4 Limitations and recommendations for future research

In situ remediation of groundwater is difficult to simulate under laboratory conditions, as groundwater itself is a complex solution. Groundwater composition varies from one well to another, sometimes even when the wells are very close in distance, due to heterogeneity and small-scale preferential flow channels. Future researchers should attach great importance to this whenever a groundwater system is taken into consideration. Regarding technical limitations, this study examined mineral transformation or microbial community changing based on sediments at the start and end of the experiment, yet lacking direct evidences to reveal the status in between, which limited our understanding of the biogeochemical processes. Effluent concentrations of ROC could have also helped us understanding the chemical and microbial activities. Future study should consider sampling for sediment characterization and microbial community analysis at different stages, and including measurement of influent and effluent concentrations of ROC.

It is difficult to mimic real field conditions by laboratory column simulation of field groundwater remediation. This study tried its best in performing field-based column experiments, so as to apply fresh natural groundwater and sediment for the simulation, while making the most of column experiment's simplicity. Nonetheless, the study is limited for lack of process-based quantification. The numerical modelling simulation of the experiments can reproduce the concentration changes and mineral transformations during experiments, helping researchers identify and quantify the key processes governing arsenic immobilization and iron mineral transformation in anoxic groundwater systems. Future studies should conduct reactive transport modelling

based on the experiment results to further our understanding of the biogeochemical processes from more quantitative perspectives.

To date, *in situ* mitigation strategies for groundwater contamination aiming at formation of stable minerals using chemicals, e.g. iron and nitrate for magnetite formation, often underestimate the role of reactive organic carbon in fueling functional microbial activities in oligotrophic groundwater system. Future studies should carefully consider the combined use of reactive organic carbon, to stimulate functional microbial activities and produce target minerals *in situ* for mitigation.

List of references

Acton, G., Yin, Q.Z., Verosub, K.L., Jovane, L., Roth, A., Jacobsen, B., Ebel, D.S., 2007. Micromagnetic coercivity distributions and interactions in chondrules with implications for paleointensities of the early solar system. Journal of Geophysical Research: Solid Earth 112(B3).

Ahmad, A., Bhattacharya, P., 2019. Arsenic in drinking water: is 10 μg/L a safe limit? Current Pollution Reports 5, 1-3.

Ahmad, A., van der Wens, P., Baken, K., de Waal, L., Bhattacharya, P., Stuyfzand, P., 2020. Arsenic reduction to< 1 μg/L in Dutch drinking water. Environment International 134, 105253.

Ahmann, D., Krumholz, L.R., Hemond, H.F., Lovley, D.R., Morel, F.M., 1997. Microbial mobilization of arsenic from sediments of the Aberjona watershed. Environmental Science & Technology 31(10), 2923-2930.

Alam, M.F., Villholth, K.G., Podgorski, J., 2021. Human arsenic exposure risk via crop consumption and global trade from groundwater-irrigated areas. Environmental Research Letters 16(12), 124013.

Allen, H.E., Fu, G., Deng, B., 1993. Analysis of acid-volatile sulfide (AVS) and simultaneously extracted metals (SEM) for the estimation of potential toxicity in aquatic sediments. Environmental Toxicology and Chemistry 12(8), 1441-1453.

Aredes, S., Klein, B., Pawlik, M., 2012. The removal of arsenic from water using natural iron oxide minerals. Journal of Cleaner Production 29-30, 208-213.

Arrigo, K.R., 2005. Marine microorganisms and global nutrient cycles. Nature 437(7057), 349-355.

Benner, S.G., Blowes, D.W., Ptacek, C.J., 1997. A Full-Scale Porous Reactive Wall for Prevention of Acid Mine Drainage. Groundwater Monitoring & Remediation 17(4), 99-107.

Benner, S.G., Hansel, C.M., Wielinga, B.W., Barber, T.M., Fendorf, S., 2002. Reductive dissolution and biomineralization of iron hydroxide under dynamic flow conditions. Environmental Science & Technology 36(8), 1705-1711.

Borch, T., Kretzschmar, R., Kappler, A., Cappellen, P.V., Ginder-Vogel, M., Voegelin, A., Campbell, K., 2009. Biogeochemical redox processes and their impact on contaminant dynamics. Environmental science & technology 44(1), 15-23.

Bostick, B.C., 2001. Characterization of ion sorption on metal sulfide minerals using macroscopic and spectroscopic approaches, Department of Geological and Environmental Sciences. Stanford University.

Bostick, B.C., Fendorf, S., 2003. Arsenite sorption on troilite (FeS) and pyrite (FeS_2). Geochimica et Cosmochimica Acta 67(5), 909-921.

Bowell, R.J., Alpers, C.N., Jamieson, H.E., Nordstrom, D.K., Majzlan, J., 2014. The environmental geochemistry of arsenic—an overview. Reviews in Mineralogy and Geochemistry 79(1), 1-16.

Brandis-Heep, A., Gebhardt, N.A., Thauer, R.K., Widdel, F., Pfennig, N., 1983. Anaerobic acetate oxidation to CO 2 by Desulfobacter postgatei: I. Demonstration of all enzymes required for the operation of the citric acid cycle. Archives of microbiology 136, 222-229.

Brassington, R., 1988. Sources of information, Field Hydrogeology (Geological Society of London Professional Handbook). Open Univesity Press, Milton Keynes & Halsted Press, New York, pp. 30-35.

Burton, E.D., Johnston, S.G., Bush, R.T., 2011. Microbial sulfidogenesis in ferrihydrite-rich environments: Effects on iron mineralogy and arsenic mobility. Geochimica et Cosmochimica Acta 75(11), 3072-3087.

Burton, E.D., Johnston, S.G., Kocar, B.D., 2014. Arsenic Mobility during Flooding of Contaminated Soil: The Effect of Microbial Sulfate Reduction. Environmental Science & Technology 48(23), 13660-13667.

Byrne, J.M., Klueglein, N., Pearce, C., Rosso, K.M., Appel, E., Kappler, A., 2015. Redox cycling of Fe(II) and Fe(III) in magnetite by Fe-metabolizing bacteria. Science 347(6229), 1473-1476.

Callahan, B.J., McMurdie, P.J., Rosen, M.J., Han, A.W., Johnson, A.J.A., Holmes, S.P., 2016. DADA2: High-resolution sample inference from Illumina amplicon data. Nature methods 13(7), 581-583.

Cardoso, R.B., Sierra-Alvarez, R., Rowlette, P., Flores, E.R., Gomez, J., Field, J.A., 2006. Sulfide oxidation under chemolithoautotrophic denitrifying conditions. Biotechnology and bioengineering 95(6), 1148-1157.

Chakraborty, A., Picardal, F., 2013. Neutrophilic, nitrate-dependent, Fe (II) oxidation by a Dechloromonas species. World Journal of Microbiology and Biotechnology 29, 617-623.

Chaudhuri, S.K., Lack, J.G., Coates, J.D., 2001. Biogenic magnetite formation through anaerobic biooxidation of Fe (II). Applied and Environmental Microbiology 67(6), 2844-2848.

Chowdhury, S.R., Yanful, E.K., Pratt, A.R., 2011. Arsenic removal from aqueous solutions by mixed magnetite–maghemite nanoparticles. Environmental earth sciences 64, 411-423.

Chowdhury, T., 1998. Borehole sediment analysis probable source and mechanism of arsenic release to groundwater in affected districts of West Bengal, India, Int. Conf. on Arsenic Pollution of Groundwater in Bangladesh: Causes, effects and remedies. pp. 157-158.

Chowdhury, T.R., Basu, G.K., Mandal, B.K., Biswas, B.K., Samanta, G., Chowdhury, U.K., Chanda, C.R., Lodh, D., Roy, S.L., Saha, K.C., 1999. Arsenic poisoning in the Ganges delta. Nature 401(6753), 545-546.

Chowdhury, T.R., Mandal, B.K., Samanta, G., Basu, G.K., Chowdhury, P., Chanda, C., Karan, N.K., Lodh, D., Dhar, R.K., Das, D., 1997. Arsenic in groundwater in

six districts of West Bengal, India: the biggest arsenic calamity in the world: the status report up to August, 1995, Arsenic: exposure and health effects. Springer, pp. 93-111.

Dai, H., 2022. Bioavailability of Dissolved Organic Matter in Reducing Groundwater. Southern University of Science and Technology

Das, S., Bora, S.S., Yadav, R.N.S., Barooah, M., 2017. A metagenomic approach to decipher the indigenous microbial communities of arsenic contaminated groundwater of Assam. Genomics Data 12, 89-96.

Delany, J., Lundeen, S., 1991. The LLNL thermochemical data base--revised data and file format for the EQ3/6 package. Lawrence Livermore National Lab.(LLNL), Livermore, CA (United States).

Deng, Y., Li, Y., Li, X., Sun, Y., Ma, J., Lei, M., Weng, L., 2018. Influence of calcium and phosphate on pH dependency of arsenite and arsenate adsorption to goethite. Chemosphere 199, 617-624.

Dittmar, J., Voegelin, A., Maurer, F., Roberts, L.C., Hug, S.J., Saha, G.C., Ali, M.A., Badruzzaman, A.B.M., Kretzschmar, R., 2010. Arsenic in Soil and Irrigation Water Affects Arsenic Uptake by Rice: Complementary Insights from Field and Pot Studies. Environmental Science & Technology 44(23), 8842-8848.

Dixit, S., Hering, J.G., 2003. Comparison of arsenic (V) and arsenic (III) sorption onto iron oxide minerals: implications for arsenic mobility. Environmental science & technology 37(18), 4182-4189.

Dos Santos Afonso, M., Stumm, W., 1992. Reductive dissolution of iron (III)(hydr) oxides by hydrogen sulfide. Langmuir 8(6), 1671-1675.

Duan, Y., Liu, J., Yang, Y., Han, L., Li, Z., Gu, Y., Ma, Y., Palomo, A., Tuo, X., Zheng, Y., 2024. Large Quantity EDTA Addition and Cold Storage in Dark Recommended for Preserving Inorganic Arsenic Speciation in Reducing Groundwater. ACS ES&T Water.

Egli, R., 2013. VARIFORC: An optimized protocol for calculating non-regular first-order reversal curve (FORC) diagrams. Global and Planetary Change 110, 302-320.

Fendorf, S., Michael, H.A., van Geen, A., 2010. Spatial and temporal variations of groundwater arsenic in South and Southeast Asia. Science 328(5982), 1123-1127.

Feng, S., Guo, H., Sun, X., Han, S., Li, Y., 2022. Relative importance of hydrogeochemical and hydrogeological processes on arsenic enrichment in groundwater of the Yinchuan Basin, China. Applied Geochemistry 137, 105180.

Gebhardt, N.A., Thauer, R.K., Linder, D., Kaulfers, P.-M., Pfennig, N., 1985. Mechanism of acetate oxidation to CO 2 with elemental sulfur in Desulfuromonas acetoxidans. Archives of microbiology 141, 392-398.

Glodowska, M., Stopelli, E., Schneider, M., Lightfoot, A., Rathi, B., Straub, D., Patzner, M., Duyen, V.T., Berg, M., Kleindienst, S., Kappler, A., 2020. Role of in Situ Natural Organic Matter in Mobilizing As during Microbial Reduction

of FeIII-Mineral-Bearing Aquifer Sediments from Hanoi (Vietnam). Environmental Science & Technology 54(7), 4149-4159.

Goldberg, S., 2002. Competitive adsorption of arsenate and arsenite on oxides and clay minerals. Soil Science Society of America Journal 66(2), 413-421.

Grabb, K.C., Buchwald, C., Hansel, C.M., Wankel, S.D., 2017. A dual nitrite isotopic investigation of chemodenitrification by mineral-associated Fe(II) and its production of nitrous oxide. Geochimica et Cosmochimica Acta 196, 388-402.

Gran, G., 1952. Determination of the equivalence point in potentiometric titrations. Part II. Analyst 77(920), 661-671.

Grubba, D., Majtacz, J., Mąkinia, J., 2021. Sulfate reducing ammonium oxidation (SULFAMMOX) process under anaerobic conditions. Environmental Technology & Innovation 22, 101416.

Gu, Z., de Silva, S., Reichman, S.M., 2020. Arsenic Concentrations and Dietary Exposure in Rice-Based Infant Food in Australia. International Journal of Environmental Research and Public Health 17(2), 415.

Guo, H., Jia, Y., Wanty, R.B., Jiang, Y., Zhao, W., Xiu, W., Shen, J., Li, Y., Cao, Y., Wu, Y., 2016. Contrasting distributions of groundwater arsenic and uranium in the western Hetao basin, Inner Mongolia: implication for origins and fate controls. Science of the Total Environment 541, 1172-1190.

Hafenbradl, D., Keller, M., Dirmeier, R., Rachel, R., Roßnagel, P., Burggraf, S., Huber, H., Stetter, K.O., 1996. Ferroglobus placidus gen. nov., sp. nov., a novel hyperthermophilic archaeum that oxidizes Fe2+ at neutral pH under anoxic conditions. Archives of microbiology 166, 308-314.

Hakil, F., Amin-Ali, O., Hirschler-Réa, A., Mollex, D., Grossi, V., Duran, R., Matheron, R., Cravo-Laureau, C., 2014. Desulfatiferula berrensis sp. nov., a n-alkene-degrading sulfate-reducing bacterium isolated from estuarine sediments. International Journal of Systematic and Evolutionary Microbiology 64(Pt_2), 540-544.

Han, L., Sun, Y., Li, Z., Duan, Y., Han, S., Zhang, H., Zhao, M., Zheng, Y., 2023. Beyond the geological origin of sediment arsenic in groundwater systems: arsenic redux by redox. Science Bulletin 68(15), 1616-1620.

Han, S., Zhang, F., Zhang, H., An, Y., Wang, Y., Wu, X., Wang, C., 2013. Spatial and temporal patterns of groundwater arsenic in shallow and deep groundwater of Yinchuan Plain, China. Journal of Geochemical Exploration 135, 71-78.

Han, Y.-S., Park, J.-H., Min, Y., Lim, D.-H., 2020. Competitive adsorption between phosphate and arsenic in soil containing iron sulfide: XAS experiment and DFT calculation approaches. Chemical Engineering Journal 397, 125426.

Hansel, C.M., Benner, S.G., Fendorf, S., 2005. Competing Fe (II)-induced mineralization pathways of ferrihydrite. Environ Sci Technol 39(18), 7147-7153.

Hongshao, Z., Stanforth, R., 2001. Competitive adsorption of phosphate and arsenate on goethite. Environmental Science & Technology 35(24), 4753-4757.

Horneman, A., van Geen, A., Kent, D.V., Mathe, P., Zheng, Y., Dhar, R., O'connell, S., Hoque, M., Aziz, Z., Shamsudduha, M., 2004. Decoupling of as and fe release to bangladesh groundwater under reducing conditions. Part I: Evidence from sediment profiles1. Geochimica et Cosmochimica Acta 68(17), 3459-3473.

Hubert, C., Voordouw, G., 2007. Oil field souring control by nitrate-reducing Sulfurospirillum spp. that outcompete sulfate-reducing bacteria for organic electron donors. Applied and environmental microbiology 73(8), 2644-2652.

Huhmann, B.L., Harvey, C.F., Uddin, A., Choudhury, I., Ahmed, K.M., Duxbury, J.M., Bostick, B.C., van Geen, A., 2017. Field Study of Rice Yield Diminished by Soil Arsenic in Bangladesh. Environmental Science & Technology 51(20), 11553-11560.

Jackson, B.P., Miller, W., 2000. Effectiveness of phosphate and hydroxide for desorption of arsenic and selenium species from iron oxides. Soil Science Society of America Journal 64(5), 1616-1622.

Jamieson, J., Prommer, H., Kaksonen, A., Sun, J., Siade, A., Yusov, A., Bostick, B.C., 2018. Identifying and quantifying the intermediate processes during nitrate dependent iron(II) oxidation. Environmental Science & Technology 52(10), acs.est.8b01122.

Jang, J.-H., Dempsey, B.A., Catchen, G.L., Burgos, W.D., 2003. Effects of Zn (II), Cu (II), Mn (II), Fe (II), NO3−, or SO42− at pH 6.5 and 8.5 on transformations of hydrous ferric oxide (HFO) as evidenced by Mössbauer spectroscopy. Colloids and Surfaces A: Physicochemical and Engineering Aspects 221(1-3), 55-68.

Jung, H.B., Zheng, Y., 2006. Enhanced recovery of arsenite sorbed onto synthetic oxides by l-ascorbic acid addition to phosphate solution: calibrating a sequential leaching method for the speciation analysis of arsenic in natural samples. 40(11), 0-2180.

Jurgens, B.C., McMahon, P.B., Chapelle, F.H., Eberts, S.M., 2009. An Excel workbook for identifying redox processes in ground water.

Kappler, A., Schink, B., Newman, D.K., 2005. Fe(III) mineral formation and cell encrustation by the nitrate-dependent Fe(II)-oxidizer strain BoFeN1. Geobiology 3(4), 235-245.

Kaster, K.M., Grigoriyan, A., Jennneman, G., Voordouw, G., 2007. Effect of nitrate and nitrite on sulfide production by two thermophilic, sulfate-reducing enrichments from an oil field in the North Sea. Applied Microbiology and Biotechnology 75(1), 195-203.

Keimowitz, A.R., Mailloux, B.J., Cole, P., Stute, M., Simpson, H.J., Chillrud, S.N., 2007. Laboratory Investigations of Enhanced Sulfate Reduction as a Groundwater Arsenic Remediation Strategy. Environmental Science & Technology 41(19), 6718-6724.

Keon, N.E., Swartz, C.H., Brabander, D.J., Harvey, C., Hemond, H.F., 2001. Validation of an arsenic sequential extraction method for evaluating mobility in sediments. Environ Sci Technol 35(13), 2778-2784.

Kirk, M.F., Holm, T.R., Park, J., Jin, Q., Sanford, R.A., Fouke, B.W., Bethke, C.M., 2004. Bacterial sulfate reduction limits natural arsenic contamination in groundwater. Geology 32(11), 953-956.

Kirk Nordstrom, D., 2012. Models, validation, and applied geochemistry: Issues in science, communication, and philosophy. Applied Geochemistry 27(10), 1899-1919.

Kocar, B.D., Borch, T., Fendorf, S., 2010. Arsenic repartitioning during biogenic sulfidization and transformation of ferrihydrite. Geochimica et Cosmochimica Acta 74(3), 980-994.

Korom, S.F., 1992. Natural denitrification in the saturated zone: a review. Water resources research 28(6), 1657-1668.

Kumar, N., Noël, V., Planer-Friedrich, B., Besold, J., Lezama-Pacheco, J., Bargar, J.R., Brown, G.E., Jr., Fendorf, S., Boye, K., 2020. Redox Heterogeneities Promote Thioarsenate Formation and Release into Groundwater from Low Arsenic Sediments. Environmental Science & Technology 54(6), 3237-3244.

Kwon, M.J., O'Loughlin, E.J., Boyanov, M.I., Brulc, J.M., Johnston, E.R., Kemner, K.M., Antonopoulos, D.A., 2016. Impact of organic carbon electron donors on microbial community development under iron-and sulfate-reducing conditions. PloS one 11(1), e0146689.

Layton, A.C., Chauhan, A., Williams, D.E., Mailloux, B., Knappett, P.S.K., Ferguson, A.S., McKay, L.D., Alam, M.J., Matin Ahmed, K., van Geen, A., Sayler, G.S., 2014. Metagenomes of microbial communities in arsenic- and pathogen-contaminated well and surface water from bangladesh. Genome announcements 2(6).

Lengke, M.F., Sanpawanitchakit, C., Tempel, R.N., 2009. The oxidation and dissolution of arsenic-bearing sulfides. The Canadian Mineralogist 47(3), 593-613.

Li, Z., 2018. Microbial community and manganese influence in situ arsenic immobilization by biogenically formed magnetite. Southern University of Science and Technology.

Liu, E., Yang, Y., Xie, Z., Wang, J., Chen, M., 2022. Influence of Sulfate Reduction on Arsenic Migration and Transformation in Groundwater Environment. Water 14(6), 942.

Liu, L.Y., Xie, G.J., Xing, D.F., Liu, B.F., Ren, N.Q., 2021. Sulfate dependent ammonium oxidation: A microbial process linked nitrogen with sulfur cycle and potential application. Environmental Research 192(1), 110282.

Liu, Q., Roberts, A.P., Larrasoana, J.C., Banerjee, S.K., Guyodo, Y., Tauxe, L., Oldfield, F., 2012. Environmental magnetism: principles and applications. Reviews of Geophysics 50(4).

Liu, T., Chen, D., Luo, X., Li, X., Li, F., 2019. Microbially mediated nitrate-reducing Fe (II) oxidation: quantification of chemodenitrification and biological reactions. Geochimica et Cosmochimica Acta 256, 97-115.

Londry, K., Suflita, J., 1999. Use of nitrate to control sulfide generation by sulfate-reducing bacteria associated with oily waste. Journal of industrial microbiology & biotechnology 22(6).

Lovley, D.R., Coates, J.D., Saffarini, D.A., Lonergan, D.J., 2022. Dissimilatory iron reduction, Transition metals in microbial metabolism. CRC Press, pp. 187-215.

Lovley, D.R., Phillips, E.J., 1987. Competitive mechanisms for inhibition of sulfate reduction and methane production in the zone of ferric iron reduction in sediments. Applied and Environmental Microbiology 53(11), 2636-2641.

Lu, K.-L., Liu, C.-W., Wang, S.-W., Jang, C.-S., Lin, K.-H., Liao, V.H.-C., Liao, C.-M., Chang, F.-J., 2010. Primary sink and source of geogenic arsenic in sedimentary aquifers in the southern Choushui River alluvial fan, Taiwan. Applied Geochemistry 25(5), 684-695.

Mailloux, B.J., Alexandrova, E., Keimowitz, A.R., Wovkulich, K., Freyer, G.A., Herron, M., Stolz, J.F., Kenna, T.C., Pichler, T., Polizzotto, M.L., Dong, H., Bishop, M., Knappett, P.S.K., 2009. Microbial Mineral Weathering for Nutrient Acquisition Releases Arsenic. Applied and Environmental Microbiology 75(8), 2558-2565.

Makinia, J., Grubba, D., Majtacz, J., 2021. Sulfate reducing ammonium oxidation (SULFAMMOX) process under anaerobic conditions. Environmental Technology & Innovation 22(1), 101416.

Manning, B.A., Goldberg, S., 1996. Modeling competitive adsorption of arsenate with phosphate and molybdate on oxide minerals. Soil Science Society of America Journal 60(1), 121-131.

Manning, B.A., Goldberg, S., 1997. Arsenic (III) and arsenic (V) adsorption on three California soils. Soil Science 162(12), 886-895.

Mark Jensen, M., Thamdrup, B., Rysgaard, S., Holmer, M., Fossing, H., 2003. Rates and regulation of microbial iron reduction in sediments of the Baltic-North Sea transition. Biogeochemistry 65(3), 295-317.

McArthur, J., Ravenscroft, P., Safiulla, S., Thirlwall, M., 2001. Arsenic in groundwater: testing pollution mechanisms for sedimentary aquifers in Bangladesh. Water Resources Research 37(1), 109-117.

Mehta-Kolte, M.G., Loutey, D., Wang, O., Youngblut, M.D., Hubbard, C.G., Wetmore, K.M., Conrad, M.E., Coates, J.D., 2017. Mechanism of H_2S oxidation by the dissimilatory perchlorate-reducing microorganism Azospira suillum PS. MBio 8(1), e02023-02016.

Miao, Z., Brusseau, M.L., Carroll, K.C., Carreón-Diazconti, C., Johnson, B., 2012. Sulfate reduction in groundwater: characterization and applications for remediation. Environmental geochemistry and health 34(4), 539-550.

Mihajlov, I., 2014. The vulnerability of low-arsenic aquifers in Bangladesh: A multi-scale geochemical and hydrologic approach. Columbia University.

Mladenov, N., Zheng, Y., Miller, M.P., Nemergut, D.R., Legg, T., Simone, B., Hageman, C., Rahman, M.M., Ahmed, K.M., McKnight, D.M., 2010.

Dissolved organic matter sources and consequences for iron and arsenic mobilization in Bangladesh aquifers. Environmental science & technology 44(1), 123-128.

Mozumder, M.R.H., Benjamin, C.B., Magdi, S., Islam, M.A., Elizabeth, M.S., Tyler, E., Brian, J.M., Imtiaz, C., Kazi, M.A., Alexander, 2020. Similar retardation of arsenic in gray Holocene and orange Pleistocene sediments: Evidence from field-based column experiments in Bangladesh. Water Research 183, 116081.

Mukherjee, A., Gupta, S., Coomar, P., Fryar, A.E., Guillot, S., Verma, S., Bhattacharya, P., Bundschuh, J., Charlet, L., 2019. Plate tectonics influence on geogenic arsenic cycling: From primary sources to global groundwater enrichment. Science of the Total Environment 683, 793-807.

Müller, H., Bosch, J., Griebler, C., Damgaard, L.R., Nielsen, L.P., Lueders, T., Meckenstock, R.U., 2016. Long-distance electron transfer by cable bacteria in aquifer sediments. The ISME journal 10(8), 2010-2019.

Müller, H., Marozava, S., Probst, A.J., Meckenstock, R.U., 2020. Groundwater cable bacteria conserve energy by sulfur disproportionation. The ISME journal 14(2), 623-634.

Muxworthy, A.R., Dunlop, D.J., 2002. First-order reversal curve (FORC) diagrams for pseudo-single-domain magnetites at high temperature. Earth and Planetary Science Letters 203(1), 369-382.

Muyzer, G., Stams, A.J.M., 2008. The ecology and biotechnology of sulphate-reducing bacteria. Nature Reviews Microbiology 6(6), 441-454.

Newell, A.J., 2005. A high-precision model of first-order reversal curve (FORC) functions for single-domain ferromagnets with uniaxial anisotropy. Geochemistry, Geophysics, Geosystems 6(5).

Niazi, N.K., Burton, E.D., 2016. Arsenic sorption to nanoparticulate mackinawite (FeS): an examination of phosphate competition. Environmental pollution 218, 111-117.

Nickson, R., McArthur, J., Burgess, W., Ahmed, K.M., Ravenscroft, P., Rahmanñ, M., 1998. Arsenic poisoning of Bangladesh groundwater. Nature 395(6700), 338-338.

Nickson, R.T., McArthur, J.M., Ravenscroft, P., Burgess, W.G., Ahmed, K.M., 2000. Mechanism of arsenic release to groundwater, Bangladesh and West Bengal. Applied Geochemistry 15(4), 403-413.

Nordstrom, D.K., 2000. An overview of arsenic mass poisoning in Bangladesh and West Bengal, India. Minor elements, 21-30.

O'Day, P.A., Vlassopoulos, D., Root, R., Rivera, N., 2004. The influence of sulfur and iron on dissolved arsenic concentrations in the shallow subsurface under changing redox conditions. Proceedings of the National Academy of Sciences 101(38), 13703-13708.

O'reilly, S., Strawn, D., Sparks, D., 2001. Residence time effects on arsenate adsorption/desorption mechanisms on goethite. Soil Science Society of America Journal 65(1), 67-77.

Oude Elferink, S.J., Akkermans-van Vliet, W., Bogte, J.J., Stams, A.J., 1999. Desulfobacca acetoxidans gen. nov., sp. nov., a novel acetate-degrading sulfate reducer isolated from sulfidogenic granular sludge. International Journal of Systematic and Evolutionary Microbiology 49(2), 345-350.

Paar, H., Ruhl, A.S., Jekel, M., 2015. Influences of nanoscale zero valent iron loadings and bicarbonate and calcium concentrations on hydrogen evolution in anaerobic column experiments. Water Research 68, 731-739.

Pantke, C., Obst, M., Benzerara, K., Morin, G., Ona-Nguema, G., Dippon, U., Kappler, A., 2012. Green rust formation during Fe (II) oxidation by the nitrate-reducing Acidovorax sp. strain BoFeN1. Environmental science & technology 46(3), 1439-1446.

Patel, B., Gundaliya, R., Desai, B., Shah, M., Shingala, J., Kaul, D., Kandya, A., 2023. Groundwater arsenic contamination: impacts on human health and agriculture, ex situ treatment techniques and alleviation. Environmental Geochemistry and Health 45(5), 1331-1358.

Pi, K., Wang, Y., Xie, X., Ma, T., Liu, Y., Su, C., Zhu, Y., Wang, Z., 2017. Remediation of arsenic-contaminated groundwater by in-situ stimulating biogenic precipitation of iron sulfides. Water Research 109, 337-346.

Pike, C.R., Roberts, A.P., Dekkers, M.J., Verosub, K.L., 2001a. An investigation of multi-domain hysteresis mechanisms using FORC diagrams. Physics of the Earth and Planetary Interiors 126(1-2), 11-25.

Pike, C.R., Roberts, A.P., Verosub, K.L., 1999. Characterizing interactions in fine magnetic particle systems using first order reversal curves. Journal of Applied Physics 85(9), 6660-6667.

Pike, C.R., Roberts, A.P., Verosub, K.L., 2001b. First order reversal curve diagrams and thermal relaxation effects in magnetic particles. Geophysical Journal International 145(3), 721-730.

Planer-Friedrich, B., 2023. Sulfur being an overlooked promoter of groundwater arsenic contamination. Nature Water 1(2), 134-135.

Podgorski, J., Berg, M., 2020. Global threat of arsenic in groundwater. Science 368(6493), 845-850.

Polizzotto, M.L., Harvey, C.F., Sutton, S.R., Fendorf, S., 2005. Processes conducive to the release and transport of arsenic into aquifers of Bangladesh. Proceedings of the National Academy of Sciences 102(52), 18819-18823.

Poulton, S.W., Krom, M.D., Raiswell, R., 2004. A revised scheme for the reactivity of iron (oxyhydr) oxide minerals towards dissolved sulfide. Geochimica et cosmochimica acta 68(18), 3703-3715.

Poulton, S.W., Krom, M.D., Rijn, J.V., Raiswell, R., 2002. The use of hydrous iron (III) oxides for the removal of hydrogen sulphide in aqueous systems. Water Research 36(4), 825-834.

Poulton, S.W., Krom, M.D., van Rijn, J., Raiswell, R., Bows, R., 2003. Detection and removal of dissolved hydrogen sulphide in flow-through systems via the

sulphidation of hydrous iron (III) oxides. Environmental Technology 24(2), 217-229.

Qian, J., Liu, R., Wei, L., Lu, H., Chen, G.-H., 2015. System evaluation and microbial analysis of a sulfur cycle-based wastewater treatment process for Co-treatment of simple wet flue gas desulfurization wastes with freshwater sewage. Water Research 80, 189-199.

Quast, C., Pruesse, E., Yilmaz, P., Gerken, J., Schweer, T., Yarza, P., Peplies, J., Glöckner, F.O., 2012. The SILVA ribosomal RNA gene database project: improved data processing and web-based tools. Nucleic acids research 41(D1), D590-D596.

Radloff, K.A., Manning, A.R., Mailloux, B., Zheng, Y., Rahman, M.M., Huq, M.R., Ahmed, K.M., van Geen, A., 2008. Considerations for conducting incubations to study the mechanisms of As release in reducing groundwater aquifers. Applied geochemistry 23(11), 3224-3235.

Radloff, K.A., Zheng, Y., Michael, H.A., Stute, M., Bostick, B.C., Mihajlov, I., Bounds, M., Huq, M.R., Choudhury, I., Rahman, M.W., Schlosser, P., Ahmed, K.M., van Geen, A., 2011. Arsenic migration to deep groundwater in Bangladesh influenced by adsorption and water demand. Nature Geoscience 4(11), 793-798.

Rakshit, S., Matocha, C.J., Coyne, M.S., 2008. Nitrite reduction by siderite. Soil Science Society of America Journal 72(4), 1070-1077.

Ratering, S., Schnell, S., 2001. Nitrate-dependent iron (II) oxidation in paddy soil. Environmental Microbiology 3(2), 100-109.

Raven, K.P., Jain, A., Loeppert, R.H., 1998. Arsenite and arsenate adsorption on ferrihydrite: kinetics, equilibrium, and adsorption envelopes. Environmental science & technology 32(3), 344-349.

Ravenscroft, P., Brammer, H., Richards, K., 2009. Arsenic pollution: a global synthesis. John Wiley & Sons.

Ravenscroft, P., Burgess, W.G., Ahmed, K.M., Burren, M., Perrin, J., 2005. Arsenic in groundwater of the Bengal Basin, Bangladesh: Distribution, field relations, and hydrogeological setting. Hydrogeology Journal 13, 727-751.

Rawson, J., Prommer, H., Siade, A., Carr, J., Berg, M., Davis, J.A., Fendorf, S., 2016. Numerical modeling of arsenic mobility during reductive iron-mineral transformations. Environmental science & technology 50(5), 2459-2467.

Rawson, J., Siade, A., Sun, J., Neidhardt, H., Berg, M., Prommer, H., 2017. Quantifying reactive transport processes governing arsenic mobility after injection of reactive organic carbon into a Bengal Delta aquifer. Environmental science & technology 51(15), 8471-8480.

Rios-Del Toro, E.E., Cervantes, F.J., 2019. Anaerobic ammonium oxidation in marine environments: contribution to biogeochemical cycles and biotechnological developments for wastewater treatment. Reviews in Environmental Science and Bio/Technology 18(1), 11-27.

Roberts, A.P., Liu, Q., Rowan, C.J., Chang, L., Carvallo, C., Torrent, J., Horng, C.-S., 2006. Characterization of hematite (α-Fe_2O_3), goethite (α-FeOOH), greigite (Fe_3S_4), and pyrrhotite (Fe_7S_8) using first-order reversal curve diagrams. Journal of Geophysical Research: Solid Earth 111(B12).

Roberts, A.P., Pike, C.R., Verosub, K.L., 2000. First-order reversal curve diagrams: A new tool for characterizing the magnetic properties of natural samples. Journal of Geophysical Research: Solid Earth 105(B12), 28461-28475.

Rochette, E.A., Bostick, B.C., Li, G., Fendorf, S., 2000. Kinetics of Arsenate Reduction by Dissolved Sulfide. Environmental Science & Technology 34(22), 4714-4720.

Rockafellow-Baldoni, M., Spayd, S.E., Hong, J.-Y., Meng, Q., Ohman-Strickland, P., Robson, M.G., 2018. Arsenic exposure and cancer risk reduction with local ordinance requiring whole-house dual-tank water treatment systems. Human and Ecological Risk Assessment: An International Journal 24(5), 1256-1267.

Saalfield, S.L., Bostick, B.C., 2009. Changes in Iron, Sulfur, and Arsenic Speciation Associated with Bacterial Sulfate Reduction in Ferrihydrite-Rich Systems. Environmental Science & Technology 43(23), 8787-8793.

Saint-Jacques, N., Brown, P., Nauta, L., Boxall, J., Parker, L., Dummer, T.J.B., 2018. Estimating the risk of bladder and kidney cancer from exposure to low-levels of arsenic in drinking water, Nova Scotia, Canada. Environment International 110, 95-104.

Schmidt, C.W., 2014. Low-Dose Arsenic: In Search of a Risk Threshold. Environmental Health Perspectives 122(5), A130-A134.

Schwertmann, U., Taylor, R.M., 1989. Iron oxides. Minerals in soil environments 1, 379-438.

Senn, D.B., Hemond, H.F., 2002. Nitrate controls on iron and arsenic in an urban lake. Science 296(5577), 2373-2376.

Shiklomanov, I.A., 1993. World fresh water resources, in: Gleick, P.H. (Ed.) Water in crisis: A guide to the world's fresh water resources. Oxford University Press, New York, pp. 13-24.

Smedley, P.L., Kinniburgh, D., 2002. A review of the source, behaviour and distribution of arsenic in natural waters. Applied geochemistry 17(5), 517-568.

Smirnov, A.V., 2006. Low-temperature magnetic properties of magnetite using first-order reversal curve analysis: Implications for the pseudo-single-domain state. Geochemistry, Geophysics, Geosystems 7(11).

Smith, R.L., Kent, D.B., Repert, D.A., Böhlke, J., 2017. Anoxic nitrate reduction coupled with iron oxidation and attenuation of dissolved arsenic and phosphate in a sand and gravel aquifer. Geochimica et Cosmochimica Acta 196, 102-120.

Sollo, F.W., Larson, T.E., Mcgurk, F.F., 1971. Colorimetric methods for bromine. Environmental Science & Technology 5(3), 240-246.

Sørensen, J., 1987. Nitrate reduction in marine sediment: pathways and interactions with iron and sulfur cycling. Geomicrobiology Journal 5(3-4), 401-421.

Sørensen, J., Thorling, L., 1991. Stimulation by lepidocrocite (7-FeOOH) of Fe(II)-dependent nitrite reduction. Geochimica et Cosmochimica Acta 55(5), 1289-1294.

Stenger, V.A., Kolthoff, I.M., 2002. The Detection and Colorimetric Estimation of Micro Quantities of Bromide. Journal of the American Chemical Society 57(5), 831-833.

Stolze, L., Battistel, M., Rolle, M., 2022. Oxidative Dissolution of Arsenic-Bearing Sulfide Minerals in Groundwater: Impact of Hydrochemical and Hydrodynamic Conditions on Arsenic Release and Surface Evolution. Environmental Science & Technology 56(8), 5049-5061.

Straub, K.L., Benz, M., Schink, B., Widdel, F., 1996. Anaerobic, nitrate-dependent microbial oxidation of ferrous iron. Appl. Environ. Microbiol. 62(4), 1458-1460.

Straub, K.L., Schönhuber, W.A., Buchholz-Cleven, B.E., Schink, B., 2004. Diversity of ferrous iron-oxidizing, nitrate-reducing bacteria and their involvement in oxygen-independent iron cycling. Geomicrobiology Journal 21(6), 371-378.

Stumm, W., Morgan, J.J., 1996. Aquatic chemistry : chemical equilibria and rates in natural waters.

Stute, M., Zheng, Y., Schlosser, P., Horneman, A., Dhar, R.K., Datta, S., Hoque, M.A., Seddique, A.A., Shamsudduha, M., Ahmed, K.M., van Geen, A., 2007. Hydrological control of As concentrations in Bangladesh groundwater. Water Resources Research 43(9).

Sultana, M., Härtig, C., Planer-Friedrich, B., Seifert, J., Schlömann, M., 2011. Bacterial Communities in Bangladesh Aquifers Differing in Aqueous Arsenic Concentration. Geomicrobiology Journal 28(3), 198-211.

Sun, J., 2015. Developing Improved Strategies of Remediating Arsenic Contaminated Aquifers. Columbia University.

Sun, J., Chillrud, S.N., Mailloux, B.J., Bostick, B.C., 2016a. In situ magnetite formation and long-term arsenic immobilization under advective flow conditions. Environmental science & technology 50(18), 10162-10171.

Sun, J., Chillrud, S.N., Mailloux, B.J., Stute, M., Singh, R., Dong, H., Lepre, C.J., Bostick, B.C., 2016b. Enhanced and stabilized arsenic retention in microcosms through the microbial oxidation of ferrous iron by nitrate. Chemosphere 144, 1106-1115.

Sun, J., Prommer, H., Siade, A.J., Chillrud, S.N., Mailloux, B.J., Bostick, B.C., 2018. Model-Based Analysis of Arsenic Immobilization via Iron Mineral Transformation under Advective Flows. Environmental science & technology 52(16), 9243-9253.

Sun, J., Quicksall, A.N., Chillrud, S.N., Mailloux, B.J., Bostick, B.C., 2016c. Arsenic mobilization from sediments in microcosms under sulfate reduction. Chemosphere 153, 254-261.

Sun, Y., 2021. Mechanism of arsenic mobilization and immobilization in reducing groundwater of Quaternary aquifer, Yinchuan Plain. Peking University.

Sun, Y., Sun, J., Nghiem, A.A., Bostick, B.C., Ellis, T., Han, L., Li, Z., Liu, S., Han, S., Zhang, M., Xia, Y., Zheng, Y., 2021. Reduction of iron (hydr)oxide-bound arsenate: Evidence from high depth resolution sampling of a reducing aquifer in Yinchuan Plain, China. Journal of Hazardous Materials 406, 124615.

Tufano, K.J., Benner, S.G., Mayer, K.U., Marcus, M.A., Nico, P.S., Fendorf, S., 2009. Aggregate-scale heterogeneity in iron (hydr) oxide reductive transformations. Vadose Zone Journal 8(4), 1004-1012.

Tufano, K.J., Fendorf, S., 2008. Confounding impacts of iron reduction on arsenic retention. Environmental Science & Technology 42(13), 4777-4783.

Turpeinen, R., Kairesalo, T., Häggblom, M.M., 2004. Microbial community structure and activity in arsenic-, chromium- and copper-contaminated soils. Fems Microbiology Ecology 47(1), 39-50.

UNESCO-IGRAC, 2018. Groundwater Overview. Making the invisible visible, UN-Water Category III. International Groundwater Resources Assessment Centre, UNESCO, pp. 1-60.

Van de Graaf, A.A., Mulder, A., de Bruijn, P., Jetten, M., Robertson, L.A., Kuenen, J.G., 1995. Anaerobic oxidation of ammonium is a biologically mediated process. Applied and environmental microbiology 61(4), 1246-1251.

van Geen, A., Rose, J., Thoral, S., Garnier, J.M., Zheng, Y., Bottero, J.Y., 2004. Decoupling of As and Fe release to Bangladesh groundwater under reducing conditions. Part II: Evidence from sediment incubations 1 1Associate editor: G. Sposito. Geochimica et Cosmochimica Acta 68(17), 3475-3486.

van Geen, A., Zheng, Y., Goodbred Jr, S., Horneman, A., Aziz, Z., Cheng, Z., Stute, M., Mailloux, B., Weinman, B., Hoque, M., 2008. Flushing history as a hydrogeological control on the regional distribution of arsenic in shallow groundwater of the Bengal Basin. Environmental science & technology 42(7), 2283-2288.

van Houten, B.H.G.W., Roest, K., Tzeneva, V.A., Dijkman, H., Smidt, H., Stams, A.J.M., 2006. Occurrence of methanogenesis during start-up of a full-scale synthesis gas-fed reactor treating sulfate and metal-rich wastewater. Water Research 40(3), 553-560.

van Houten, R.T., Yun, S.Y., Lettinga, G., 1997. Thermophilic sulphate and sulphite reduction in lab-scale gas-lift reactors using H2 and CO2 as energy and carbon source. Biotechnology and Bioengineering 55(5), 807-814.

Vandieken, V., 2005. Microbiological and Biogeochemical Studies of Microbial Mn(IV) and Fe(III) Reduction in Arctic Sediments (Svalbard).

Wang, F., Peng, S., Fan, L., Li, Y., 2022. Improved sulfate reduction efficiency of sulfate-reducing bacteria in sulfate-rich systems by acclimatization and multiple-grouting. Alexandria Engineering Journal 61(12), 9993-10005.

Wang, R., Yang, C., Zhang, M., Xu, S.-Y., Dai, C.-L., Liang, L.-Y., Zhao, H.-P., Zheng, P., 2017. Chemoautotrophic denitrification based on ferrous iron oxidation: reactor performance and sludge characteristics. Chemical Engineering Journal 313, 693-701.

Wang, Y., Li, P., Li, B., Webster, G., Weightman, A.J., Jiang, Z., Jiang, D., Deng, Y., Wang, Y., 2014. Bacterial Diversity and Community Structure in High Arsenic Aquifers in Hetao Plain of Inner Mongolia, China. Geomicrobiology Journal 31(4), 338-349.

Weber, K.A., Achenbach, L.A., Coates, J.D., 2006. Microorganisms pumping iron: anaerobic microbial iron oxidation and reduction. Nature Reviews Microbiology 4(10), 752-764.

Weber, K.A., Picardal, F.W., Roden, E.E., 2001. Microbially catalyzed nitrate-dependent oxidation of biogenic solid-phase Fe (II) compounds. Environmental Science & Technology 35(8), 1644-1650.

Xia, D., Yi, X., Lu, Y., Huang, W., Xie, Y., Ye, H., Dang, Z., Tao, X., Li, L., Lu, G., 2019. Dissimilatory iron and sulfate reduction by native microbial communities using lactate and citrate as carbon sources and electron donors. Ecotoxicology and Environmental Safety 174, 524-531.

Xie, X., Wang, Y., Ellis, A., Su, C., Li, J., Li, M., 2011. The sources of geogenic arsenic in aquifers at Datong basin, northern China: Constraints from isotopic and geochemical data. Journal of Geochemical Exploration 110(2), 155-166.

Yang, Q., Flanagan, S.V., Chillrud, S., Ross, J., Zeng, W., Culbertson, C., Spayd, S., Backer, L., Smith, A.E., Zheng, Y., 2020. Reduction in drinking water arsenic exposure and health risk through arsenic treatment among private well households in Maine and New Jersey, USA. Science of the Total Environment 738, 139683.

Yu, Y., Lee, C., Kim, J., Hwang, S., 2005. Group-specific primer and probe sets to detect methanogenic communities using quantitative real-time polymerase chain reaction. Biotechnology and bioengineering 89(6), 670-679.

Zecchin, S., Colombo, M., Cavalca, L., 2019. Exposure to different arsenic species drives the establishment of iron- and sulfur-oxidizing bacteria on rice root iron plaques. World Journal of Microbiology and Biotechnology 35(8), 117.

Zhang, D., Cui, L., Madani, R.M., Wang, H., Zhu, H., Liang, J., 2019. Effect of nitrite and nitrate on sulfate reducing ammonium oxidation. Water Science and Technology 80(4), 634-643.

Zhang, L., Sun, H., Zhang, X.-x., Ren, H., Ye, L., 2018. High diversity of potential nitrate-reducing Fe (II)-oxidizing bacteria enriched from activated sludge. Applied microbiology and biotechnology 102, 4975-4985.

Zhang, Z., Zhang, C., Yang, Y., Zhang, Z., Tang, Y., Su, P., Lin, Z., 2022. A review of sulfate-reducing bacteria: Metabolism, influencing factors and application in wastewater treatment. Journal of Cleaner Production 376, 134109.

Zhao, L., Dong, H., Kukkadapu, R., Agrawal, A., Liu, D., Zhang, J., Edelmann, R.E., 2013. Biological oxidation of Fe(II) in reduced nontronite coupled with nitrate reduction by Pseudogulbenkiania sp. Strain 2002. Geochimica et Cosmochimica Acta 119, 231-247.

Zheng, Y., 2007. The heterogeneity of arsenic in the crust: a linkage to occurrence in groundwater. Quaternary Sciences (Chinese) 27, 1-15.

Zheng, Y., 2017. Lessons learned from arsenic mitigation among private well households. Current environmental health reports 4, 373-382.

Zheng, Y., Stute, M., Van Geen, A., Gavrieli, I., Dhar, R., Simpson, H., Schlosser, P., Ahmed, K., 2004. Redox control of arsenic mobilization in Bangladesh groundwater. Applied Geochemistry 19(2), 201-214.

Zheng, Y., van Geen, A., Stute, M., Dhar, R., Mo, Z., Cheng, Z., Horneman, A., Gavrieli, I., Simpson, H.J., Versteeg, R., Steckler, M., Grazioli-Venier, A., Goodbred, S., Shahnewaz, M., Shamsudduha, M., Hoque, M.A., Ahmed, K.M., 2005. Geochemical and hydrogeological contrasts between shallow and deeper aquifers in two villages of Araihazar, Bangladesh: Implications for deeper aquifers as drinking water sources. Geochimica et Cosmochimica Acta 69(22), 5203-5218.